The NIMA-Related Kinases as Regulators of Ciliary Assembly, Disassembly, and Length

by

Laura K. Hilton

B.Sc., Simon Fraser University, 2008

Thesis Submitted In Partial Fulfillment of the
Requirements for the Degree of
Doctor of Philosophy

in the
Department of Molecular Biology and Biochemistry
Faculty of Science

SIMON FRASER UNIVERSITY

Fall 2013

Approval

Name: **Laura Kathleen Hilton**

Degree: **Doctor of Philosophy**

Title of Thesis: ***The NIMA-Related Kinases as Regulators of Ciliary Assembly, Disassembly, and Length***

Examining Committee: **Chair: Dr. Fiona Brinkman**
Professor

Dr. Lynne Quarmby
Senior Supervisor
Professor

Dr. Christopher Beh
Supervisor
Associate Professor

Dr. William Davidson
Supervisor
Professor

Dr. Michel Leroux
Internal Examiner
Professor
Molecular Biology and Biochemistry

Dr. Karl Lechtreck
External Examiner
Assistant Professor
Department of Cellular Biology
University of Georgia at Athens

Date Defended/Approved: September 18, 2013

Partial Copyright Licence

Abstract

Cilia are microtubule-based, membrane-enclosed organelles that project from the surface of most eukaryotic cells. Cilia perform important signalling functions in development and homeostasis, and disruption of these functions in humans and other metazoans is associated with diseases known as ciliopathies. Previously, it was hypothesized that the NIMA-related kinases (Neks) evolved to coordinate ciliogenesis and ciliary resorption with the cell cycle. In this work, I examine the events surrounding pre-mitotic resorption in *Chlamydomonas*, and the roles of two Neks in ciliary regulation, thereby advancing our understanding of the mechanisms that regulate ciliogenesis, ciliary resorption, and ciliary length.

Pre-mitotic ciliary resorption occurs to free the basal body to act as a spindle pole during mitosis, although little is known of the mechanisms or signals that regulate this event. Here, I show that pre-mitotic resorption culminates in a severing event that separates the basal body from the transition zone in *Chlamydomonas*. This severing may be essential for cell cycle progression in *Chlamydomonas* and other organisms.

Mutations in mammalian Nek1 are associated with defective ciliogenesis and severe ciliopathies, and signalling to the nucleus may be important for the etiology of these ciliopathies. Here, I show that Nek1 cycles through the nucleus. Nek1 is therefore a candidate to transduce signals between the cilium and nucleus.

Previous work demonstrated that RNAi of the *Chlamydomonas* Nek CNK2 caused a slight increase in flagellar length. I characterized a new *cnk2-1* null mutant and discovered that it contributes to the regulation of flagellar resorption and length control by regulating the rate of flagellar disassembly. My work with cnk2-1 and a mutant strain defective in a second ciliary kinase, lf4-7, revealed that flagellar length is controlled by a feedback system, wherein rates of both flagellar assembly and disassembly are modulated when flagella are too long.

Keywords: Cilia; resorption; ciliogenesis; Nek; cell cycle; *Chlamydomonas*

To my parents,

for your endless encouragement and enthusiasm

and

To Neill,

for everything you do for me

Acknowledgements

I thank my lab mates, past and present: Jaime Kirschner, Courtney Choutka, Fabian Meili, Paul Buckoll, Mette Lethan, and especially Julie Pike, for making life both in and out of the lab fun. I am grateful to many wonderful undergrads over the years who have made outstanding contributions to this work, especially Marianne Schwarz, Kavisha Gunawardane, James Kim, and Stephanie Campbell. I thank Mark White and Melissa Trapp, for introducing me to the Quarmby Lab. Finally, I am incredibly grateful to my mentor, Lynne, for encouraging me to go to grad school, for following through with years of patience, motivation, and encouragement, and for being such an incredible role model for a young female scientist like me.

Table of Contents

List of Figures

List of Acronyms

BB	Basal Body
TZ	Transition Zone
PKD	Polycystic Kidney Disease
NIMA	Never in Mitosis gene A
Nek	NIMA-related kinase
CNK	*Chlamydomonas* NIMA-related Kinase
FA	Flagellar Autotomy
ADF	Acid Deflagellation
FLA	Flagellar Assembly
LF	Long Flagella
PSOS	Proximal Site of Severing
SOFA	Site of Flagellar Autotomy
IFT	Intraflagellar Transport
NPHP	Nephronophthisis
MKS	Meckel Syndrome
SRPS	Short Rib-Polydactyly Syndrome
RP	Retinitis Pigmentosa
CDK	Cyclin-dependent kinase
HDAC	Histone Deacetylase
NES	Nuclear Export Signal
NLS	Nuclear Localization Signal
EGFP	Enhanced Green Fluorescent Protein
DDR	DNA Damage Response
TEM	Transmission Electron Microscopy

1. Introduction

Sections 1.1 and 1.3 of this chapter are adapted and updated from *Cellular Domains*, First Edition, Editor I.R. Nabi, Authors Laura K. Hilton and Lynne M. Quarmby, “Cilia”, Pages 245-266, © 2011 Wiley-Blackwell, with permission.

As first author on this chapter, I conducted an extensive literature review, wrote half of the text, generated/assembled all of the figures, and created a table of >100 known ciliary proteins and their functions. LMQ wrote half of the text and contributed to the conception and design of the figures.

1.1. Cilia: Structure and Function

Cilia are membrane-covered, microtubule-based structures that project from the surface of eukaryotic cells. The earliest eukaryotic cells were ciliated and most extant lineages retain cilia [Richards and Cavalier-Smith, 2005]. The primordial cilium may have functioned both as a processing centre for signal transduction and as a device of motility [Satir et al., 2008; Quarmby and Leroux, 2010]. Some cilia have retained both functions whereas others have become highly specialized. Cilia are sometimes referred to as flagella, especially in the case of the motile flagella of sperm or some protists like *Chlamydomonas*, but should not be confused with the unrelated prokaryotic flagellum.

The fundamental structure of the cilium is conserved, both at the level of proteins and ultrastructurally. Cilia are organized into four defined zones: the basal body, the transition zone, the cilium proper and the tip (Figure 1.1). Each of these regions may be more or less elaborated in different cell types. As this work considers the roles of most of these regions in normal ciliary function, I will begin with a review of our current knowledge of ciliary structure and function.

1.1.1. The Basal Body

Basal bodies (BBs) are the interphase form of centrioles (reviewed in [Marshall, 2008]). Centrioles come in pairs of orthogonally-oriented short cylinders of nine triplet microtubules: The ABC triplet is composed of one complete microtubule (the A-tubule; made of 13 protofilaments) and two partial microtubules (B- and C-tubules with 11 protofilaments each) that "piggy-back" on the A tubule (Figure 1.1, [Marshall and Rosenbaum, 2001]). With each cell cycle centrioles undergo replication: a new "daughter" centriole forms next to each original "mother" centriole [Marshall and Rosenbaum, 2001]. At prophase the original pair separates, with each mother taking its daughter along into one of the daughter cells. The microtubule-driven separation of centrioles during cell division facilitates efficient separation of daughter cell components. During interphase, centrioles dock to the plasma membrane and elaborate into the BBs from which cilia are built [Reiter et al., 2012]. In addition to providing the foundation for cilia, BBs serve as microtubule organizing centres (MTOCs), directly impacting the structure of the cytoplasmic cytoskeleton.

BBs have a structural polarity that has been examined most thoroughly in Chlamydomonas (Figure 1.1; [Ringo, 1967; Johnson and Porter, 1968; Cavalier-Smith, 1974; Holmes and Dutcher, 1989; O'Toole et al., 2003]). In Chlamydomonas, a highly stereotyped system of fibres emanating from the BBs serves to position the two flagella, the nucleus and the eyespot. While the specifics of this fibre system may be unique to the green algae, it is generally the case that the establishment of apical-basal and planar cell polarity are tightly linked to BB placement in metazoans [Marshall, 2010].

In cells that possess only a single cilium, the mother centriole invariably serves as the BB of the cilium [Vorobjev and Chentsov, 1982]. With few exceptions, ciliated cells lose their cilia prior to entry into mitosis, presumably to provide flexibility and precision in centriole separation and positioning during cell division [Parker et al., 2010]. However, in some organisms, such as *C. elegans* and *Drosophila*, only terminally differentiated cells are ciliated. This means that once centrioles become basal bodies, they never return to serve as centrioles again. In these cases, it is not uncommon to find that basal bodies are degenerate and comprised of only singlet or doublet microtubules,

and become less distinguished from the microtubules of the ciliary axoneme [Marshall, 2008].

Key elaborations of the basal body include the transition fibres/distal appendages that facilitate docking of the basal body to the cell membrane [Weiss et al., 1977]. All cilia have these fibres, which are thought to play important roles as scaffolds for the assembly and loading of intraflagellar transport (IFT) complexes (reviewed in [Reiter et al., 2012]). A number of components of the distal appendages have been identified, including CEP123, CEP164, CCDC41, and Odf1, and loss of any of these components interferes with ciliary membrane docking and ciliogenesis [Graser et al., 2007; Singla et al., 2010; Joo et al., 2013; Sillibourne et al., 2013; Tanos et al., 2013].

1.1.2. The Transition Zone

The transition from the basal body ABC triplet microtubules to the AB doublets occurs at the proximal end of the transition zone (TZ; [O'Toole et al., 2003]). Assembly of the TZ on the BB is a key step in the formation of cilia, but to date only two genes have been implicated specifically in this process (UNI1 and UNI2; [Piasecki and Silflow, 2009]. In some cilia, such as the flagella of green algae, the transition zone contains highly stereotyped and distinctive electron-dense structures [Ringo, 1967; O'Toole et al., 2003]. In other cells, such as the primary cilia of mammalian cells, the TZ is more difficult to define ultrastructurally. However, TZs can usually be identified by the presence of Y-link structures that connect the doublet microtubules to the membrane forming a “ciliary necklace” that decorates the transition zone membrane [Gilula and Satir, 1972] The only protein component of these Y-links identified thus far is CEP290 in *Chlamydomonas* [Craige et al., 2010], although many proteins that localize to TZs and have related functions are candidates to be components of the Y-link complex [Reiter et al., 2012].

Perhaps one of the most important functions of the ciliary transition zone is to “gate” the entry and exit of membrane and soluble proteins into the ciliary compartment. In *Chlamydomonas*, loss of CEP290 causes abnormal accumulation or reduction of IFT proteins in flagella, alters the behavior of retrograde IFT, and reduces flagellar levels of PKD2, a membrane protein associated with polycystic kidney disease in humans [Craige et al., 2010]. In *C. elegans* and mammalian cells, transition zone proteins associated

with Meckel syndrome (MKS) and nephronopthisis (NPHP) form a complex that similarly gates the entry and exit of both membrane and soluble ciliary components [Garcia-Gonzalo et al., 2011; Williams et al., 2011]. These components have further roles in ciliogenesis that will be addressed in Section 1.3.

1.1.3. The Cilium

Underlying the membrane, providing structural support and a scaffold for assembly and function, is the axoneme. The axoneme most often consists of nine doublet microtubules that run the length of the cilium. In some cases, such as in *C. elegans* sensory cilia, *Chlamydomonas* gametes, and mammalian olfactory cilia, the doublet microtubules transition to singlets toward the distal end of the cilium [Silverman and Leroux, 2009]. With few exceptions, motile cilia have a central pair of singlet microtubules that participate in regulating motility – these cilia are designated 9+2. Most non-motile cilia, such as mammalian primary cilia, olfactory cilia, and photoreceptor outer segments, lack this central pair and are designated 9+0.

The axoneme of a non-motile 9+0 axoneme is relatively streamlined; the nine outer doublet microtubules are composed of α- and β-tubulin with various post-translational modifications, including acetylated α-tubulin, and glutamylation and glycosylation of both tubulin isoforms [Gaertig and Wloga, 2008]. The 9-fold symmetry established by the basal bodies continues throughout the length of the axoneme.

The motile 9+2 cilium, such as that of *Chlamydomonas*, builds on the basic structure of the 9+0 cilium, but when examined in cross-section a number of important distinguishing features are readily apparent (Figure 1.1). The outer doublets are decorated with rows of inner and outer dyneins, radial spoke complexes, and inter-doublet connections known as the nexin links (e.g., [Nicastro et al., 2006]). Recent tomographic studies have revealed that the nexin link is the Dynein Regulatory Complex, which plays a major role in regulating motility [Heuser et al., 2009]. Ten or more heavy chain dyneins and a multitude of associated proteins form the outer and inner arm dyneins [King and Kamiya, 2009]. Different species of dynein are restricted to specific domains along the length of the flagella [Yagi et al., 2009]. Further spatial organization is found in the distinct identities of each of the nine outer doublet microtubules [Wargo et

al., 2005]. Each singlet microtubule of the central pair has distinct projections, with the C1 tubule having longer projections than the C2 tubule. Rotation of the central pair relative to the outer doublets may regulate the waveform of ciliary beating [Omoto et al., 1999].

The “membrane-matrix” fraction of the cilium includes the lipids and proteins of the ciliary membrane, the IFT (Intra-Flagellar Transport) particles involved in ciliary assembly, and the as yet poorly defined soluble fraction of the compartment [Pazour et al., 2005]. IFT particles are made of two protein complexes that span the space between the outer doublet microtubules and the ciliary membrane (see Section 1.3 Ciliogenesis). Although the ciliary membrane is continuous with the plasma membrane, its lipid and protein composition is distinct [Reiter et al., 2012]. Predominant among ciliary membrane proteins are signaling proteins such as receptors and ion channels [Dunlap, 1977; Berbari et al., 2009]. The mechanisms that maintain the entire ciliary compartment, keeping it distinct from the plasma membrane and the cytoplasm, are active areas of investigation. In addition to the ciliary gate functions of the transition zone (see Section 1.1.2), this selectivity may involve the regulation of ciliary import in a mechanism similar to that of nuclear import [Dishinger et al., 2010; Kee et al., 2012], and include the active export of non-ciliary components by IFT [Lechtreck et al., 2009; Lechtreck et al., 2013].

1.1.4. The Ciliary Tip

The tip of cilia and flagella remains one of the most enigmatic structures within the cilium, and very little is known about its structure, composition, and function. Electron microscopy has demonstrated that, in the motile flagella of *Chlamydomonas* and *Tetrahymena*, the basic structure of the ciliary tip includes a plate and ball structure that anchors the central pair to the ciliary membrane, and a plug inserted into the A tubule of each outer doublet [Dentler, 1980]. The function and composition of these structures is not yet defined. However the flagellar tip must perform three essential functions necessary for maintaining the axoneme: regulating the turnover of flagellar subunits, loading and unloading intraflagellar transport (IFT) cargo, and regulating the activity of microtubule motors that transport IFT cargo along the axoneme [Sloboda, 2005]. The microtubule plus-end binding protein EB1 localizes to the flagellar tip in

Chlamydomonas, and has an essential role in the assembly of primary cilia [Pedersen et al., 2003; Schroder et al., 2007]. It is not yet clear, however, whether this is due to the known microtubule-stabilizing functions of EB1 or some other, yet unknown function at the flagellar tip.

1.1.5. Ciliary Function

Cilia evolved as sensory organelles [Satir et al., 2008; Quarmby and Leroux, 2010]. While all cilia likely perform at least rudimentary signaling functions, some are highly specialized for sensory functions. A common feature of sensory cilia is that receptor molecules are concentrated within the cilium. This can be observed in photoreceptor cells, where the light-detecting machinery is condensed in the cell's outer segment; in olfactory cilia, where the G-protein coupled receptors and associated G-proteins activate cAMP signaling and neuron depolarization from within the cilium; and in neuronal cilia, where particular somatostatin and serotonin receptors localize exclusively to primary cilia [Whitfield, 2004; Berbari et al., 2009]. Thus a number of normal signaling functions are entirely dependent on the presence of a healthy cilium.

A growing number of human diseases are attributed to sensory dysfunction of cilia. For example, the products of cystic kidney disease genes, such as polycystin-1 and -2 (PC1 and PC2; autosomal dominant polycystic kidney disease), fibrocystin (autosomal recessive PKD), and various nephronophthisis (NPHP) proteins, localize to cilia [Nauli and Zhou, 2004]. In response to flow, PC1 and PC2 initiate downstream signaling events that include Ca^{2+} influx and transcriptional changes [Zhou, 2009]. Cilia are also critical for developmental and homeostatic Hedgehog (Hh) and Wnt signaling. In mammals, the Hh receptor PTCH1 and downstream Hh effectors localize to cilia, and proper localization of these components is essential for normal Hh signaling [Goetz and Anderson, 2010]. For Wnt signaling, the presence or absence of a cilium determines whether canonical or non-canonical Wnt signaling is activated [Lai et al., 2009]. The Hippo pathway, an important regulator of cell growth and proliferation, is negatively regulated by the TZ-localized ciliopathy protein NPHP4 [Habbig et al., 2011]. The cilium is the site of localization of PDGF receptor α (PDGFRα), and is essential for cell migration and wound healing [Schneider et al., 2005; Clement et al., 2013]. The roles of

these pathways in tumorigenesis also strongly implicate the cilium as an important organelle in cancer.

Nephronophthisis, the most severe form of juvenile cystic kidney disease, has joined a rapidly expanding group of heterogeneic ciliopathies associated with early development and physiological homeostasis: Bardet-Beidl syndrome (BBS), Meckel syndrome (MKS), Joubert syndrome (JBTS), NPHP, isolated and syndromic forms of retinitis pigmentosa (RP), and a growing number of skeletal disorders (reviewed in [Waters and Beales, 2011]). These disorders are highly pleiotropic, and symptoms can include retinal degeneration, cysts of the kidney and liver, facial malformations, neural tube defects, mental retardation, polydactyly, and obesity. While the disorders are clinically distinct, some genes contribute pathogenic alleles to multiple disorders. For example, nonsense mutations in CEP290 cause MKS, the most severe of these disorders, while hypomorphic mutations can cause RP, NPHP, BBS, or JBTS [Chang et al., 2006; Sayer et al., 2006; Frank et al., 2008; Leitch et al., 2008]. Many of the abnormalities in these disorders have connections to Wnt, Hh, and planar cell polarity signals, all of which have cilia-dependent functions in development [Zaghloul and Katsanis, 2009]. A major hypothesis in the etiology of these ciliopathies, currently, is that they arise from “leakiness” of the ciliary compartment [Reiter et al., 2012]. That is, mutations in BBS, MKS, JBTS, and NPHP disease genes cause things like transmembrane receptors to aberrantly leak into or out of the cilium. For example, mutations in these genes can phenocopy Hedgehog signalling mutants, and the Hh effector SMO fails to efficiently localize to mutant cilia [Garcia-Gonzalo et al., 2011; Chih et al., 2012].

Although all cilia are sensory, some are also motile. Ciliary beating drives the swimming behavior of unicellular organisms, such as Paramecium, *Tetrahymena* and *Chlamydomonas*, colonial and multicellular protists such as *Volvox*, and metazoans like Planaria. The gametes of multicellular organisms, for example mammalian sperm, can be propelled by cilia (often known as flagella in this context). In complex tissues, motile cilia can drive the flow of fluid over a surface. In mammals, this includes respiratory epithelia, ependymal cells lining the brain cavities, and the epithelial cells that drive fluid flow in oviducts. Whether propelling a cell over distance or moving or moving fluids over a surface, the molecular machinery that drives underlying ciliary beat is conserved.

Commensurate with the diversity of motile cilia in the human body, a number of disease states derive directly from the loss of ciliary motility. Among the first ciliopathies defined is Kartagener's Syndrome, also known as Primary Ciliary Dyskinesia (PCD). This disorder is caused by loss of ciliary motility, often due to mutations in axonemal dynein subunits [Leigh et al., 2009]. Predominant symptoms include chronic bronchitis due to inefficient clearance of mucus from the airway. Because motile cilia in the vertebrate embryonic node are essential establishing left-right asymmetry, approximately 50% of PCD patients have the placement of their organs reversed (reviewed in [Lee, 2011]). The motile cilia of ventricular ependymal cells help maintain circulation of cerebrospinal fluid (CSF), without which CSF builds up in the brain causing hydrocephalus.

The coordination of ciliary assembly and disassembly with the cell cycle is also important for normal physiology. I will next review the important connections between cilia and the cell cycle, and the features of the cell cycle that necessitate this coordination.

1.2. Cilia, the Cell Cycle, and the Neks

Most cells lose their cilia prior to cell division by resorption, the tip-down disassembly of the axoneme returning ciliary components to the cell body. This appears to be a requirement for cell cycle progression because the basal bodies serve as centrioles at the spindle poles during cell division, and must therefore be free to migrate throughout the cell (Figure 1.2). In rare examples where the cilia are free to migrate with the basal body, such as meiosis in butterfly sperm, cilia may remain attached to the basal body throughout the cell cycle [Quarmby and Parker, 2005]. However, in *Chlamydomonas* and mammalian cells, the two model systems I have used in this study, ciliary retention is not conducive to cell cycle progression. In *Chlamydomonas,* this is likely due to the presence of a rigid cell wall through which the cilium projects. If the basal bodies remained attached to the flagellum, with its many connections to the plasma membrane, the basal bodies would not be able to facilitate spindle assembly and mitosis. In multicellular organisms, mitotic spindle orientation can be restricted by the need for asymmetric cell division, or for division to occur in a particular plane to maintain

tissue architecture, so disassembling the cilium gives the centrosomes complete freedom to execute these processes with fidelity.

Because the cilium disassembles as the cell divides, the daughter cells must build new cilia. However, while many of the stages of ciliogenesis are well characterized, very little is known about the signals that coordinate ciliogenesis with mitotic exit. In Section 5.3 I will elaborate more on some potential components of this coordination pathway, including Nek1, the subject of Chapter 2.

Chlamydomonas cells divide by a multiple fission mechanism; that is, at each cell division they divide n times to produce 2^n daughter cells, where n is dependent only on the size of the mother cell prior to division. Small cells will divide once to produce only two daughters, while large cells can divide up to four times to produce 16 daughters. *Chlamydomonas* cells easily switch between being phototrophic (using photosynthesis to fix CO_2) or auxotrophic (consuming fixed sources of carbon like acetate), and will continue to grow and divide asynchronously so long as there is a continual supply of light or fixed carbon. When cells are transferred to the dark and deprived of fixed carbon, all cells that have reached a minimum size threshold (commitment size) will divide [Umen and Goodenough, 2001].

Cultures of *Chlamydomonas* cells can be synchronized by alternating exposure to light and dark, with CO_2 as the only available source of carbon [Bisova et al., 2005]. This facilitates observation of ciliary resorption and ciliogenesis events related to the cell cycle [Parker et al., 2010]. In some mammalian tissue culture cell types, synchrony can be similarly achieved by regulating nutrient content. For example, retinal pigment epithelium (RPE) cells can be forced into quiescence by depleting serum from the media, at which point cells will generate cilia. Subsequently restoring serum to the media then causes the cells to synchronously resorb their cilia and divide [Pugacheva et al., 2007].

This synchrony strategy has been employed to test the roles of signalling pathways in coordinating resorption and ciliogenesis with the cell cycle, although still relatively little is known about these processes. One important regulatory step occurs when the cell-cycle kinase aurora A phosphorylates and activates the histone

deacetylase HDAC6, which then goes on to deacetylate ciliary microtubules [Pugacheva et al., 2007; Plotnikova et al., 2012]. Furthermore, siRNA of HDAC6 inhibits ciliary resorption upon growth factor stimulation of cell division [Pugacheva et al., 2007]. The tubulin deacetylation itself is not likely the direct cause of ciliary resorption since acetylated tubulin is not essential for the assembly or maintenance of cilia [Kozminski et al., 1993; Shida et al., 2010]. Thus, tubulin deacetylation appears to play a key role in regulating pre-mitotic ciliary disassembly, possibly by signalling to still-unidentified resorption machinery.

Another component of the pre-mitotic resorption pathway in mammalian cells is the dynein light chain protein Tctex-1, which is required to be phosphorylated and recruited to the TZ for pre-mitotic resorption to proceed [Li et al., 2011]. The centrosomal protein Nde1 interacts with another dynein light chain, LC8, to negatively regulate ciliary length and promote pre-mitotic resorption [Kim et al., 2011]. That both Tctex-1 and Nde1 have roles in regulating cytoplasmic dynein activity may implicate the retrograde IFT motor in pre-mitotic ciliary resorption.

Based on data described below, the Quarmby lab hypothesized that the NIMA-related kinases, or Neks, may have evolved to coordinate cilia with the cell cycle [Quarmby and Mahjoub, 2005]. The Neks are serine/threonine kinases found throughout eukaryotes, defined by similarity of the N-terminal kinase domain to the *Aspergillus* cell cycle kinase NIMA, with highly divergent C-terminal regulatory domains (reviewed in [Fry et al., 2012]). Some members of this family are activated by dimerization and autophosphorylation, but there is no known commonality of activating phosphorylation events or of substrates [Fry et al., 2012]. An extensive phylogenetic analysis of the Nek family revealed that the last common ancestor of all eukaryotes, which was ciliated, possessed at least five Neks [Parker et al., 2007]. Today, organisms that have ciliated cells that re-enter the cell cycle have more representatives of these five clades than those whose ciliated cells are terminally differentiated [Parker et al., 2007]. For example, *Chlamydomonas* and humans have at least one representative of each of these clades, but plants, which have neither cilia nor centrioles, have representatives of only one of these clades [Parker et al., 2007]. This suggests that cells that co-ordinate cilia with the cell cycle maintained a greater diversity of Neks for this purpose, while non-ciliated organisms lost most members of this family as a consequence of the loss of cilia.

The founding member of the Nek family is the lone Nek NIMA (never in mitosis gene A), found in the non-ciliated fungus *Aspergillus nidulans.* It was named for a conditional mutation that prevented cells from entering mitosis at the restrictive temperature [Osmani et al., 1991]. Therefore early studies on Nek family members focused on cell cycle roles for the Neks. For example, Nek2, which belongs to the same clade as *Aspergillus* NIMA, localizes to the centrosome and plays a critical role in centrosome disjunction, the separation of the centrioles that occurs as they duplicate at the onset of mitosis (Reviewed in [Fry et al., 2012]). Nek9, Nek6, and Nek7 participate in a mitotic signalling cascade that is required for normal mitotic spindle assembly [Belham et al., 2003; O'Regan and Fry, 2009]. However, none of these early studies on the roles of Neks in cell cycle considered their functions in cilia.

The first evidence that Neks might play a role in regulating cilia and the cell cycle came when the Quarmby Lab discovered that the causative mutation in a *Chlamydomonas* deflagellation mutant, *fa2*, disrupted a gene encoding a Nek [Mahjoub et al., 2002]. Consistent with the previously described roles for Neks in cell cycle regulation, *fa2* mutants exhibit a delay in G2-M progression that manifests as unusually large cells [Mahjoub et al., 2002]. Coincident with the identification of FA2, a novel hypothesis for the etiology of polycystic kidney disease was emerging. First, it was discovered that the *C. elegans* orthologs of the human polycystins localize to the cilia of male sensory neurons and are required for male mating behaviour [Barr and Sternberg, 1999; Barr et al., 2001]. Shortly thereafter, the causative mutation in the *orpk* mouse model of PKD was identified in the *Tg737* gene, which encodes the mouse ortholog of *Chlamydomonas* IFT88 and is required for ciliogenesis [Pazour et al., 2000]. These data pointed the finger squarely at a role for cilia in the development of cystic kidneys.

At the time, of the seven remaining mouse models for cystic kidneys, one was caused by a mutation in Nek1 and the other in Nek8 [Upadhya et al., 2000; Liu et al., 2002]. The Quarmby lab demonstrated that Nek8 localizes to the proximal half of the cilium, and showed that the causative mutation in the mouse model disrupted its ciliary localization [Mahjoub et al., 2005; Trapp et al., 2008]. These data prompted the screen of a cohort of patients with a severe juvenile cystic kidney disease called nephronophthisis, and identified causative mutations in human Nek8 that disrupt its ciliary localization [Otto et al., 2008]. Furthermore, Nek1 localizes to centrosomes, and

its overexpression inhibits post-mitotic ciliogenesis [Mahjoub et al., 2005; White and Quarmby, 2008]. More recently, causative mutations in Nek1 were identified in the embryonic-lethal skeletal ciliopathy Short Rib-Polydactyly Syndrome (SRPS) [Thiel et al., 2011; Chen et al., 2012a; Chen et al., 2012b; El Hokayem et al., 2012].

Thus far we know little about the cell cycle-related functions of the two ciliopathy Neks, Nek1 and Nek8. However, some of the previously mentioned cell cycle Neks have recently been re-examined for novel ciliary functions. Nek2 has been localized to the distal end of the basal body in ciliated interphase cells, and Nek2 siRNA delays ciliary resorption until after the centrioles have duplicated and separated [Spalluto et al., 2012]. Similarly, Nek7 knock-out mouse embryonic fibroblasts are characterized by reduced overall ciliation and a population of cells with multiple primary cilia [Salem et al., 2010]. It is possible that the effects of Nek2 and Nek7 on cilia are directly responsible for their effects on cell cycle since resorption of the cilium appears to be an important signal for cell cycle progression [Jackson, 2011].

1.3. Ciliogenesis

After a cell has completed mitosis, the first step in creating a new cilium is to dock the basal body at the plasma membrane [Marshall, 2008]. This process typically involves docking of the basal body to a specialized ciliary vesicle, which subsequently fuses to the plasma membrane. The migration of the basal body to the surface of the cell involves intracellular polarity cues, as the cilium forms at the apical surface of the cell. The transition zone and its associated fibres are then assembled and this structure anchors the cilium in its permanent position in the plasma membrane.

As soon as the ciliary vesicle has docked to the centriole (or before it docks to the plasma membrane, if the ciliary vesicle step is omitted) the transition zone and its associated Y-link structures have already begun to form. The docking of the centriole and the formation of the transition zone are regulated by complex interactions between the MKS and NPHP proteins [Reiter et al., 2012]. This interaction network has been defined in both mammalian and *C. elegans* model systems [Garcia-Gonzalo et al., 2011; Sang et al., 2011; Williams et al., 2011; Chih et al., 2012], although little is known of the

functions of these proteins in *Chlamydomonas*. Importantly, the formation of the transition zone establishes the ciliary gate early on in ciliogenesis, separating the cilium from the cell body before axoneme outgrowth even begins [Reiter et al., 2012].

The cilium is assembled via the addition of ciliary components to the distal tip. IFT complexes A and B, assembled from distinct subunits, transport cargo from the cell body towards the tip of the axoneme in IFT "trains" containing multiple A and B complexes (Figure 1.3). Anterograde transport (toward the + end of the ciliary microtubules and the distal tip of the cilium) is mediated by kinesin-2, which is thought to associate with complex B, while retrograde transport is mediated by cytoplasmic dynein in association with complex A [Cole, 2009]. Mutations in complex B subunits obliterate ciliogenesis [Pazour et al., 2000; Brazelton et al., 2001], while mutations in complex A subunits cause accumulation of material at the ciliary tip [Iomini et al., 2009; Jonassen et al., 2012]. In addition to carrying the building blocks of the ciliary axoneme, there is growing evidence that IFT trains also participate in the transport of membrane proteins along the axoneme.

A subset of the proteins related to the ciliopathy BBS also participate in IFT, and are important for membrane biogenesis and membrane protein trafficking in cilia. These BBS proteins assemble into a complex referred to as the BBSome, which includes Rabin8/Sec2p, a guanine nucleotide exchange factor (GEF) for the Rab8/Sec4p vesicular trafficking small GTPase [Nachury et al., 2007]. Since Rab8 is required for ciliogenesis, it has been hypothesized that Rabin8 and Rab8 regulate the docking and fusion of vesicles to the ciliary membrane to create new ciliary membrane (reviewed by [Das and Guo, 2011]). In *C. elegans*, anterograde IFT is mediated by two kinesin motors, kinesin-II and OSM-3, which cooperate to transport IFT complexes in the proximal half of the cilium. The BBSome is important for regulating the association between these two motors [Ou et al., 2005; Pan et al., 2006]. In *Chlamydomonas* and mammals, appears to function as an adaptor between IFT complexes and membrane cargoes, and is required for the import of some membrane proteins into cilia and for the export of others [Lechtreck et al., 2009; Jin et al., 2010; Lechtreck et al., 2013].

At least one IFT protein (IFT20) is involved not only in the ciliary IFT trains, but also in vesicular traffic [Follit et al., 2006]. IFT20 is thought to facilitate the trafficking of

vesicles carrying ciliary membrane proteins from the Golgi to the base of the cilia. These vesicles then fuse with the plasma membrane near the transitional fibres, delivering membrane proteins and lipids to the IFT particles for transport into the cilium. Baldari and Rosenbaum [2010] have proposed that axonemal components might also be targeted to the cilium via association with cilia-destined vesicles.

Ciliogenesis also involves new synthesis of many ciliary proteins, including tubulin, and axonemal dyneins [Lefebvre et al., 1978]. Recent RNAseq analysis identified 1850 genes that are upregulated during flagellar regeneration in *Chlamydomonas* [Albee et al., 2013]. In metazoans, the expression of ciliary genes is coordinated by the activity of RFX transcription factors, which bind to a highly sterotyped site in the promoter region of the majority of ciliary genes [Swoboda et al., 2000; Chen et al., 2006]. A subset of genes that are required for the assembly and function of motile cilia are regulated by the FOXJ1 transcription factor [Yu et al., 2008]. However, *Chlamydomonas* and other bikonts lack either RFX or FOXJ1 homologs, and very little is known about the promoter sequences that regulate ciliary gene transcription [Chu et al., 2010; Piasecki et al., 2010]. Nonetheless, transcriptional upregulation of ciliary genes is likely one of the key events that coordinates ciliogenesis with cell cycle exit.

1.4. Ciliary Resorption and Deflagellation

Ciliary resorption occurs in most organisms prior to mitosis, and, in *Chlamydomonas*, in response to growth on solid agar plates. Much less is known about the mechanisms that govern ciliary resorption than ciliogenesis. Given the dynamic nature of ciliary microtubules, at the very least we can say that resorption occurs when the rate of disassembly exceeds the rate of assembly. The *Chlamydomonas* temperature sensitive *fla10-1* mutant carries a point mutation in the motor domain of the anterograde IFT kinesin motor, and flagellar assembly halts at the restrictive temperature, causing flagella to gradually resorb [Kozminski et al., 1995; Iomini et al., 2001; Marshall and Rosenbaum, 2001; Marshall et al., 2005]. The drug ciliabrevin similarly causes anterograde IFT reduction leading to resorption [Engel et al., 2011]. Although it has been assumed that retrograde IFT was required for ciliary resorption by returning disassembled ciliary components to the cell body, this may not actually be the

case. Temperature sensitive *Chlamydomonas* mutants with defects in IFT B complex particles gradually resorb at the restrictive temperature, and accumulate large amounts of IFT material and other ciliary components in a large bulge at the tip of the short flagella [Iomini et al., 2009]. This observation indicates that neither retrograde IFT, nor the ability to clear ciliary components from the ciliary tip, are required to shorten flagella. Another *Chlamydomonas* mutant, *dhc1b-3*, which carries a temperature sensitive mutation in the motor domain of the retrograde IFT dynein, can maintain full-length flagella for up to 24 hours at the restrictive temperature, and appears only to have a defect in its ability to regenerate flagella following mitosis [Engel et al., 2012]. Therefore retrograde IFT may participate in the return of ciliary components to the cell body, but it is not required for the disassembly of the axoneme that leads to ciliary resorption. The mechanisms that do facilitate ciliary resorption remain elusive.

In rare cases, deflagellation is used as an alternative to resorption prior to mitosis, but in *Chlamydomonas* and the cells lining the human respiratory tract deflagellation occurs in response to stress (reviewed in [Quarmby, 2004],[Coggins et al., 1980]). Most of what we know about deflagellation has been discovered in *Chlamydomonas*. The deflagellation response can be activated by acidifying the media with a weak organic acid, such as acetic acid, that can permeate the cell membrane and acidify the cytoplasm [Hartzell et al., 1993]. This drop in pH triggers an influx of Ca2+ from the media, which activates the severing machinery at the site of flagellar autotomy (SOFA) at the distal end of the transition zone [Lewin and Lee, 1985; Quarmby and Hartzell, 1994]. Deflagellation can also be induced by permeabilizing the cells in the presence of calcium [Lewin and Burrascano, 1983]. Upon severing of the microtubule axoneme, the flagellar membrane pinches off to seal the membrane over the transition zone, and the flagellum is shed into the environment. Forward genetics approaches have identified mutations in two genes that are required for **a**cid-induced **d**e**f**lagellation, *adf1* and *adf2*, but these mutants all deflagellate normally when permeabilized in the presence of calcium, indicating that the severing machinery is intact ([Finst et al., 1998], F. Meili, P. Buckoll, M. Lethan, and J. Pike, unpublished data). In contrast, mutations in one of the two known flagellar autotomy (FA) genes prevent deflagellation in response to any known stimulus [Finst et al., 2000; Mahjoub et al., 2002]. FA1 is a scaffolding protein with a Ca2+/CaM binding motif [Finst et al., 2000], and FA2 is a kinase from the NIMA-

related kinase family (see Section 1.2. Cilia, the Cell Cycle, and the Neks, [Mahjoub et al., 2002]). Both FA1 and FA2 localize to the SOFA [Mahjoub et al., 2004; Parker, 2008].

Although resorption and deflagellation seem like dramatically different processes, there is good evidence that they share commonalities. Parker et al. [2003] made a number of observations that suggest a connection. First, *fla10-1* mutants don't just resorb at the restrictive temperature, they often deflagellate instead, indicating that the severing machinery can be activated by the loss of IFT. Second, *fla10-1 fa* double mutants, which are incapable of deflagellation, resorb more slowly at the restrictive temperature than *fla10-1* single mutants. Remarkably, this suggests that the severing machinery contributes to flagellar resorption, possibly by removing axonemal components at the base of the flagellum. Third, *fa1* and *fa2* mutants, when treated with the same pH shock stimulus that induces deflagellation in wild-type cells, resorb their flagella. This indicates that the signal for deflagellation can be relayed into a signal for resorption when deflagellation is not possible. Together, these data indicate that there may be overlap in the signalling pathways and/or the machinery that control both flagellar resorption and deflagellation. In this study, I will also address a role for axonemal severing in pre-mitotic resorption in *Chlamydomonas* (see Chapter 3).

1.5. Ciliary Length Control

As I have mentioned already, ciliary microtubules are dynamic, although they behave somewhat differently from cytoplasmic microtubules. First, isolated *Chlamydomonas* flagellar microtubules are stable in solution for extended periods of time and do not undergo dramatic microtubule catastrophes the way isolated cytoplasmic microtubules do. Second, microtubule depolymerizing drugs like colchicine prevent the elongation of flagellar microtubules and are often used to inhibit ciliogenesis, but do not cause full-length flagella to resorb [Rosenbaum et al., 1969]. These observations initially led to the conclusion that ciliary microtubules are highly stable *in vivo* and undergo very little turnover [Tilney and Gibbins, 1968].

However, a number of observations confirm that ciliary microtubules are, in fact, dynamic. First, *in vivo* ^{35}S labeling studies reveal that both the microtubule axoneme and

its associated appendages are undergoing constant turnover, even at steady-state length [Song and Dentler, 2001]. Second, experiments that measure the incorporation of tagged tubulin subunits into otherwise unlabelled axonemes show that tubulin turnover is ongoing in steady-state length flagella, but only at the distal tips [Marshall and Rosenbaum, 2001; Hao et al., 2011]. This last point especially suggests that, at steady state length, flagella are undergoing constant disassembly that is balanced by constant assembly. This has been coined the balance point model, and it explains how dynamic ciliary microtubules manage to maintain a steady-state length, which then becomes a function of the rates of assembly and disassembly. When the rate of assembly exceeds the rate of disassembly, cilia will elongate, and when disassembly exceeds assembly they will shorten.

The question of length control then becomes a question of how the rates of assembly and disassembly are regulated. There are abundant data from experiments using *Chlamydomonas* which demonstrate that the rate of flagellar assembly is inversely proportional to the length of the flagella, which may be due to the fact that axonemal components must be transported by IFT to the ciliary tip for assembly [Marshall and Rosenbaum, 2001; Marshall et al., 2005; Engel et al., 2009]. As the flagellum elongates, the time it takes IFT to transport cargo to the tip increases, so the rate of delivery decreases. This is further supported by the observation that the rate of injection of IFT particles into the flagellum decreases as flagella elongate [Ludington et al., 2013]. Unlike assembly, the rate of disassembly appears to be constant and length-independent, as demonstrated by the linear rate of resorption in *fla10-1* mutant flagella at the restrictive temperature [Marshall et al., 2005]. Based on these observations, steady-state ciliary length could be achieved when the length-dependent rate of assembly matches the length-independent rate of disassembly, and active regulation of these rates would not be required [Wemmer and Marshall, 2007].

However, the existence of mutants that produce long cilia in *Chlamydomonas* and other organisms suggests that the rates of assembly and disassembly may be under more control than is implied by the balance point model. For example, *Chlamydomonas lf4* mutants can have flagella almost four times longer than those of wild-type cells [Asleson and Lefebvre, 1998; Berman et al., 2003], and mutations in the mouse and human homologs of *LF4* cause long cilia and retinal degeneration [Omori et al., 2010;

Ozgül et al., 2011; Tucker et al., 2011]. Recently, the length defect in *lf4* mutant flagella was attributed to an accelerated rate of assembly, apparent from the increased rate of injection of IFT particles into the flagellum [Ludington et al., 2013]. These data suggest that the wild-type function of the LF4 protein, which is a kinase, is to inhibit the rate of assembly, supporting my hypothesis that flagellar length is actively regulated by feedback control of the rates of assembly and disassembly (see Chapter 4). My work places another *Chlamydomonas* kinase, CNK2, in a signalling pathway that actively regulates rates of assembly and disassembly to control flagellar length.

1.6. Research aims

In this study, I have examined the events of pre-mitotic resorption of flagella, and the roles of two Neks in ciliogenesis, ciliary resorption, and length control. In Chapter 2, I use mouse tissue culture cell lines to examine the localization of a kinase required for ciliogenesis, Nek1. Although full-length Nek1 localizes to centrosomes [White and Quarmby, 2008], sequence analysis predicted that it possesses nuclear localization and nuclear export signals. When cells expressing EGFP-Nek1 were treated with Leptomycin B, which blocks CRM1-dependent nuclear export, Nek1 became trapped in the nucleus, indicating that the protein continually cycles in and out of the nucleus. I went on to functionally define one of at least two nuclear import signals. My data indicate that Nek1 may transduce signals between the cilium and the nucleus to control ciliogenesis.

In Chapter 3, I used *Chlamydomonas* cells to characterize a novel ciliary severing event that occurs during pre-mitotic resorption. Jeremy Parker and Qasim Rasi observed by immunofluorescence that two acetylated tubulin foci remain embedded in the *Chlamydomonas* mother cell wall after cell division is completed. Dennis Diener of the Rosenbaum lab used electron microscopy to identify these “flagellar remnants” as degenerated transition zones. I performed live-cell imaging of pre-mitotic resorption, and observed these flagellar remnants left behind in the mother cell wall once resorption was complete and cortical rotation had begun. We hypothesize that pre-mitotic resorption culminates in a severing event that frees the basal body from the transition zone, and that this may be essential for cell cycle progression so that the basal bodies may migrate freely to act as spindle poles in mitosis.

In Chapter 4, I characterize a novel *Chlamydomonas* mutant strain with a null mutation in the gene encoding a NIMA-related kinase, CNK2. Previous work by Quarmby lab graduate student Brian Bradley demonstrated that CNK2 localizes to flagella, and that RNAi of CNK2 causes slightly long flagella while overexpression causes slightly short flagella [Bradley and Quarmby, 2005]. Similar to the RNAi results, I find that the *cnk2-1* cells have slightly long flagella, and are defective in flagellar resorption in response to a number of stimuli that cause resorption in wild-type cells. My data indicate that both the subtle length phenotype and the resorption defect can be attributed to a reduced rate of disassembly in the *cnk2-1* mutant. Strikingly, we uncovered a synthetic long flagella phenotype of *cnk2-1 lf4-7* double mutants, whose flagella are much longer those of either single mutant. I concluded that this occurs because of a decreased rate of disassembly caused by *cnk2-1* and an increased rate of assembly caused by *lf4-7*. I demonstrate that the rates of both flagellar assembly and disassembly are regulated in response to longer-than-optimal flagellar length, revealing for the first time the presence of a feedback control loop that maintains wild-type flagellar length.

1.7. Figures

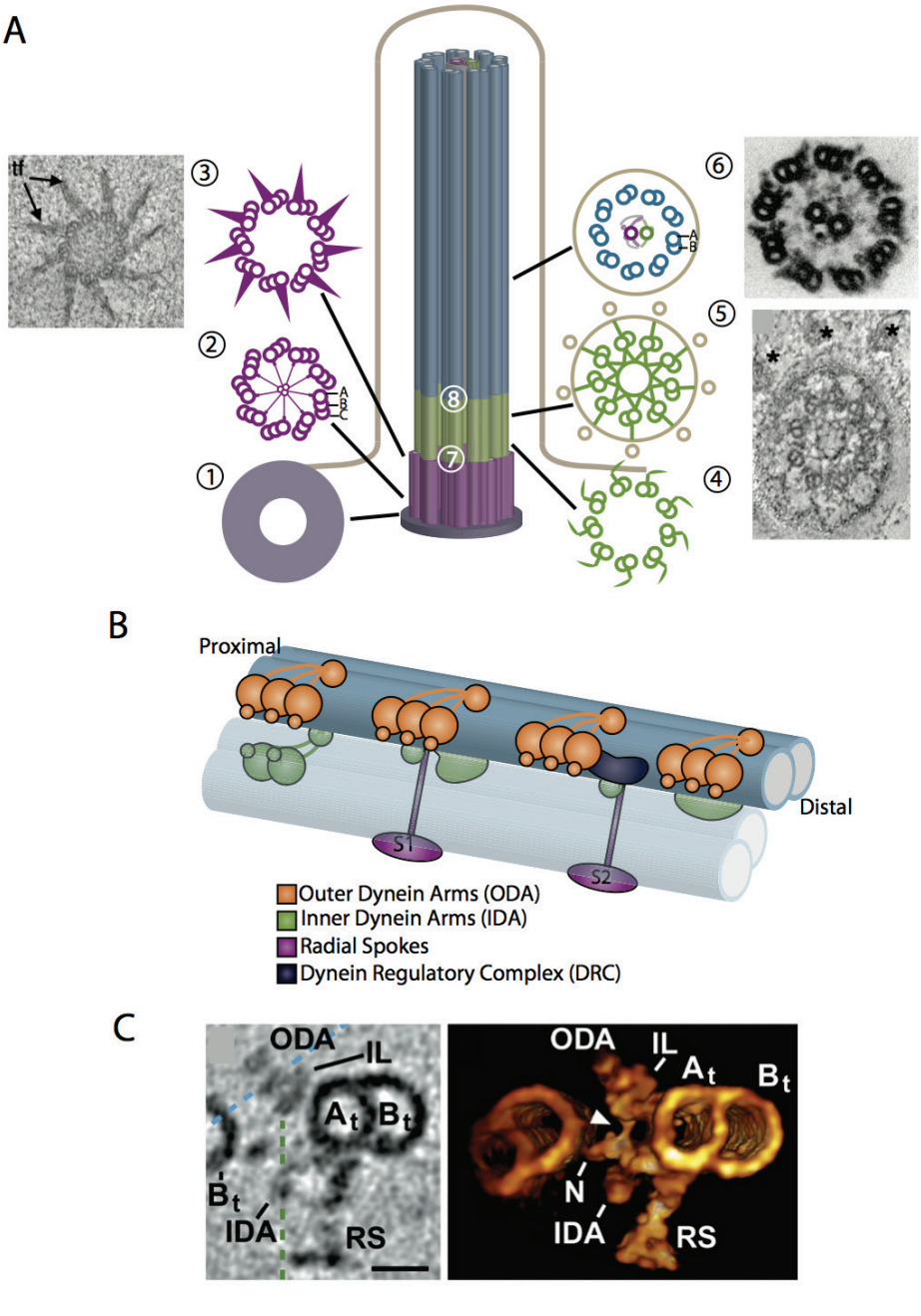
A
tf
③
②
①
⑧
⑦
⑥
⑤
④
B
Proximal
Distal
S1
S2
Outer Dynein Arms (ODA)
Inner Dynein Arms (IDA)
Radial Spokes
Dynein Regulatory Complex (DRC)
C
ODA
IL
At
Bt
IDA
RS
N

Figure 1.1. Anatomy of a cilium.
This diagram of a cilium including cross-sections is based on data from *Chlamydomonas*. (A) A ciliary basal body (BB; pink), transition zone (TZ; green), and axoneme (blue) are shown, with cross sections through each region shown on either side. Adapted from O'Toole et al. [2003]. (1) A ring of amorphous material at the proximal end of the BB. (2) The proximal end of the BB has a "cartwheel" structure at its center with nine triplet microtubule (MT) "blades" surrounding it. The A, B, and C tubules are indicated. (3) Transition fibres that anchor the BB to the plasma membrane are shown as triangular projections from the blades. An electron tomography (ET) image of this section of the BB is shown adjacent. From O'Toole et al., [2003] with permission. (4) Transition fibres from the distal end of the BB continue through the proximal end of the transition zone (TZ). (5) Stellate fibres within the MT ring of the TZ, and the termination of the transition fibres in pores surrounding the TZ. An ET image of this section of the TZ is shown adjacent; asterisks indicate the pores in the surrounding ciliary membrane From O'Toole et al., [2003] with permission. (6) The arrangement of 9 outer doublet MTs and the central pair are shown, with the A and B tubules indicated. A TEM image of an axoneme is shown adjacent, with central pair and outer doublet projections visible Reprinted from Sakato and King [2004] with permission from Elsevier. (7) The recently-identified proximal site of severing where the TZ severs from the BB before mitosis. (8) The site of flagellar autotomy (SOFA) where the axoneme severs during the deflagellation stress response. (B) A simplified representation of the 96 nm repeat pattern in which inner and outer arm dyneins and radial spokes are arrayed. (C) Cryo-ET image and volume rendering of 160 averaged sections through two adjacent outer doublet MTs. RS – Radial Spoke; ODA – outer dynein arm; IDA – inner dynein arm; N – Nexin link/DRC; IL – Dynein tail complex (from Nicastro et al., [2006]. Reprinted with permission from AAAS).Figure 1.1 reprinted from Cellular Domains, First Edition, Editor I.R. Nabi, Authors Laura K. Hilton and Lynne M. Quarmby, "Cilia", Pages 245-266. © 2011 Wiley-Blackwell, with permission.

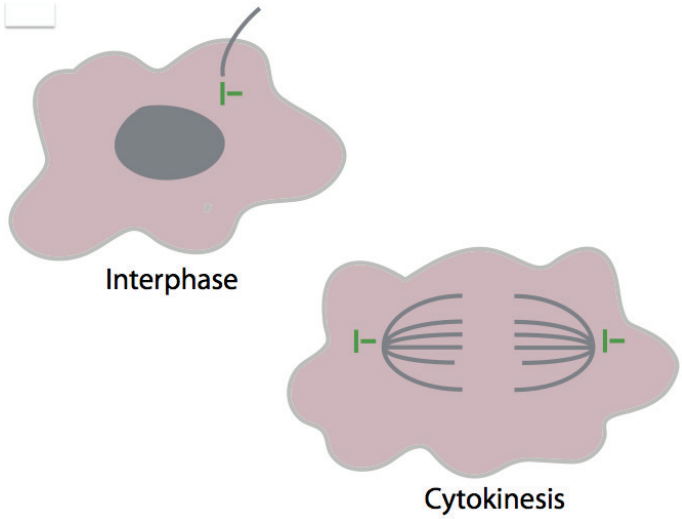

Figure 1.2. Cilia and the Cell Cycle
During interphase, the centrosome is located adjacent to the plasma membrane of the cell and the mother centriole becomes the BB that nucleates a cilium. Before cell division, the cilium is resorbed. The centrioles then duplicate and participate in cytokinesis. After cell division, new cilia are built from the older of the two centrioles. Reprinted from Cellular Domains, First Edition, Editor I.R. Nabi, Authors Laura K. Hilton and Lynne M. Quarmby, “Cilia”, Pages 245-266. © 2011 Wiley-Blackwell, with permission.

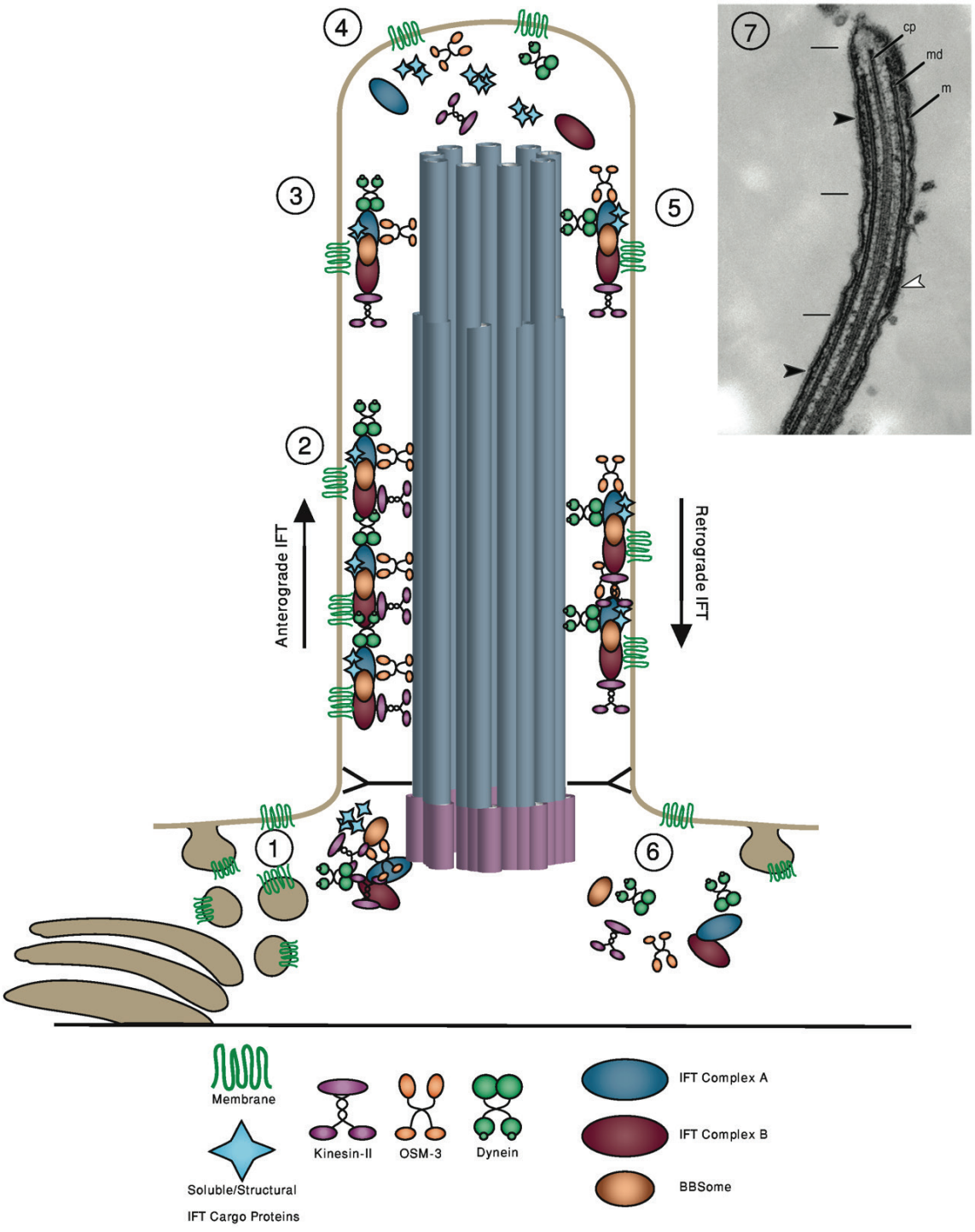
4
3
5
2
1
6
7
cp
md
m
Anterograde IFT
Retrograde IFT
Membrane
Soluble/Structural
IFT Cargo Proteins
Kinesin-II
OSM-3
Dynein
IFT Complex A
IFT Complex B
BBSome

Figure 1.3. Intraflagellar Transport.
(1) IFT components accumulate at the basal body and are assembled on the transition fibres. Membrane proteins arrive at the base of the cilium from the Golgi via vesicular transport pathways. (2) IFT particles transport cargo along the ciliary axoneme in IFT trains. In certain species, such as C. elegans, OSM-3 supplements Kinesin-II driven anterograde transport. (3) In these species, OSM-3 is the sole molecular motor responsible for driving anterograde transport along the distal singular MTs. (4) At the distal tip of the cilium, IFT complexes disassemble, and structural components may be added at the tip of the axoneme. As ciliary components are turned over, IFT complexes are reassembled for transport back to the cell body. (5) IFT trains transport ciliary components using cytoplasmic dynein as the exclusive molecular motor for retrograde transport. (6) Retrograde IFT complexes are disassembled at the BB, and membrane components are degraded using the endosomal recycling pathway. (7) TEM of Chlamydomonas flagella showing three IFT trains. Black arrowheads indicate the longer anterograde trains and the white arrowhead indicates a shorter retrograde train cp: central pair; md: microtubule doublet; m: membrane. (© Pigino et al., 2009. Originally published in The Journal of Cell Biology. 187: 135-148). This complete figure is reprinted from Cellular Domains, First Edition, Editor I.R. Nabi, Authors Laura K. Hilton and Lynne M. Quarmby, “Cilia”, Pages 245-266. © 2011 Wiley-Blackwell, with permission.

2. The NIMA-related kinase NEK1 cycles through the nucleus

Laura K. Hilton, Mark C. White, and Lynne M. Quarmby

Department of Molecular Biology and Biochemistry, Simon Fraser University, Burnaby, British Columbia, Canada, V5A 1S6

Reprinted from Biochemical and Biophysical Research Communications, Vol. 389, Pages 52-56, © 2009, with permission from Elsevier.

As the first author, I generated, expressed, and localized the 1-321 Nek1 sub-clone, interpreted all the data, and wrote the manuscript. MCW conducted the remainder of the experiments and helped with data analysis. LMQ was involved with the conception and design of the experiments, data analysis, and writing of the manuscript.

2.1. Abstract

Mutations in *NEK1* in mice are causal for cystic kidneys, and model the ciliopathy polycystic kidney disease caused by abnormal ciliary structure or signaling. NEK1 has previously been shown to localize near centrosomes and to play a role in centrosomal stability and ciliogenesis. Recent data suggest that the etiology of kidney cysts involves aberrant signaling from the primary cilium to the nucleus. Here we demonstrate that NEK1 contains functional nuclear localization signals, is exported from the nucleus via a nuclear export signal-dependent pathway and that the protein cycles through the nucleus. Our data suggest that NEK1 is a candidate to transduce messages from the ciliary basal-body region to the regulation of nuclear gene expression.

2.2. Introduction

NEK1 is a member of the NIMA-related kinase (Nek) family, members of which are defined by similarity in their kinase domains to that of the essential *Aspergillus nidulans* cell cycle kinase NIMA (never in mitosis A) [Letwin et al., 1992; Quarmby and Mahjoub, 2005]. Two mouse models for polycystic kidney disease (PKD), *kat* and *kat*^{2J}, are caused by mutations in NEK1, and therefore implicate NEK1 in the etiology of PKD [Upadhya et al., 2000]. The *kat* strains present a recessive, pleiotropic phenotype that includes progressive cystic kidneys, runting, facial dysmorphism, hydrocephalus, and anemia [Janaswami et al., 1997; Vogler et al., 1999; Upadhya et al., 2000]. Despite extensive phenotypic characterization, little is known of the cellular functions of NEK1.

NEK1 is found associated with centrosomes, where it remains throughout the cell cycle [Mahjoub et al., 2005; Shalom et al., 2008; White and Quarmby, 2008]. It has recently been implicated in the maintenance of centrosomes and in the formation of the primary cilium [Evangelista et al., 2008; Shalom et al., 2008; White and Quarmby, 2008]. It remains unknown, however, whether defects in NEK1 cause cystic kidneys directly, by failing to relay a particular signal to the cell; or indirectly, by interfering with the structure of the primary cilium.

Recent evidence indicates that signals for both proliferation and differentiation are received by the primary cilium [Caspary et al., 2007; Christensen et al., 2007]; therefore it is not surprising that some cystogenic proteins are active in both cilium and nucleus. ADPKD is caused by mutations in either gene encoding polycystin-1 (PC1) or polycystin-2 (PC2), large membrane proteins that localize to the primary cilia in renal epithelia (reviewed in [Zhou, 2009]). In response to mechanical stimuli proteolytic cleavage releases the C-terminal tail of PC1, which then translocates to the nucleus to alter gene expression independently or in association with the transcription factor STAT-6 [Chauvet et al., 2004; Low et al., 2006]. PC2 helps stimulate this cleavage [Bertuccio et al., 2009]; thus the polycystins function co-operatively in altering gene expression through cilium-to-nucleus signaling. ARPKD is caused by mutations in the gene encoding fibrocystin, another membrane protein that localizes to cilia, which similarly undergoes proteolytic cleavage in response to Ca^{2+} signals, and the released C-terminal tail translocates to the nucleus [Hiesberger et al., 2006]. Similarly, mutations in inversin

cause an autosomal recessive cystic kidney disease (NPHP2, [Otto et al., 2003]) and inversin affects nuclear signaling through the Wnt pathway [Simons et al., 2005].

The presence of one or more predicted nuclear localization signals (NLSs) and nuclear export signals (NESs) in NEK1 suggest that NEK1 might also be directly involved in communicating a change in state to the transcriptional machinery of the cell. Dysfunctional communication with the nucleus is likely to be an important aspect of cystogenesis, accounting for changes in proliferation and differentiation status [Simons et al., 2005; Low et al., 2006]. Therefore, we set out to test whether NEK1 is capable of translocating to the nucleus, and if so, to define the functional nuclear transit signals. In this paper we demonstrate that endogenous NEK1 cycles through the nucleus, indicating that NEK1 may be capable of carrying signals between the primary cilium and the nucleus. In addition, we report the functional definition of two NLSs and the use of an NES-dependent nuclear export pathway.

2.3. Materials and Methods

2.3.1. Cell lines and cell culture

Inner medullary collecting duct (IMCD3) murine renal epithelial cells were maintained in a 1:1 mixture of DMEM and Ham's F12 medium supplemented with 10% fetal bovine serum (DMEM-F12 (+), Invitrogen, Carlsbad, CA). All experiments were carried out on cells that had been passaged fewer than ten times, and grown to confluence on coverslips. Transient transfections were carried out with 4 µg of plasmid and Lipofectamine 2000 (Invitrogen) in OPTI-MEM reduced-serum media according to the manufacturer's protocol. After 6 hours, cells were washed with PBS and incubated in DMEM-F12 (+) overnight. For nuclear export experiments, cells were treated with either 5ng/µl Leptomycin B or a solvent control for six hours, 24 hours post-transfection.

2.3.2. Antibodies and Microscopy

For microscopy, cells grown on coverslips were fixed with methanol at -20^{o}C for ten minutes and rehydrated in PBS. If immunofluorescence was required, coverslips

were incubated with primary antibody diluted in PBS for one hour, and then washed twice for 15 minutes in PBS. This was repeated for secondary antibody. Coverslips were then incubated with 1 µg/mL 4',6-diamidino-2-phenylindole (DAPI) for 10 minutes at room-temperature to stain nuclei. Coverslips were mounted with MOWIOL 4-88 (Calbiochem, San Diego, CA). Microscopy was carried out on the Delta Vision system (Applied Precision, Issaquah, WA) as described previously [Cokol et al., 2000; Mahjoub et al., 2004]. By visual inspection, we considered the distribution of NEK1 signal to be "nuclear/cytoplasmic" when there was a clear signal in both compartments; a substantially greater distribution of NEK1 signal to either the nucleus or cytoplasm was counted as "nuclear" or "cytoplasmic", respectively. At least 300 cells were scored for each construct. Primary antibodies include mouse monoclonal anti-myc (Clone 9E10; 1:2000; Clontech, Palo Alto, CA) and rabbit polyclonal anti-NEK1 (1:100; from Dr. Y. Chen, University of Texas Health Science Center, San Antonio; [Polci et al., 2004]). Secondary antibodies include Alexa Fluor 488-conjugated goat anti-rabbit IgG (1:500; Molecular Probes, Eugene, OR) and Alexa Fluor 594-conjugated goat anti-mouse IgG (1:2000; Molecular Probes).

2.3.3. Molecular Constructs

Sequence representing the full-length NEK1 cDNA (GenBank accession no. AY850065) was cloned into the SacI-SalI sites of pEGFP-C2 (Clontech), and truncations were made using standard molecular biology techniques. To generate myc-NEK1, the full-length NEK1 sequence was cloned into the Sal1 site of the pCMV-myc plasmid.

2.4. Results

2.4.1. NEK1 cycles through the nucleus in IMCD3 cells

Although two classical NLSs have been previously predicted for NEK1 (364KKRR367, 580RKRK583) using the PredictNLS tool (available through the PredictProtein server at https://www.predictprotein.org/ [Cokol et al., 2000]), mutating one or both of these NLSs does not interfere with the nuclear localization of C-terminally truncated NEK1 (our unpublished data; [Feige et al., 2006]). These data indicated that

an additional sequence participated in the transport of NEK1 into the nucleus, either an NLS or a region that interacted with another protein that itself had an NLS. We re-examined the NEK1 sequence for new NLS predictions using the updated PredictNLS database and uncovered a single bipartite predicted NLS between residues 355-378 (NLS in Figure 2.1). The NES prediction tool NetNES v1.1 (http://www.cbs.dtu.dk/services/NetNES/; [la Cour et al., 2004]) predicts two leucine-rich NESs for NEK1: NES1 at residues 764-774, and NES2 at residues 1131-1138 (NES1 and NES2 in Figure 1).

While full-length NEK1 is predominantly cytoplasmic, the presence of multiple predicted NLS and NES in NEK1 led us to investigate the nuclear translocation of NEK1. The nuclear export-blocking drug Leptomycin B (LMB) binds to CRM1, an essential factor in NES-dependent nuclear export in mammalian cells, and prevents the interaction of CRM1 with NES-containing proteins [Kudo et al., 1998]. To test the effects of LMB on the sub-cellular localization of NEK1, we transfected IMCD3 cells with myc-NEK1 and treated cells with LMB for 6 hours beginning 24 hours post-transfection. In cells treated with LMB, but not in control cells, full-length myc-NEK1 accumulates in the nucleus (Figure 2.2, A and B). When untransfected cells are treated with LMB, endogenous NEK1 also accumulates in the nucleus (Figure 2.2, C and D). This indicates that NEK1 has at least one functional NES that is blocked by LMB.

In attempts to identify the NES, we mutated both predicted NESs individually and together (LQL772AQA; LRL1134AQA). These mutations did not cause nuclear accumulation of the protein (data not shown). Several different scenarios could explain these negative results. It is possible that the mutations disrupted protein structure in such a way as to interfere with import. Alternatively, the functional NES may be cryptic. Finally, it is possible that NEK1 exits the nucleus via interaction with another NES-bearing protein.

The LMB experiments demonstrated the existence of NES-dependent nuclear export of NEK1. However, in tissue culture cells we always observe a predominantly cytoplasmic localization of endogenous NEK1. In order to obtain the result that we did in the LMB experiment, NEK1 must be cycling through the nucleus, accumulating in the

nucleus only when export is blocked. This implies the existence of functional NLSs in NEK1.

2.4.2. NEK1 has at least two functional NLSs

To define functional NLSs within NEK1, we generated a series of EGFP-tagged NEK1 truncations (Figure 2.1) and transfected them into IMCD3 cells. EGFP alone distributes to both nucleus and cytoplasm (Figure 2.3 A) because it is smaller than the passive diffusion threshold of the nuclear pore complex [Keminer and Peters, 1999]. The EGFP-tagged kinase domain (residues 1-258) is predominantly cytoplasmic (Figure 2.3 B), while EGFP-NEK1 1-321, 1-352 and 1-686 are predominantly nuclear (Figure 2.3 C, D and E). The EGFP-tagged basic domain (residues 258-353) and the EGFP-coiled-coil domain (residues 353-686) are also predominantly nuclear, indicating that there is a functional NLS in both the basic and the coiled-coil domains (Figure 2.3 F and G). The ability of the 1-321 construct to localize to the nucleus indicates that the functional NLS within the basic domain lies within residues 258-321. However, no stretches of basic amino acids occur within this region and consequently it is clear that although this region can direct nuclear import, no canonical NLS exists within this sequence.

We proceeded to test functionality of the predicted bipartite NLS, which is in the coiled-coil domain, by mutating two stretches of basic amino acids in the NLS, KK357AG and KR366AG, in the 353-686 construct. As predicted, nuclear localization of this construct is severely disrupted (Figure 2.3 H). Including the basic domain in NLS-mutated EGFP-NEK1 (residues 258-686, Figure 2.3 I) rescues nuclear localization of the construct. Taken together, these data confirm that the predicted NLS is functional, and that the basic domain harbors a second cryptic NLS. Our data demonstrate that each of the two NLSs is sufficient on its own to direct nuclear localization of NEK1.

2.5. Discussion

We have established the presence of two functional NLSs and the nuclear export of NEK1 via an NES-dependent pathway. Only one NLS, located at the beginning of the coiled-coil region of NEK1, functions as predicted on the basis of sequence. A second,

cryptic NLS lies within the basic region C-terminal to the kinase domain. The NES-dependent export of NEK1 is confirmed through experiments with leptomycin-B (LMB), which causes both transiently expressed myc-NEK1 and endogenous NEK1 to accumulate in the nucleus (Figure 2.3). Furthermore, the LMB experiments demonstrate that endogenous NEK1 cycles through the nucleus, making it an excellent candidate for conveying signals between the primary cilium and the nucleus.

While NEK1 is continually cycling through the nucleus, it remains unknown what physiological signals will cause the protein to accumulate in the nucleus. A recent report demonstrated that NEK1 translocates to the nucleus in response to nuclear DNA damage [Chen et al., 2008]; however, the upstream signals that regulate this activity with respect to functional nuclear transit signals are unknown. Recent reports have identified three phosphorylated residues on mouse NEK1, which could help regulate the activity of NEK1 nuclear transit signals [Ballif et al., 2004; Zanivan et al., 2008]. Aberrant regulation of NEK1 nuclear localization and its activity within the nucleus could contribute to cystogenesis.

We have recently shown that NEK1 affects ciliogenesis [White and Quarmby, 2008]. In the current paper we have shown that NEK1 cycles through the nucleus. NEK1 therefore may be one of a cohort of cystogenic proteins that affects both ciliary and nuclear signaling. Our data add support to the idea that defective ciliary signaling is transduced into aberrant regulation of nuclear gene expression, which may be an important component of the etiology of kidney cysts.

2.6. Acknowledgements

This work was funded by an operating grant from the Canadian Institutes of Health Research (MOP-37861) to L.M.Q. We thank Michel Leroux and his laboratory members for use of their tissue culture facilities. We are grateful to Yumay Chen for the anti-NEK1 antibody. The intellectual engagement of members of the Quarmby lab is also appreciated.

2.7. Figures

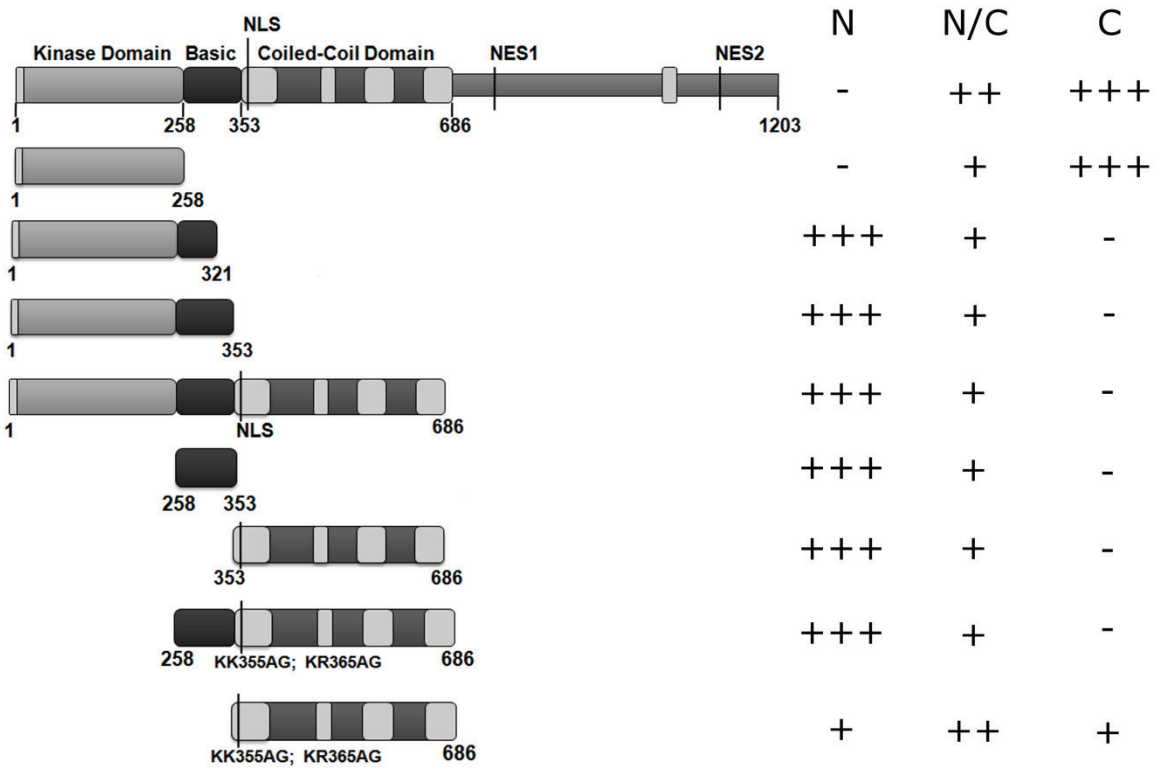

Figure 2.1. Predominant Localization of Different NEK1 Constructs.
This schematic shows the different domains of the NEK1 protein, and the distribution of predicted nuclear translocation signals. The various NEK1 truncations shown were expressed as GFP fusions in IMCD3 cells, and their predominant localization is indicated as nuclear (N), cytoplasmic (C), or both (N/C). +++: strong localization; ++: moderate localization; +: weak localization; -: no localization.

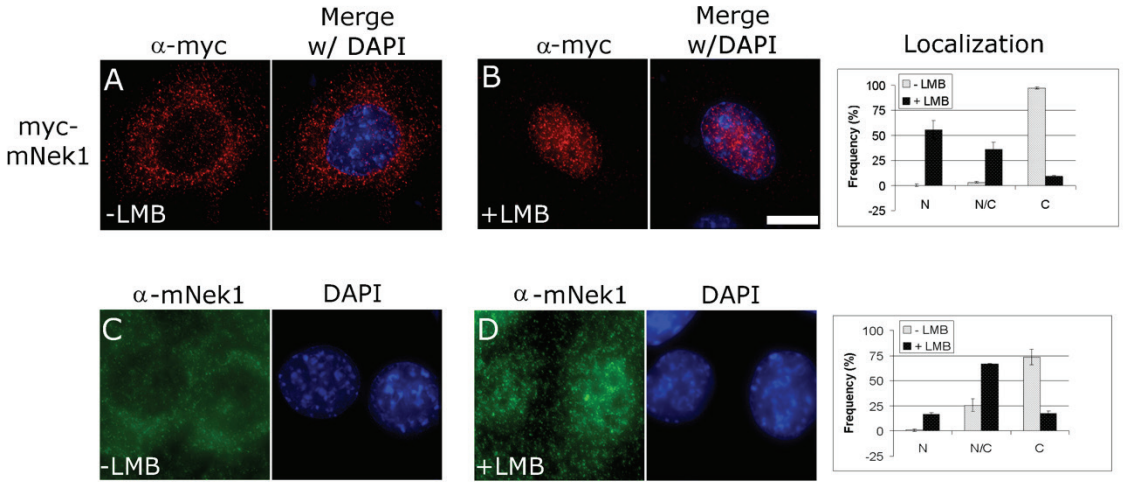

Figure 2.2. NEK1 Cycles Through the Nucleus.
(A, B) IMCD3 cells were transfected with myc-NEK1. Twenty-four hours post-transfection, cells were left untreated (LMB-) or treated with leptomycin B (LMB+) for 6 hours, then fixed for immunofluorescence and stained with anti-myc (red) and DAPI (blue). (C, D) Un-transfected IMCD3 cells were subjected to the same LMB experiment, then cells were fixed and stained with anti-NEK1 antibody (green) and DAPI (blue). The frequency of the observed localization of myc-NEK1 or endogenous NEK1 [nuclear (N), cytoplasmic (C), or both (N/C)] is indicated. Scale bar represents 5 μm.

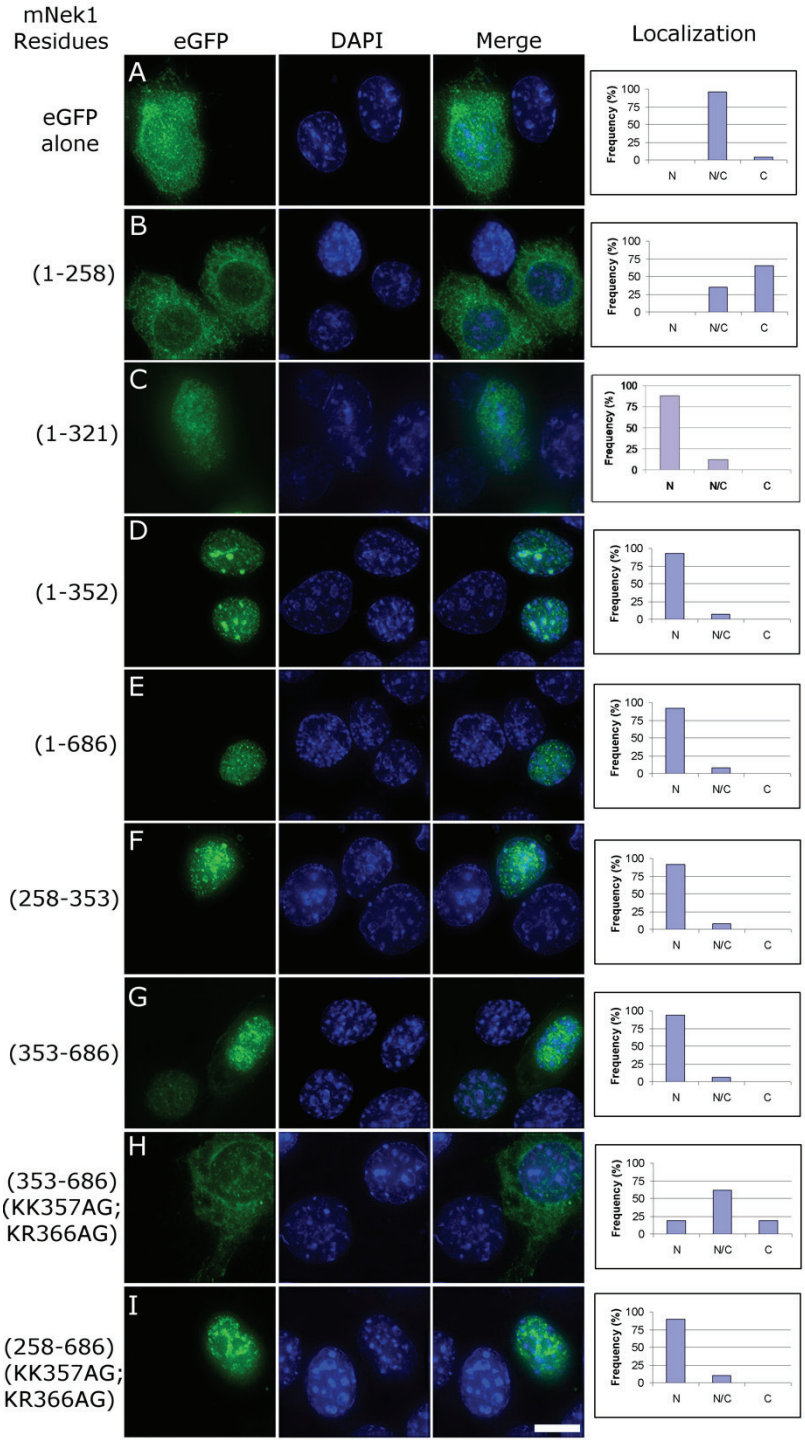

Figure 2.3. NEK1 Has Two Functional NLSs.
IMCD3 cells were transfected with GFP-NEK1 fusion constructs (green) using the indicated residues of NEK1, then fixed for immunofluorescence and stained with DAPI (blue). The frequency of the observed localization of each construct [nuclear (N), cytoplasmic (C), or both (N/C)] is indicated. Scale bar represents 5 μm.

3. Centrioles Are Freed from Cilia by Severing Prior to Mitosis

Jeremy D.K. Parker[1], Laura K. Hilton[1], Dennis R. Diener[2], M. Qasim Rasi[1], Moe R. Mahjoub[1], Joel L. Rosenbaum[2], and Lynne M. Quarmby[1]

[1]Department of Molecular Biology and Biochemistry, Simon Fraser University, Burnaby, British Columbia, Canada, V5A 1S6

[2]Department of Molecular, Cellular, and Developmental Biology, Yale University, New Haven, CT

Reprinted from Cytoskeleton, Vol. 67, Pages 425-430, © 2010 Wiley-Liss, Inc., with permission.

As co-first author, I conducted live cell imaging of 19 pre-mitotic resorption events, analyzed the data for all of the pre-mitotic resorption experiments (Figure 1), and assisted with writing the manuscript. JDKP conducted imaging of 1 live pre-mitotic resorption event, (Figure 2B) carried out immunofluorescence experiments (Figure 3A), synchronized and fixed cells for EM, and wrote most of the manuscript. DD carried out all EM sectioning and imaging (Figure 3B-D). MQR helped with immunofluorescence imaging. MRM created the pre-mitotic resorption video shown in Figure 2A. JLR provided comments on the manuscript. LMQ helped conceive of and design experiments and contributed to writing the manuscript.

3.1. Abstract

Cilia are necessary for normal tissue development and homeostasis. Cells are generally ciliated in interphase, but not in mitosis. The precise mechanism of pre-mitotic ciliary loss has been controversial, with data supporting either sequential disassembly through the transition zone or, alternatively, a severing event at the base of the cilia. Here we show by live cell imaging and immunofluoresence microscopy that resorbing flagella leave remnants associated with the mother cell wall. We postulated that the remnants are the product of severing of doublet microtubules between the basal bodies and the flagellar transition zone, thereby freeing the centrioles to participate in spindle

organization. We show via TEM that flagellar remnants are indeed flagellar transition zones encased in vesicles derived from the flagellar membrane. This transition zone vesicle can be lodged within the cell wall or it can be expelled into the environment. This process is observable in *Chlamydomonas,* first because the released flagellar remnants can remain associated with the cell by virtue of attachments to the cell wall, and second because the *Chlamydomonas* transition zone is particularly rich with electron-dense structure. However, release of basal bodies for spindle-associated function is likely to be conserved among the eukaryotes.

3.2. Introduction

Eukaryotic cilia/flagella (the terms are interchangeable) are composed of four distinct structural regions. Within the cytoplasm of the cell is the basal body, which is anchored to the plasma membrane via transitional fibres [O'Toole et al., 2003]. Microtubules of the basal body are continuous with the transition zone (TZ) and ciliary microtubules, which extend typically 5-15 μm out from the cell, and along with the ciliary membrane, form the cilium proper. At the distal end of the cilium is a cap structure that bears attachments to the ciliary membrane and is the major site of ciliary subunit addition and subtraction [Dentler and Rosenbaum, 1977; Johnson and Rosenbaum, 1992]. The TZ region is the site of several important activities (reviewed in Pazour and Bloodgood [2008]): in addition to anchoring the cilium at the surface of the cell through Y fibres that connect with the base of the ciliary membrane, it is the region where the triplet microtubules of the basal body become doublet microtubules of the cilium proper; it forms a putative flagellar pore complex that regulates the traffic of proteins into and out of the cilium; and it forms a diffusion barrier that prevents mixing of flagellar and cell body membrane components. In addition, the distal end of the TZ is where the central pair microtubules of motile cilia are nucleated. This distal region of the TZ is also the site of severing during deflagellation, the stress-induced event that is the quickest mode of ciliary loss [Quarmby, 2009].

We have previously proposed that deflagellation is mediated by the microtubule-severing ATPase, katanin p60, but genetic evidence has been lacking [Lohret et al., 1998; Lohret et al., 1999]. Using an RNAi knock-down approach, we recently showed

that in wild-type (flagellated) *Chlamydomonas* cells, reduction of the levels of katanin is lethal [Rasi et al., 2009]. In contrast, we observed that katanin levels can be efficiently reduced in mutant backgrounds that lack flagella, implying that katanin plays an essential function that is abrogated in cells lacking cilia [Rasi et al., 2009]. One possible explanation is that katanin serves to release basal bodies from their transition zones, thus freeing them to migrate and facilitate proper placement of the spindle poles.

In this report, TEM images reveal structures encased in vesicles and embedded in post-mitotic mother cell walls. These images are consistent with the predicted TZs encased in membrane derived from the flagella. This transition zone vesicle can be lodged within the cell wall or it can be expelled into the environment, as we show by live cell imaging. Additionally, our live cell imaging has allowed us to discover that pre-mitotic resorption of flagella is faster than reported rates of experimentally-induced flagellar resorption in non-dividing cells (e.g. [Marshall et al., 2005; Pan and Snell, 2005])

3.3. Materials and Methods

Chlamydomonas strains were obtained from the *Chlamydomonas* Genetics Center. Wild-type *Chlamydomonas* 137c mt(-) (CC-124) was used for all EM experiments, *pf6* mutant cells (CC-1029) were used for live cell imaging experiments. Cells were maintained on TAP medium with 1.5% agar [Harris, 2009].

For IFM experiments, cultures enriched for dividing cells were obtained by transferring cells growing asynchronously in TAP liquid cultures to liquid minimal medium (MI) [Harris, 2009], for 24 hours in the dark. Cells were then resuspended in fresh TAP in bright light for ~12 hours, then returned to MI in the dark to induce division and assayed by phase-contrast microscopy for the presence of an abundance of large cells suggestive of imminent division.

IFM was performed as described previously [Rasi et al., 2009]. For EM, synchronous cultures were fixed by adding an equal volume of 5% glutaraldehyde in MI medium. The cells were shipped overnight (from Burnaby to New Haven) and processed the following day by fixing 30 minutes at RT in 2.5% glutaraldehyde in MI with 0.1%

tannic acid, postfixed in 1% osmium tetroxide in 100 mM cacadylate buffer pH 7.2 for 1 hour at 4˚C, and stained *en bloc* with 1% uranyl acetate. The fixed cells were sedimented and embedded in 1% agarose, dehydrated, and embedded in Epon resin. Sections were viewed with a JEOL 1230 electron microscope and images were collected with an Orca HR digital camera (Hamamatsu). Micrographs were rotated, cropped, and their brightness and contrast were adjusted in Photoshop (Adobe).

For live cell imaging, cultures enriched for dividing cells were obtained by transferring cells growing asynchronously in TAP liquid cultures to liquid minimal medium (MI) [Harris, 2009], for 24 hours in the dark. Cells were then resuspended in fresh TAP in bright light for 6 hours, then embedded in 0.5% low melting point agarose in MI and imaged in the dark on a Delta Vision system (Applied Precision, Issaquah WA). Images were captured once every minute for 6 hours. Flagellar length was measured in five-minute intervals using SoftWorx software (Applied Precision). Only cells with flagella longer than 4 μm at the start of imaging were included in our analyses.

3.4. Results

In the *Chlamydomonas* cell cycle, a haploid vegetative cell grows until it passes a commitment point, then some time later divides N times to produce 2^N daughter cells (N is typically 1-4 [Umen and Goodenough, 2001]). The parental cell is surrounded by a cell wall with two tunnels at the anterior end through which the flagella pass into the surrounding medium. Prior to the first division the flagella resorb, though details of how this occurs are sketchy, and the cell rotates within the cell wall. The progeny cells remain encased in the cell wall of the parental cell (the "mother cell wall") until they assemble flagella of their own, become motile and “hatch”.

To more carefully examine the resorption of flagella prior to division, live cells were imaged with time-lapsed photomicroscopy as they approached and completed mitosis. Imaging was facilitated by using a mutant with immotile flagella (*pf6*). To enrich for cells entering cell division, cells were held in the dark in minimal medium, then released to light in rich medium. Cells were observed over the next 6 hours and when a

substantial fraction of the population of cells were greater than ~9 μm in diameter, live cells were imaged as described in materials and methods.

Using this technique, we captured twenty-one cells that remained in focus through flagellar resorption and cell division allowing us to describe this process quantitatively. Comparing the lengths of the two flagella on a given cell revealed that the initiation and rate of resorption of the pair was tightly coupled (Figure 3.1A). As is commonly observed for paralyzed mutants, the *pf6* flagella are generally shorter than those of wild-type, and we did not observe any flagella greater than 10 μm in length. It is important to note that most of the cells in these samples were entering the division cycle and we cannot know a priori which ones had already begun to resorb their flagella. For this reason, we used the onset of cytoplasmic rotation as our time anchor (Figure 3.1B). The pause between the completion of flagellar resorption and cytoplasmic rotation indicates that mitosis is occurring [Holmes and Dutcher, 1989]. This period was generally 10-20 min in the cells captured on video, though one was much longer (45 min) and two were not seen to rotate. We observed an average rate of resorption of 0.17 μm/min in the final 20 minutes of resorption where the flagellar length decreased in a linear fashion (N= 9 cells from 3 independent experiments, using only one flagellum per cell; standard deviation of 0.05; range 0.09 to 0.26). We note that although there is variability in previously reported resorption rates, our data supports the conclusion that pre-mitotic flagellar resorption is substantially faster than flagellar resorption induced by $NaPP_i$ or by a shift to the restrictive temperature of the fla10-1 anterograde IFT mutant [Marshall et al., 2005; Pan and Snell, 2005].

Although we and others have documented flagella of various lengths (presumably partially resorbed) detached from the basal bodies yet still adhering to cells during division, in all twenty-one cells observed here, the flagella resorbed completely, leaving only a small round spot visible, typically associated with the mother cell wall in a position consistent with the flagellar tunnels (Figure 3.2A). In two of the twenty-one cells recorded by live cell imaging, the cell appeared to eject a small particle from cell wall tunnel and these particles were lost to the surrounding media (e.g. Figure 3.2B). We speculate that these spots were remnants of the resorbed flagella, which were lodged in the flagellar tunnel in the cell wall, and were dislodged by the rotation of the protoplast. If these, and the small spots seen associated with the mother cell wall of most cells

entering mitosis, are in fact small vesicular remnants of the resorbed flagella, they may be generated by severing from the basal body and may contain residual microtubules or tubulin. Consistent with this hypothesis, we previously reported pairs of “dots” observed by anti-acetylated tubulin IFM in locations consistent with the flagellar tunnels of the mother cell wall [Rasi et al., 2009] and proposed that these were isolated TZs.

To determine whether these dots were indeed shed TZs, we grew cultures enriched for dividing cells and processed duplicate aliquots for immunofluorescence microscopy (IFM) and TEM. Taken together with our earlier published observations [Rasi et al., 2009] we have observed greater than 300 unhatched daughter clusters by IMF. In 80% of these, the anti-acetylated tubulin antibody recognized two small dots near unhatched daughter cells, in a position consistent with the flagellar tunnels of the mother cell wall (for example see Figure 3.3A, arrow). Though the tunnels in the cell wall were only occasionally seen in TEM section, these often contained small vesicles that enveloped electron dense material with characteristics of a TZ (Figure 3.3B-G). In none of these cases were microtubules still evident, but in longitudinal section the central part of the “H” of the TZ was clearly visible (Figure 3.3C-E) and in some cases (e.g. Figure 3.3E) the vesicle appeared to include little more than the central hub of the TZ. In cross section the central circle of the TZ could be seen (Figure 3.3F and G) and even though the microtubule doublets were no longer present the 9 fold symmetry sometimes was detectable (Figure 3.3F) as were links between the central hub and the surrounding membrane (Figure 3.3G). For the TZ to be contained within a vesicle, it must have been severed from the basal body.

3.5. Discussion

Due to the small size of the basal body and attached transition zone, and the transient nature of flagellar resorption, the exact sequence of events late in flagellar resorption in *Chlamydomonas* has been controversial. Johnson and Porter [1968] observed by TEM, flagella attached to transition zones, but severed from basal bodies, in agreement with our previous IMF observations and with the TEM images presented here. Cavalier-Smith [1974] and Gaffal [1988], however, made observations that led to the widely-held interpretation that flagella are sequentially disassembled via resorption,

starting at the distal end and proceeding proximally until the entire flagellum and transition zone are gone, and the basal bodies are free of flagellar microtubules. Subtle differences in strains, culture conditions, or fixation may be contributing to these conflicting observations, but the greatest limitation of all three studies with respect to this issue is that very few dividing cells were observed. To resolve this question, we enriched for dividing cells, which enabled us to observe hundreds of cells by immunofluorescent microscopy in addition to numerous by TEM and twenty-one by live cell video microscopy. Consequently, our data is less sensitive to rare events.

We and others have documented flagellar remnants that were microns long still attached to dividing Chlamydomonas though, as we now appreciate, they were no longer attached to the basal bodies. This observation demonstrated that severing the flagella can occur before resorption is complete. Rare TEM images also supported this idea and suggested that pre-mitotic severing occurred between the basal body and the TZ [Johnson and Porter, 1968]. For this to be true there must be two sites where the axoneme can be severed: just distal to the TZ, as occurs during pH-induced autotomy [Quarmby, 2009]; and, between the basal body and the TZ [Rasi et al., 2009]. Two different sites of severing suggest two different molecular machineries are involved, but it is likely that they share components [Parker and Quarmby, 2003]. A requirement for the microtubule-severing ATPase, katanin in severing proximal to the TZ may be the reason a knockdown of the 60 kD subunit of katanin is lethal in flagellated cells [Rasi et al., 2009].

Even though severing of partially resorbed flagella from the basal bodies before division has been documented [Piasecki and Silflow, 2009; Rasi et al., 2009], this relatively rare event was not observed in the experiments reported here. All of the cells captured on video fully resorbed their flagella before division. The cell must send two different signals to its flagella prior to cell division; one to resorb, possibly so that the axonemal tubulin can be reutilized during mitosis; and a second to abscise, perhaps to free the basal body to perform other roles in mitosis and cell division. We hypothesize that the signal to resorb is given long enough before abscission that normally the flagella resorb fully before severing of the TZ. Occasionally, resorption may not begin early enough and severing occurs before resorption is complete to rid the cell of its flagella

before division starts. This may explain the perplexing images presented in earlier works [Piasecki and Silflow, 2009; Rasi et al., 2009].

The most generally cited speculation for why flagella are lost before mitosis is to free the basal bodies to participate as centrioles in organizing the spindle. Ciliary loss is common and is consistently observed when the presence of cilia would otherwise restrict the plane of division, for example, in highly organized tissues. It should be emphasized that we do not fully understand the roles of the Chlamydomonas basal bodies during mitosis and cytokinesis. However, it is likely that migration and positioning of the basal bodies is critical for one or both of these processes and thus, in this cell, it is likely that the cell wall necessitates flagellar loss and release of the basal body. Because the flagella exit the cell through two tunnels in the cell wall, the basal bodies cannot separate and the cell can not rotate while the flagella are in place.

We propose that the TZ vesicle is abandoned by the cell because the transition zone and its associated fibres and plasma membrane and cell wall connections are not easily disassembled for the recycling of component molecules, as happens with components of the flagellum proper [Lefebvre et al., 1978]. Consistent with this idea, we observed several TZ vesicles which retained visible connections with the surrounding membrane. This model is conceptually similar to how the microtubules of cytokinetic midbodies are not recycled, but rather (topologically) cast outside the cytoplasm [Mullins and McIntosh, 1982]. Intriguingly, Rab11 is implicated in both formation of both midbodies [Wilson et al., 2005] and cilia [Mazelova et al., 2009], leading us to propose that the abscission events of premitotic cilia loss and cytokinesis may have common components.

Understanding the mechanism of pre-mitotic flagellar resorption gives some insight into flagellar regrowth under different circumstances. Post-deflagellation, the transition zone remains in the cell and the basal bodies remain docked to the membrane; thus the cell can quickly re-grow new flagella [Rosenbaum and Child, 1967]. During experimentally induced resorption, for example using a medium low in calcium and high in monovalent cations, flagella shorten via an unknown mechanism, but do not fully disappear (data not shown). Thus, the basal bodies and transition zones are not likely to be extensively modified by the induction of resorption, explaining the rapid

regrowth of flagella when these cells are returned to normal medium (data not shown). In contrast to regrowth after deflagellation or induced resorption, assembly of a new flagellum post-mitosis requires docking of the basal bodies to the apical membrane as well as assembly of a TZ.

Some *Chlamydomonas* mutants with defects in flagellar assembly (the *fla* mutants) deflagellate precociously: they tend to deflagellate in the absence of the stress stimuli that are normally used to induce deflagellation [Parker and Quarmby, 2003]. At the time, these data suggested to us that there was a relationship between flagellar resorption and the severing of axonemal microtubules. The new data presented here provides direct evidence that in *Chlamydomonas*, normal pre-mitotic flagellar disassembly involves a microtubule-severing event between a basal body and its flagellar transition zone. However, the relationship between this event and deflagellation remains enigmatic. Release of basal bodies by severing from TZs has been observed in another green alga, *Chlorogonium* [Hoops and Witman, 1985]. In the case of *Chlorogonium*, the TZ and flagella remain attached to the cell and functional while the basal bodies migrate and serve as spindle pole foci. Although the retention of functional flagella makes the *Chlorogonium* situation unusual, it does reflect the common theme of pre-mitotic release of basal bodies from the TZ. We expect that a similar severing event occurs in all cells that bear complex TZs, and may occur in others as well.

3.6. Conclusions

Here we provide evidence that pre-mitotic flagellar resorption in *Chlamydomonas* involves microtubule severing between the flagellar TZ and the basal bodies, and that the TZ is not itself resorbed or otherwise recycled, as is the majority of the axoneme. It is not yet known whether a similar severing event is required to release the basal bodies of other ciliated cells that divide, such as mammalian cells bearing primary cilia. Although all cilia have a TZ that mediates attachment to the ciliary membrane, not all contain TZs that are as structurally elaborate as those in *Chlamydomonas* [Sanders and Salisbury, 1989; O'Toole et al., 2003]. Thus, it is not clear whether all will require a severing event to release the basal bodies prior to mitosis or whether some of the simpler transition zones might be amenable to disassembly akin the resorption of the cilium proper.

3.7. Acknowledgements

This work was funded by a Natural Sciences and Engineering Research Council Discovery Grant to L.M.Q. and by National Institutes of Health grant GM-14642 to J.L.R.

3.8. Figures

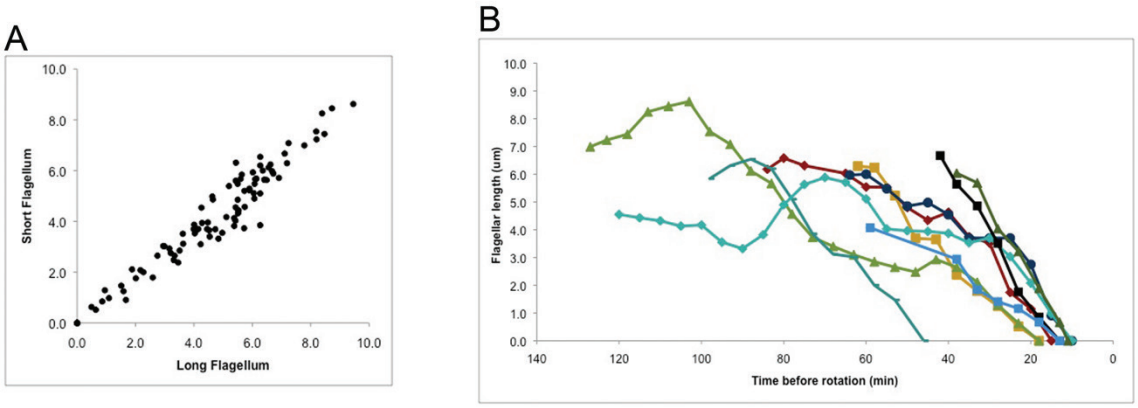

Figure 3.1. Flagellar Length Measurements During Resorption.
A. The length of the longer flagellum is plotted against the length of the shorter flagellum during resorption for each of six mitotic cells from two separate experiments. **B**. The length of a single flagellum from each of 9 mitotic cells from 3 separate experiments was measured once every five minutes during resorption. The beginning of cortical rotation is set as time 0.

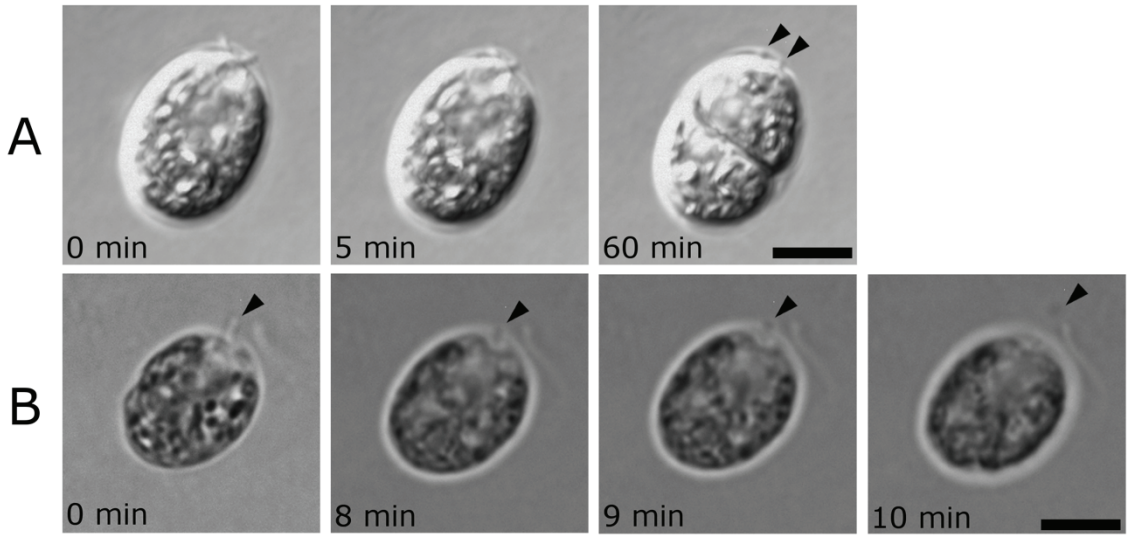

Figure 3.2. Imaging of Dividing Chlamydomonas Cells Reveals Formation of Remnant Vesicles in Living Cells.

Panels are time-lapse DIC (A) and phase contrast (B) images of flagellar resorption of single cells. In all cells examined thus far, remnants are visible upon completion of resorption. Arrowheads indicate remnants and times indicate minutes after the first image shown (not all cells are captured at the onset of resorption). Scale bars, 5 μm. **A.** Resorption is gradual until the entire axoneme is gone except for two remnants left in association with the cell wall. The remnants (indicated by arrowheads) remain in this position even after cytoplasmic rotation and cytokinesis, indicating that they are associated with the mother wall and not with a daughter cell. **B.** The left flagellum shortens gradually until it is not visible, then a remnant is ejected through the flagellar tunnel in the cell wall and comes to rest near the cell.

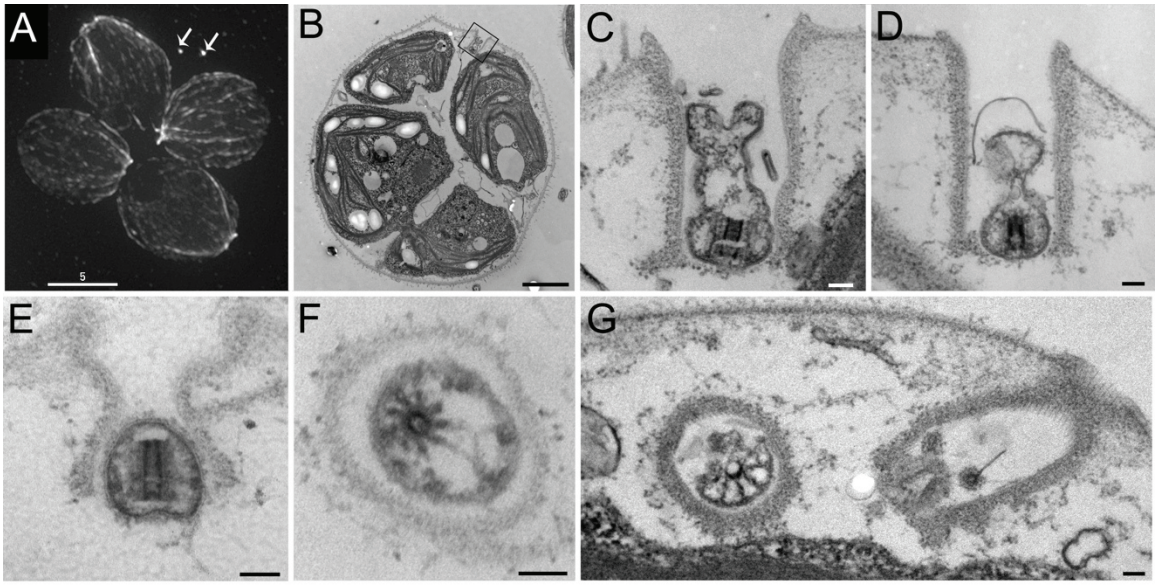

Figure 3.3. Flagellar Remnants Visualized by Immunofluorescence Microscopy Appear to be Flagellar Transition Zones (TZs) When Visualized by Electron Microscopy (EM).

A. Unhatched *Chlamydomonas* daughter cells stained for anti-acetylated tubulin and anti-α-tubulin. We typically see two flagellar remnants in a position consistent with the anterior flagellar tunnels of the mother cell wall (arrows). A pair of spots such as shown here are clearly visible in 80% of unhatched cells in our preparations (N > 300). Scale bar, 5μm. **B-G.** Cells from the same (E and F) culture as A, or a similar culture (B-D and G) visualized by thin-section EM. **B.** These cells are completing their second round of division and remain encased in their mother cell wall. The box surrounds a flagellar tunnel in the mother cell wall. Scale bar, 2 μm. **C.** This magnified view of the boxed area from B shows a vesicle that contains a flagellar transition zone seen in longitudinal section. This remnant vesicle clearly sits within the flagellar tunnel of the cell wall. The TZ appears to be split in two along the cross-piece of the canonical electron-dense H. Scale bar, 100 nm. **D.** A remnant vesicle lies within its mother cell wall with electron dense material resembling the hub of a transition zone. Scale bar, 100 nm. **E.** In this case the remnant vesicle closely encases the electron dense material resembling the hub of a transition zone. Scale bar, 100 nm. **F.** A cross-section through a remnant vesicle reveals a disintegrating transition zone. No microtubule doublets are present, but nine projections remain attached to the central core of the TZ . The hub has an eccentric location in the vesicle. Electron dense masses on the inside of the membrane are probably the remains of the Y links that once connected the microtubules to the flagellar membrane. Scale bar, 100 nm. **G.** The two flagellar tunnels of one cell are seen, one containing a cross section of a partial transition zone, the other, with no clearly identifiable flagellar remnant. Scale bar, 100 nm.

4. The *Chlamydomonas cnk2-1* Mutant Supports a Feedback Model for Flagellar Length Control

The following chapter has submitted for review at *Current Biology*. The authors of the paper were as follows:

Laura K. Hilton, Kavisha Gunawardane, Joo Wan Kim, Marianne C. Schwarz, and Lynne M. Quarmby

Department of Molecular Biology and Biochemistry, Simon Fraser University, Burnaby, British Columbia, Canada, V5A 1S6

As first author, I conceived of, designed, and interpreted all of the experiments and wrote the manuscript. KG conducted one of the three experiments that contributed to each of Figures 4E and 4F. JWK conducted the solid media resorption experiment (Figure 2C). MCS performed one of the experiments that contributed to Figure 4E, and isolated the *lf4 cnk2* double mutant. LMQ helped with conception, design, and interpretation and with writing the manuscript.

4.1. Abstract

Background: Many of the diverse functions of cilia depend upon tight control of their length. Steady-state length reflects a balance between rates of ciliary assembly and disassembly, two parameters likely controlled by a length sensor of unknown identity or mechanism.

Results: A null mutation in *Chlamydomonas* CNK2, a member of the evolutionarily conserved family of NIMA-related kinases, reveals feedback regulation of assembly and disassembly rates. The *cnk2*-1 mutant cells have a mild long flagella (lf) phenotype as a consequence of reduced rates of flagellar disassembly. This is in contrast to the strong lf mutant, *lf4*-7, which exhibits an aberrantly high rate of assembly. Cells carrying both mutations have even longer flagella than *lf4*-7 single mutants. In addition to their high rate of assembly, *lf4*-7 mutants have a CNK2-dependent increase

in disassembly rate. Finally, *cnk2*-1 cells have a decreased rate of turnover of flagellar subunits at the tip of the flagellum, demonstrating that the effects on disassembly are compensated by a reduced rate of assembly.

Conclusion: We propose a model wherein CNK2 and LF4 modulate rates of disassembly and assembly respectively in a feedback loop that is activated when flagella exceed optimal length.

4.2. Introduction

Cilia are dynamic, microtubule-based organelles that project from the surface of most eukaryotic cells. Perturbations in ciliary length are associated with certain ciliopathies, diseases that arise from defects in ciliary structure or function. For example, long cilia have been associated with retinitis pigmentosa [Omori et al., 2010; Ozgül et al., 2011; Tucker et al., 2011] and Meckel syndrome [Tammachote et al., 2009] in humans. Short cilia often arise from defects in the machinery of ciliary assembly or the composition and structural integrity of cilia, but long cilia arise from defects in the processes that regulate ciliary length. Mutations that cause abnormally long cilia are therefore valuable for studying these processes.

Cilia are regenerated *de novo* at least once per cell cycle in interphase. Components of the growing cilia are transported to the tip by molecular motors through a process known as intraflagellar transport (IFT) (e.g. [Qin et al., 2004; Hao et al., 2011]). Anterograde IFT, utilizing kinesin-2 motor proteins, delivers components to the ciliary tip, while retrograde IFT, utilizing cytoplasmic dynein motor proteins, returns IFT components to the cell body (reviewed in [Pedersen and Rosenbaum, 2008]). As cilia elongate, the rate at which IFT delivers cargo to the tip decreases; consequently, the rate of ciliary assembly is inversely proportional to the length of the cilium [Marshall and Rosenbaum, 2001; Marshall et al., 2005; Engel et al., 2009].

In contrast to assembly, the rate of ciliary disassembly appears to be constant and length independent (e.g. [Marshall et al., 2005]). As the ciliary microtubules are dynamic and there is constant turnover of microtubule subunits at the distal tip of the cilium [Marshall and Rosenbaum, 2001; Song and Dentler, 2001], steady-state length is

achieved at the balance point, when the rate of assembly is equal to the rate of disassembly [Marshall and Rosenbaum, 2001; Marshall et al., 2005; Engel et al., 2009].

It has been argued that little or no regulation of assembly and disassembly is required *per se* to maintain wild-type ciliary length [Ludington et al., 2012; Ludington et al., 2013] However, the existence of mutations that alter ciliary length, especially long cilia mutants, suggest that the normal function of these mutated components is to regulate ciliary length, possibly by regulating the rates of assembly and/or disassembly.

The NIMA-related protein kinases (Neks) are a family that may have co-evolved with centrioles to regulate cilia and cell cycle functions [Parker et al., 2007]. A growing body of evidence suggests that members of the Nek family have roles in regulating ciliary disassembly. First, the *Chlamydomonas* Nek FA2 is essential for deflagellation, a form of disassembly where cells sever the ciliary axoneme and shed their flagella into the environment in response to stress [Mahjoub et al., 2002]. The ciliate *Tetrahymena thermophila* possesses more than 30 Neks, and so far four of them have been shown to negatively regulate ciliary length [Wloga et al., 2006]. In mammalian cells, siRNA of Nek2 delays pre-mitotic resorption until after centrosome duplication and separation [Spalluto et al., 2012], and Nek7 knockout causes cells to become aberrantly multiciliated [Salem et al., 2010]. Overexpression of mouse Nek1 prevents ciliogenesis and destabilizes centrioles [White and Quarmby, 2008].

Previously, we showed that another *Chlamydomonas* Nek, CNK2, localizes to flagella, and that RNAi of CNK2 causes slightly long flagella while overexpression causes slightly short flagella [Bradley and Quarmby, 2005]. Here we describe a new *cnk2-1* null strain that exhibits a similar mild long flagella phenotype. Importantly, we find that the *cnk2-1* null is defective in some types of ciliary resorption, consistent with a reduced basal rate of ciliary disassembly. We have discovered a genetic interaction between *cnk2-1* and the long flagella mutant *lf4*, and propose a model wherein the dysregulated flagellar assembly of *lf4* mutants [Ludington et al., 2013] is enhanced by reduced disassembly in *cnk2-1*. We also show that perturbations in flagellar length are associated with measurable changes in the rates of flagellar assembly and disassembly. Our results reveal an active length sensing mechanism that regulates ciliary length, probably through feedback control of the rates of assembly and disassembly.

4.3. Materials and Methods

4.3.1. Strains and culture conditions

The *lf4* (CC-4535), *fla10-1* (CC-1919), *adf1-6* (CC-3747), HA-tubulin (CC-3055), and wild-type 137c mt+ and mt- (CC-125 and CC-124) were obtained from the Chlamydomonas Resource Center at the University of Minnesota. The *cnk2-1* mutant strain provided by Olivier Vallon (Institut Curie, Paris, France) was generated in a 137c mt- strain [Meslet-Cladière and Vallon, 2012]. It was back-crossed to 137c mt+, and the *cnk2-1* mutant progeny back-crossed three more times to 137c. The mutant progeny were identified by PCR of the coding region of the *CrAad* insert using primers CrAad_Start_Fwd (5'- ATGGCCAAGCTGACCAGCGCC-3') and RBCS_Dw_Short (5'-CGCCTCCATTTACACGGAGCG-3'). Except where noted, experiments were performed on fourth-generation *cnk2-1* progeny, using a wild-type sibling strain for all controls.

The *lf4 cnk2-1* double mutant was generated by mating second generation *cnk2-1* with *lf4*. Complete tetrads were screened for the long flagella phenotype and for the presence of the CrAad insert by PCR to identify tetrads with a non-parental di-type. All experiments on the double mutant used *lf4, cnk2-1,* and WT sibling strains as controls.

The *fla10* mutant combinations were generated by mating *fla10-1* to the *lf4 cnk2-1* double mutant described above. Progeny were screened first for the temperature-sensitive *fla10* phenotype, then for the long flagella phenotype, and finally for resorption in the presence of IBMX to identify single *fla10* mutants, double *fla10 cnk2-1* and *fla10 lf4*, and triple *fla10 lf4 cnk2-1* mutants. Each strain was derived from a different tetrad. The *cnk2-1* HA-tubulin strain was generated by crossing fourth-generation *cnk2-1* with the HA-tubulin strain, and screening the progeny for *cnk2-1* resorption phenotypes as described above, and by immunoblotting with rat anti-HA (high-affinity clone 3F10, 1:1000, Roche). The *adf1-6 cnk2-1* double mutant was generated similarly, and progeny were screened for resorption and deflagellation phenotypes.

For all experiments, cells were maintained on tris-acetate-phosphate (TAP) plates containing 1.5% agar [Harris, 2009], and grown in liquid TAP media for at least 18 hours prior to experiments involving flagellar length measurements. For NaPPi

experiments, cells were grown in liquid TAP media and transferred to liquid M media [Harris, 2009] for at least 1 hour before NaPPi was added. For solid media flagellation experiments, cells were spread on 3% agar TAP plates.

4.3.2. Generation of CNK2 antibody and immunoblotting

To generate a CNK2 antibody, the *CNK2* cDNA [Bradley and Quarmby, 2005] was cloned into pET-DEST42 (Invitrogen), a bacterial expression vector that encodes a 6xHIS tag at the C-terminus of the recombinant protein. CNK2-6xHIS was expressed in BL21 competent cells (Invitrogen) and purified on a HisTrap-FF column (GE Life Sciences). 1 mg of purified protein was used to inoculate two rabbits (Pacific Immunology), and antisera from the final bleed from one rabbit was selected for its ability to specifically detect CNK2 in wild-type flagellar extracts, but not *cnk2-1* flagellar extracts, at a 1:5000 dilution of crude antiserum. The IC140 antibody was a generous gift from Win Sale (Emory University, Atlanta, GA). The secondary antibody for immunoblotting was horseradish peroxidase-conjugated goat anti-rabbit IgG (1:20,000, Sigma-Aldrich), detected with Luminata Forte HRP substrate (Millipore).

4.3.3. Characterizing and rescuing the cnk2-1 mutation

To identify the 5' end of the site of insertion in the *CNK2* gene, genomic DNA was isolated from *cnk2-1* and a fragment was PCR amplified using a forward primer that anneals near the *CNK2* start codon (5'-TTAGACCCGTCCTTCGCCAT-3') and a reverse primer that anneals to the 5' end of the *CrAad* insert (5'-CAGCTTTTGTTCCCTTTAGTG-3'). The PCR product was ligated into pGEM-T Easy (Promega) and sequenced using standard primers that anneal to the vector's T7 and SP6 sites (Operon). This sequence was aligned to the *CNK2* genomic sequence to identify the 5' end of the site of insertion.

To rescue the *cnk2-1* mutation, a 9.8 kb fragment of 137c genomic DNA was PCR-amplified to include the entire *CNK2* gene, plus 1.6 kb upstream and 1.8 kb downstream of the transcript start and end sites. This fragment was ligated into the EcoRI site of pBluescript SK II. The resulting clone was co-transformed into *cnk2-1* cells with pSI103, which confers resistance to paromomycin [Sizova et al., 2001], by the glass bead method [Kindle, 1990]. Transformants that grew on paromomycin-containing media

were screened for flagellar resorption during treatment with 1 mM IBMX, and strains that resorbed like wild-type were further tested by western blot to confirm expression of CNK2 protein in flagella.

4.3.4. Flagellar length measurements and immunofluorescence

For steady-state length and NaPPi, IBMX, and *fla10* experiments, 25% glutaraldehyde was added to samples of liquid culture to a final concentration of 1%. IBMX (1-isobutyl-3-methylxanthine, Sigma) was dissolved in DMSO at 100 mM and added to cells in TAP media at a final concentration of 1 mM. NaPPi (sodium pyrophosphate tetrabasic, Sigma) was dissolved in water at 200 mM and adjusted to pH 7 with concentrated HCl, and added to cells in M media to a final concentration of 20 mM. For solid media flagellation experiments, cells were scraped off of 3% agar TAP plates and resuspended directly in 1% glutaraldehyde in TAP. For pre-mitotic resorption experiments, cells were synchronized on a 14:10 light:dark cycle in Sueoka high-salt media [Harris, 2009], and embedded in 1% low-melting point agarose on a slide within 30 minutes of the dark-shift. Cells were imaged by DIC on a DeltaVision microscope, using the built-in SoftWORX image analysis software to measure flagellar lengths (Applied Precision).

Long-zero experiments were performed as described previously [Ludington et al., 2012] using the microfluidic chamber C04A and the ONIX perfusion system (CellASIC). Cells were deflagellated by perfusing the chamber with a 1:1 mix of TAP media and deflagellation buffer (40 mM sodium acetate pH 4.5, 1 mM $CaCl_2$ [Finst et al., 1998]) for 60 seconds, then continually perfusing TAP media while the cells recovered. Cells were imaged by phase contrast on a Nikon 6D microscope, and flagella were measured using ImageJ 64.

For HA-tubulin quadriflagellate cell (QFC) experiments, cells were mated and QFCs separated from un-mated cells as described previously [Marshall and Rosenbaum, 2001]. Cells were fixed in a solution containing 0.1% glutaraldehyde and 4% formaldehyde for immunofluorescence using a previously described protocol [Parker et al., 2010]. Primary antibodies include mouse monoclonal anti-α-tubulin IgG1 clone DM1A (1:300, Sigma), anti-β-tubulin IgG1 clone D66 (1:300, Sigma), and rat monoclonal

anti-HA high-affinity IgG clone 3F10 (1:300, Roche). Secondary antibodies were goat anti-mouse IgG1 Alexa Fluor 594 and goat anti-Rat IgG Alexa Fluor 488 (both 1:300, Life Technologies). Slides were imaged and analyzed on a DeltaVision microscope (Applied Precision).

4.4. Results

4.4.1. The cnk2-1 mutant is null and has a flagellar resorption defect

The *Chlamydomonas cnk2-1* mutant strain is an insertional mutant, discovered during the early stages of a long-term project to generate a robust insertional mutant library for *Chlamydomonas* complete with flanking sequence tags [Meslet-Cladière and Vallon, 2012]. The mutants are produced by transforming a derivative of the wild-type strain CC-124 with a spectinomycin resistance cassette, *CrAad*, and salmon sperm carrier DNA, and flanking sequence tags are identified by 3' RACE [Meslet-Cladière and Vallon, 2012]. For the *cnk2-1* mutant strain, 3' RACE showed that the 3' end of the insertion lies within the intron of the *CNK2* 5' UTR. We were interested in characterizing the strain further because of our earlier work on this gene [Bradley and Quarmby, 2005].

We made a forward PCR primer complementary to a sequence near the stop codon of the *CrAad* gene, and screened a number of reverse primers specific for different parts of the *CNK2* gene until we found a pair that successfully produced a PCR product. We found that pairing with a reverse primer that anneals near the *CNK2* start codon produced a PCR product. Sequencing of this PCR product revealed that the 5' end of the insertion also lies within the first *CNK2* intron in the 5' UTR (Figure 4.1A).

To separate the CrAad insertion in the *CNK2* gene from additional insertions of either CrAad or salmon sperm carrier DNA, we performed four back-crosses with the wild-type strain CC-125, and followed the insertion by PCR (Figure 4.1B, top panel). All subsequent experiments were performed on fourth generation *cnk2-1* back-crossed strains.

We next raised an antibody against purified recombinant CNK2 protein (see Section 4.2 Materials and Methods). Using this antibody in western blots, CNK2 protein is not detectable in whole cell extracts of wild-type cells (not shown), but a band of 72 kDa, the predicted size of CNK2, is detectable in flagellar extracts. This band is not present in *cnk2-1* flagellar extracts, and we conclude that the Ab is specifically recognizing CNK2 and that *cnk2*-1 is null for protein expression (Figure 4.1B).

Because we had previously shown that RNAi of *CNK2* resulted in a mild long flagella phenotype [Bradley and Quarmby, 2005], we compared flagellar lengths and found that *cnk2-1* mutant flagella are slightly longer than wild-type. Transformation of the mutant strain with a 10 kb genomic fragment containing the *CNK2* gene fully restored expression of CNK2 in flagella (Figure 4.1B) and restored wildtype flagellar length (Figure 4.1C).

We hypothesized that the *cnk2-1* cells were compensating for the loss of CNK2 protein and screened known chemical modifiers of flagellar length for enhancers of the *cnk2-1* phenotype. Sodium pyrophosphate (NaPPi) and 1-isobutyl-3-methylxanthine (IBMX) both cause gradual resorption of wild-type flagella [Lefebvre et al., 1978; Lefebvre et al., 1980]. We discovered that both chemicals induce flagellar resorption in both WT and *cnk2-1:CNK2* rescue cells, but have a greatly reduced effect on *cnk2-1* mutants (Figure 4.2A and B).

Chlamydomonas cells also resorb their flagella when they are transferred from liquid to solid media. We tested the effect of the *cnk2-1* mutation on this type of resorption by maintaining cells in liquid media for 24 hours before transferring them to solid media and comparing the fraction of flagellated cells. Under these conditions, 70% of *cnk2-1* mutant cells were flagellated after 24 hours on solid media, while wild-type and *cnk2-1:CNK2* rescue strains are 14% and 5% flagellated, respectively (Figure 4.2C).

Chlamydomonas flagella also resorb when the two flagella are unequal in length. This phenomenon is most apparent in a “long-zero” experiment: when one flagellum is amputated and the other is full-length, the long flagellum resorbs as the zero-length flagellum regenerates, and once they are equal in length they continue to regenerate together until both flagella are full-length again Rosenbaum et al. [1969]; [Ludington et

al., 2012]. To test the role of CNK2 in the resorption phase of long-zeros, we used *adf1-6* [Finst et al., 1998], a hypomorphic allele of an acid deflagellation-defective mutant in which ~10% of cells shed a single flagellum after treatment with weak organic acid. We loaded *adf1-6* or *adf1-6 cnk2-1* cells into a microfluidic chamber under continuous flow of fresh media, induced deflagellation by lowering the pH of the media to 4.0 with acetic acid for one minute, then imaged uniflagellate cells for one hour to observe flagellar length equalization. Similar to previous results with wild-type cells [Ludington et al., 2012], we consistently observed resorption of the remaining flagellum as the shed flagellum regenerated in *adf1-6* single mutants (Figure 4.3A), and did not observe any abnormal behavior such as overshoot (Figure 4.3C). However, in *adf1-6 cnk2-1* double mutants, we never observed resorption of the longer flagellum as the shed flagellum regenerated (Figure 4.3B, D). We conclude that CNK2 is required for the resorption phase of flagellar length equalization.

Finally, we investigated the role of CNK2 in pre-mitotic flagellar resorption. The final stage of flagellar resorption prior to mitosis is a microtubule-severing event that occurs between the basal body and the flagellar transition zone [Parker et al., 2010]. This severing event doesn't typically occur until tip-down resorption is nearly complete, so the by-product of this severing is a small flagellar remnant (<1 μm long) left in the mother cell wall. We reasoned that if CNK2 is an important component of the pre-mitotic resorption pathway, then we would observe a reduced rate of resorption and a high frequency of *cnk2-1* mutants undergoing early PSOS severing to produce longer flagellar remnants. However, we found that *cnk2-1* mutant flagella resorb at a rate that is very similar to wild-type, and that the flagella always resorbed completely leaving no abnormally long flagellar remnants (Figure 4.2D). We note that pre-mitotic resorption is faster than other types of resorption described here (0.35 μm/min for pre-mitotic resorption, 0.14 μm/min for long-zeros, 0.08 μm/min for IBMX in wild-type cells). Our data indicate that pre-mitotic resorption is regulated by distinct signaling pathways or disassembly mechanisms than resorption induced by chemicals or solid media.

4.4.2. *cnk2-1 lf4 double mutants have longer flagella than lf4 single mutants*

In *Chlamydomonas*, mutations in five genes (*LF1* – *LF5*) are known to cause abnormally long flagella [Barsel et al., 1988] [Asleson and Lefebvre, 1998] [Tam et al., 2013]. Cells carrying mutations in two *lf* genes have synthetic phenotypes such as aflagellate cells or suppression of regeneration defects [Barsel et al., 1988; Asleson and Lefebvre, 1998]. Relatively little is known about the functions of the *LF* gene products, but it was recently shown that *lf4* mutants have an increased rate of injection of IFT material into the flagellum relative to wild-type, suggesting that *lf4* flagella become long due to an increased rate of assembly [Ludington et al., 2013]. The *lf4* mutants also have the longest flagella of all the *lf* mutants, with some flagella reaching nearly four times wild-type length. Populations of *lf4* mutant cells have a very wide distribution of flagellar lengths, including flagella that are shorter than wild-type ([Asleson and Lefebvre, 1998; Berman et al., 2003] and Figure 4.4A).

To our surprise, we find that *lf4 cnk2-1* double mutant flagella are significantly longer than *lf4* single mutants (25.4 μm vs. 18.2 μm, $p<0.0001$, Figure 4.4A) indicating that flagella can be stable at lengths much longer than what is typical of populations of *lf4* single mutant cells. Furthermore, we observed that *lf4 cnk2-1* double mutant flagella are resistant to the effects of IBMX and NaPPi on flagellar resorption, while *lf4* single mutants resorb faster than wild-type in response to either chemical (Figure 4.4B, C).

The abnormal flagellar lengths of *cnk2-1, lf4,* and *lf4 cnk2-1* can be explained by perturbations in the rates of flagellar assembly or disassembly. We propose that when wild-type flagella grow past their prescribed length, or are otherwise induced to resorb, the disassembly rate is increased and the assembly rate is decreased. In *cnk2-1* mutants, flagella that grow too long are unable to activate disassembly, but compensate by decreasing the assembly rate. In *lf4* mutants, the long flagella are unable to inhibit assembly, but compensate by increasing the rate of disassembly in a CNK2-dependent fashion. We hypothesize that in the *lf4 cnk2-1* double mutants, a decreased rate of disassembly combined with an increased rate of assembly produces extra-long flagella.

4.4.3. Rates of flagellar assembly and disassembly are actively regulated

To test the hypothesis that the disassembly rate is increased to compensate for increased assembly in *lf4* cells we examined the rates of disassembly in the *fla10* mutant background. The *Chlamydomonas fla10-1* mutant has a temperature-sensitive defect in a subunit of kinesin-II, the anterograde IFT motor: at the restrictive temperature (33^{o}C) anterograde IFT and flagellar assembly are dramatically reduced [Walther et al., 1994; Kozminski et al., 1995; Marshall and Rosenbaum, 2001]. Under these conditions some flagella are lost by deflagellation [Parker and Quarmby, 2003], while others gradually resorb due to continued disassembly with very little assembly [Kozminski et al., 1995] [Iomini et al., 2001] [Marshall and Rosenbaum, 2001] [Marshall et al., 2005]. Thus, the rate of resorption of *fla10-1* mutant flagella at the restrictive temperature can be used to approximate the basal rate of disassembly.

We generated double mutants of *fla10-1* with *cnk2-1* and *lf4,* and a *fla10-1 lf4 cnk2-1* triple mutant. Cells were cultured at 21^{o}C for 24 hours, then incubated at 33^{o}C with samples taken for flagellar length measurements every hour for two hours (Figure 4.5). We find that *fla10-1* flagella resorb at a rate of 0.046 μm/min, whereas *fla10-1 lf4* double mutants resorb at an increased rate of 0.075 μm/min. The rate of resorption is much lower in *fla10 cnk2-1* double mutants and *fla10-1 cnk2-1 lf4* triple mutants (0.013 and 0.028 μm/min, respectively). These data support our idea that *lf4* cells, whose primary defect is increased assembly [Ludington et al., 2013] have a compensatory elevation of disassembly rate. Importantly, the data demonstrate that the basal rate of disassembly is CNK2-dependent, as is the further stimulation of disassembly in the context of *lf4*.

To test whether the converse is also true, that is, whether the rate of assembly is decreased to compensate for reduced disassembly in *cnk2-1* mutants, we first compared the rates of flagellar regeneration after deflagellation by pH shock (Figure 4.6A). *cnk2-1* mutant cells begin regenerating flagella earlier than wild-type, similar to our previously reported results for *CNK2* RNAi [Bradley and Quarmby, 2005], but overall regeneration rates do not differ between cnk2-1 and wild-type cells. Consistent with our model,

assembly rates during assembly are not affected. We predict that assembly rates are only affected when flagella are full length or longer.

The most direct way to assess the rate of flagellar assembly is to measure the rate of incorporation of new tubulin subunits at the tip of the flagellum. In *Chlamydomonas*, incorporation is assessed by mating a strain expressing epitope-tagged HA-tubulin with an untagged tubulin strain. Each pair of mated cells will form a quadriflagellate cell (QFC), a temporary dikaryon with two pairs of flagella. These QFCs retain nearly full-length flagella for up to two hours before the flagella are rapidly resorbed. As the tubulin subunits are turned over at the tip of the flagella, the unlabeled flagella will have new HA-tubulin subunits incorporated at the tip that can be detected by immunofluorescence (Figure 4.6B, [Marshall and Rosenbaum, 2001]).

If *cnk2-1* mutants have reduced disassembly but wild-type rates of assembly, we would observe new HA-tubulin incorporation at the tip of the unlabeled flagella in amounts similar to or greater than wild-type, along with a gradual increase in flagellar length over the course of the experiment. However, if as we predict flagellar assembly is decreased to compensate for decreased disassembly in *cnk2-1* cells, then we would observe a decrease in the amount of HA-tubulin incorporation relative to wild-type and a constant flagellar length. We generated a *cnk2-1* HA-tubulin strain and mated this strain with *cnk2-1* cells with unlabeled tubulin. We incubated the QFCs for 30 or 60 minutes before fixing the cells for immunofluorescence. As predicted, we observe a significantly reduced amount of new tubulin incorporation at the tip of *cnk2-1* mutant flagella compared to wild-type (Figure 4.6C, D).

4.5. Discussion

4.5.1. A ciliary length sensor regulates rates of assembly and disassembly to modify length

The maintenance of normal ciliary length is critical to the normal function of many different types of cilia. *Chlamydomonas* rely on normal ciliary motility and signalling for feeding and mating, and cells with flagella that are too long, too short, or of unequal length do not swim well (e.g. [McVittie, 1972; Asleson and Lefebvre, 1998; Engel et al.,

2011; Avasthi et al., 2012]). In humans and other vertebrates, cilia are essential for developmental and homeostatic signalling processes. When cilia grow abnormally long, many of these functions are interrupted, resulting in disease [Tammachote et al., 2009; Omori et al., 2010; Ozgül et al., 2011; Tucker et al., 2011].

We have shown here that perturbations in ciliary length are associated with changes in the rates of both assembly and disassembly. In *lf4* mutant flagella, an increase in the rate of assembly is likely the cause of the long flagella phenotype [Ludington et al., 2013], and the increase in the rate of disassembly may be a compensatory mechanism (Figure 4.5). Conversely, in *cnk2-1* mutant flagella, a decrease in the rate of disassembly is likely the cause of the long flagella phenotype (Figures 4.2, 4.3, and 4.5), while the decrease in the rate of assembly compensates to maintain near wild-type flagellar length (Figure 4.6).

We propose that a ciliary length sensor detects abnormally long cilia and modulates rates of assembly and disassembly accordingly (Figure 4.7). In our model, ciliary assembly would continue at a high rate until ciliary length exceeds some set length, then the length sensor would stimulate a reduction in the rate of assembly, possibly via the LF4 kinase, and simultaneously activate disassembly via CNK2. This model explains our observation that *lf4 cnk2-1* double mutants have very long flagella because the double mutant cells have lost their ability to control rates of both flagellar assembly and disassembly. Steady state ciliary length is ultimately a consequence of balanced rates of assembly and disassembly [Marshall and Rosenbaum, 2001; Marshall et al., 2005; Engel et al., 2009; Hao et al., 2011; Ludington et al., 2012; Ludington et al., 2013]. We propose that there exists a length sensor that operates through the two kinases, CNK2 and LF4, to provide tight control of length via feedback regulation of the rates of assembly and disassembly.

4.5.2. CNK2 as a regulator of ciliary disassembly

We have shown that the *cnk2-1* mutant, which doesn't express any detectable CNK2 protein, has slightly longer flagella than wild-type, and that it is defective in flagellar resorption in response to NaPPi, IBMX, and solid media (Figure 4.2), unequal flagellar length (Figure 4.3), and the loss of IFT at the restrictive temperature in a *fla10-1*

cnk2-1 double mutant (Figure 4.5). We propose that the defective ciliary resorption and the long flagella phenotype are both consequences of a reduction in the basal rate of flagellar disassembly. Furthermore, that *fla10-1 lf4* double mutant flagella have a higher basal rate of disassembly than *fla10-1 lf4 cnk2-1* triple mutant flagella indicates that CNK2 is required to activate flagellar disassembly when flagella grow too long (Figure 4.5).

To our knowledge, *cnk2-1* is the first *Chlamydomonas* mutant with defective flagellar resorption to be characterized, but other potential components of the resorption signaling pathway have been identified. For example, *Chlamydomonas* aurora-like kinase (CALK) becomes phosphorylated shortly after deflagellation [Pan et al., 2004], and its phosphorylation state and activity changes in response to the length of flagella [Luo et al., 2011; Cao et al., 2013], indicating that it may be a component of the flagellar length-sensing pathway. The phosphorylation state of a *Chlamydomonas* microtubule-depolymerizing kinsein, CrKinesin-13, similarly changes as flagellar length changes during regeneration and shortening, but RNAi of CrKinesin-13 causes short flagella, not long flagella as would be expected for a component of the disassembly pathway [Piao et al., 2009].

Unlike flagellar assembly, which is entirely dependent on IFT (reviewed in [Pedersen and Rosenbaum, 2008]), flagellar disassembly does not require IFT. This is apparent in the temperature-sensitive retrograde IFT mutants *fla15* and *fla17*, defective in components of the IFT-A complex, which resorb at the restrictive temperature similar to *fla10-1* [Piperno et al., 1998; Iomini et al., 2009]. The *dhc1b-3* mutant, which has a temperature-sensitive defect in the retrograde dynein motor, lacks retrograde IFT at the restrictive temperature, and while it does not resorb upon shift to the restrictive temperature, it does resorb in response to NaPPi with wild-type kinetics [Engel et al., 2012]. Therefore it is unlikely that the disassembly defect in *cnk2-1* is caused by a decrease in retrograde IFT.

Exactly how CNK2 could regulate ciliary disassembly remains enigmatic. Whereas FA2, a CNK2-related Nek required for deflagellation, localizes to the site of axonemal severing [Mahjoub et al., 2002; Mahjoub et al., 2004], CNK2 localizes along the length of the axoneme [Bradley and Quarmby, 2005]. The Neks are emerging as

regulators of cilia and cell cycle, both of which are dependent on microtubules, suggesting a role for the Neks as regulators of microtubule dynamics or of processes that depend on microtubules (reviewed in [Fry et al., 2012]). *Arabidopsis* Nek6 (a member of the same clade as mammalian Nek11 [Parker et al., 2007]) negatively regulates microtubule stability, possibly by directly phosphorylating β-tubulin [Motose et al., 2011; Motose et al., 2012], and Nek4 may perform similar functions in mammalian cells [Doles and Hemann, 2010]. CNK2 could similarly alter flagellar microtubule stability directly, by regulating the activity of tubulin post-translational modifications that affect microtubule stability, such as polyglutamylation and acetylation [Pugacheva et al., 2007; Chang et al., 2009; Lacroix et al., 2010; Sudo and Baas, 2010; O'Hagan et al., 2011], or by regulating the microtubule depolymerizing functions of other proteins, such as MCAK [Blaineau et al., 2007]. Future work to dissect the CNK2-dependent disassembly pathway will be invaluable for understanding both the mechanism and regulation of ciliary disassembly.

4.6. Acknowledgements

We are grateful to Hiro Ishikawa, Wallace Marshall, and the Nikon Imaging Center at UCSF for providing tools, equipment, and assistance with the long-zero experiments, and to Olivier Vallon for sharing the *cnk2-1* mutant strain with us. We also appreciate members of the Quarmby Lab, past and present, for their feedback on this work. This research was funded by NSERC Canada Graduate Scholarships to LKH, and NSERC Discovery and Accelerator grants to LMQ.

4.7. Figures

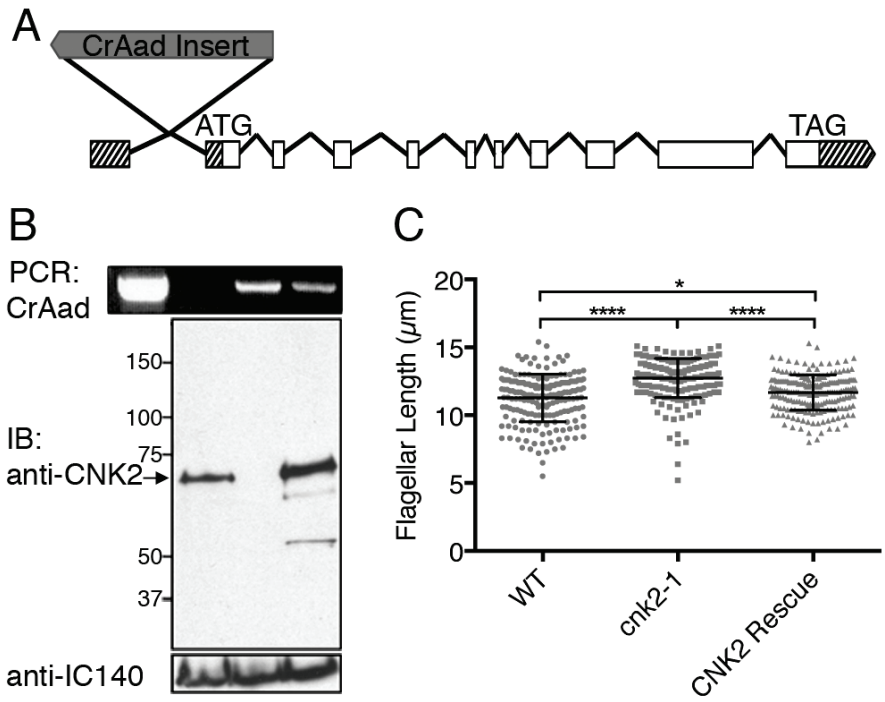

Figure 4.1. The cnk2-1 Mutation Causes a Slight Increase in Steady-State Flagellar Length.

A. The CrAad insert (grey) is inserted in the first intron within the 5' UTR of the *CNK2* gene. Hashed blocks: UTR exons; white blocks: protein coding exons. **B.** Top panel: PCR of the CrAad insert was used to identify *cnk2-1* mutant strains. Middle panel: Western blot of isolated flagella probed with anti-CNK2. Bottom panel: Anti-IC140 western blot as a control for loading of flagellar protein. (+): pALM33 plasmid containing CrAad gene; W: wild-type; C: *cnk2-1*; R: *cnk2-1:CNK2* rescue. **C.** Measurements of flagellar lengths from WT, *cnk2-1*, and *cnk2-1:CNK2* rescue strains. One flagellum from 30-100 cells from each strain were measured in each of three independent experiments. Error bars represent 95% confidence interval. Means were compared by Tukey's HSD; * $p<0.05$, **** $p<0.0001$.

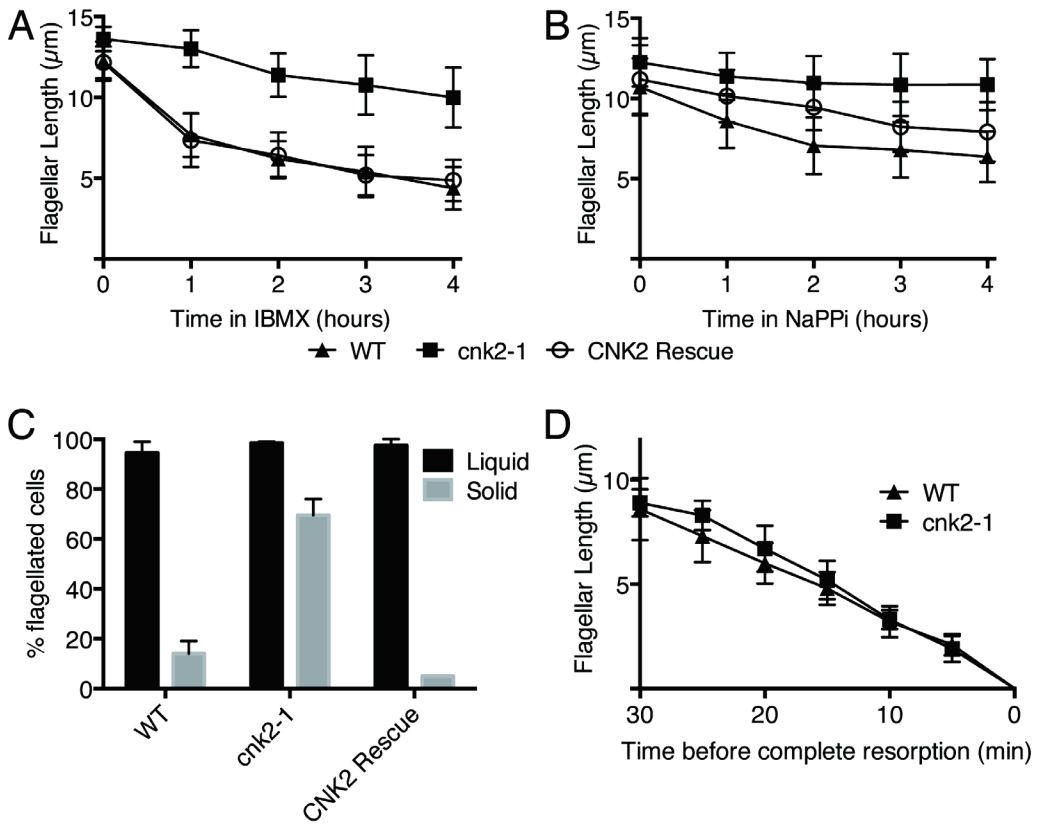

Figure 4.2. cnk2-1 Mutants are Defective in Some Types of Flagellar Resorption. Flagellar lengths of WT, *cnk2-1*, and *cnk2-1:CNK2* rescue strains were measured at hourly intervals of treatment with 1 mM IBMX (**A**) or 20 mM NaPPi (**B**). At least 30 cells were measured at each time point in two independent experiments. Error bars represent standard deviations. **C.** Cells were first maintained in liquid culture for 24 hours and the percentage of cells with flagella was scored (black bars). The cells were then transferred to solid media for 24 hours and again scored for percent flagellation (grey bars). 100 cells were counted for each strain in two independent experiments. Error bars represent standard deviations. **D.** Cells were partially synchronized then embedded in agarose at the beginning of the dark phase and imaged once every minute until resorption and cell division were complete. Flagellar length was measured once every five minutes, working backwards from the time resorption was completed (0 minutes). WT N = 6 from 3 different experiments; *cnk2-1* N = 5 from 3 different experiments, error bars represent standard deviation.

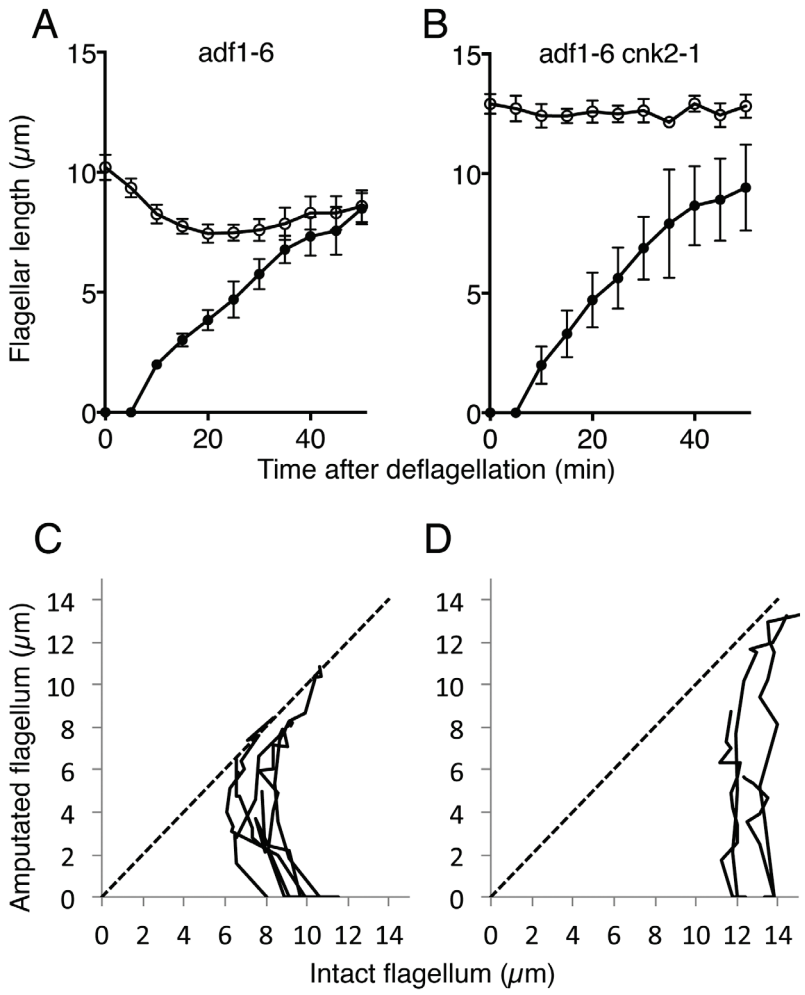

Figure 4.3. CNK2 is Required for the Resorption Phase of Flagellar Length Equalization.

adf1-6 (A, C) or *adf1-6 cnk2-1* (B, D) cells were captured in a microfluidic chamber under continuous flow of fresh media. Deflagellation of a single flagellum was induced by reducing the pH of the media to 4.5 for 1 min with 40 mM sodium acetate, then washing the low-pH buffer out to allow the flagella to regenerate. The length of each flagellum was measured every five minutes for 50 minutes after pH shock. **A, B.** The length of the amputated flagellum (red) and unamputated flagellum (blue) as a function of time post deflagellation. N = 6 cells (A) or 4 cells (B). **C, D.** The length of the amputated flagellum as a fuction of the length of the unamputated (long) flagellum.

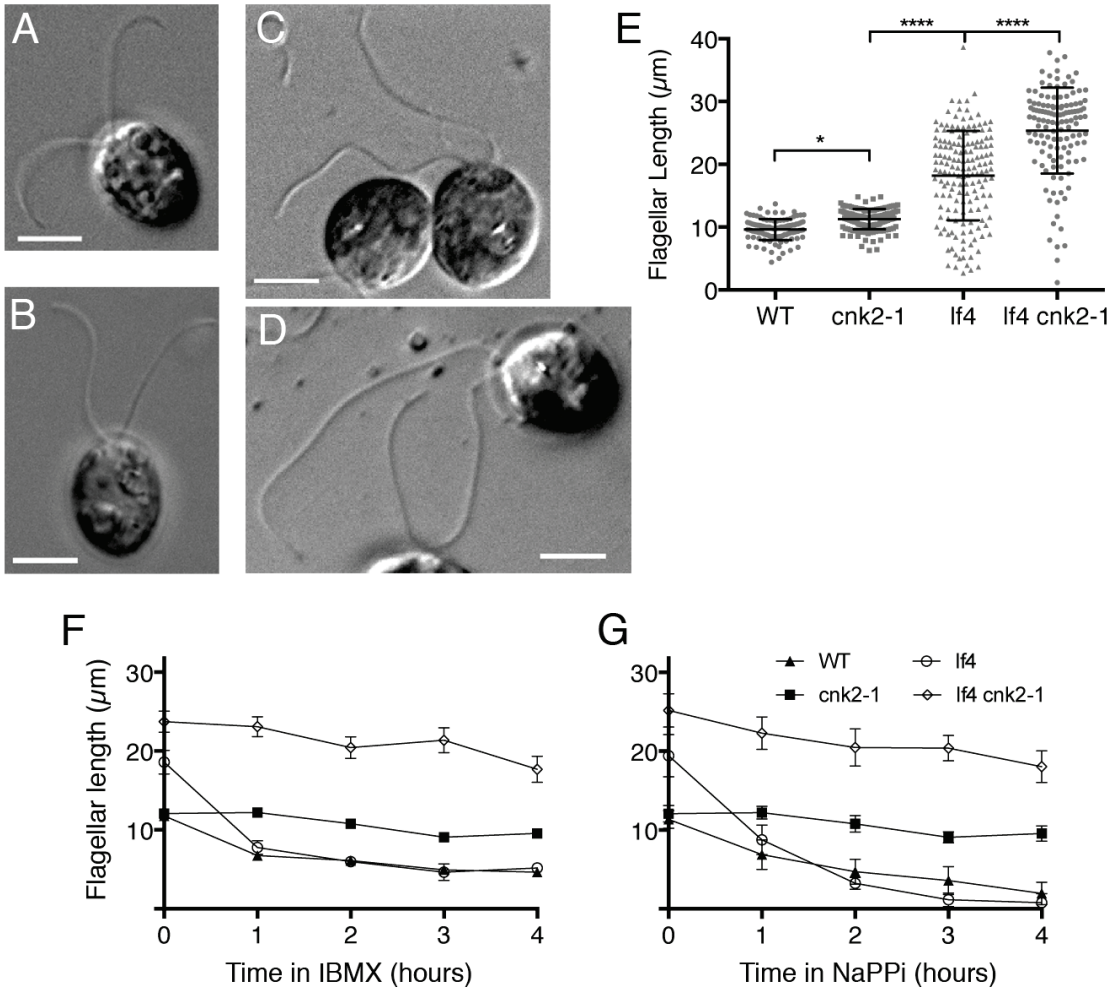

Figure 4.4. lf4 cnk2-1 Double Mutant Flagella are Longer than Single Mutant Flagella.

A-D. Representative DIC images of wild-type (A), *cnk2-1* (B), *lf4* (C), or *lf4 cnk2-1* (D) cells. Scale bar 5 μm. **E.** Distributions and average lengths of wild-type, single mutant, and double mutant flagella. One flagellum from at least fifty cells from each of two different experiments were measured. Error bars represent 95% confidence intervals. Means were compared by Tukey HSD; * $p < .05$; **** $p < .0001$. **F.** Flagellar lengths were measured at hourly intervals during treatment with 1 mM IBMX. For each strain at least 30 cells were measured from each of two independent experiments. Error bars represent 95% confidence intervals. **G.** Same as (B), except cells were treated with 20 mM NaPPi, and 25 cells were measured from one experiment.

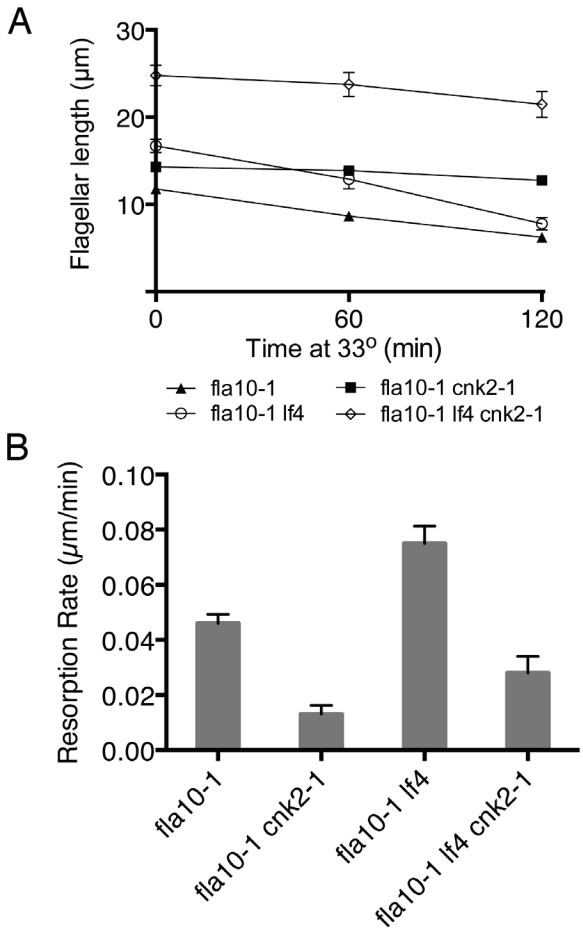

Figure 4.5. The Rate of Flagellar Disassembly is Increased in lf4 Mutant Flagella, Dependent on CNK2.

fla10-1 cells, and double or triple mutants with *lf4* and *cnk2-1*, were maintained in liquid culture at 21°C, and flagellar lengths were measured (0 minutes). Cultures were then shifted to the restrictive temperature (33°C) and lengths were measured each hour for two hours. One flagellum from at least 25 cells from each strain were measured at each time point from each of two independent experiments. **A.** Flagellar length as a function of time at 33°C. Error bars represent 95% confidence intervals. **B.** Linear regression analysis of the data in (A) gives a resorption rate for each strain. Error bars represent standard deviation.

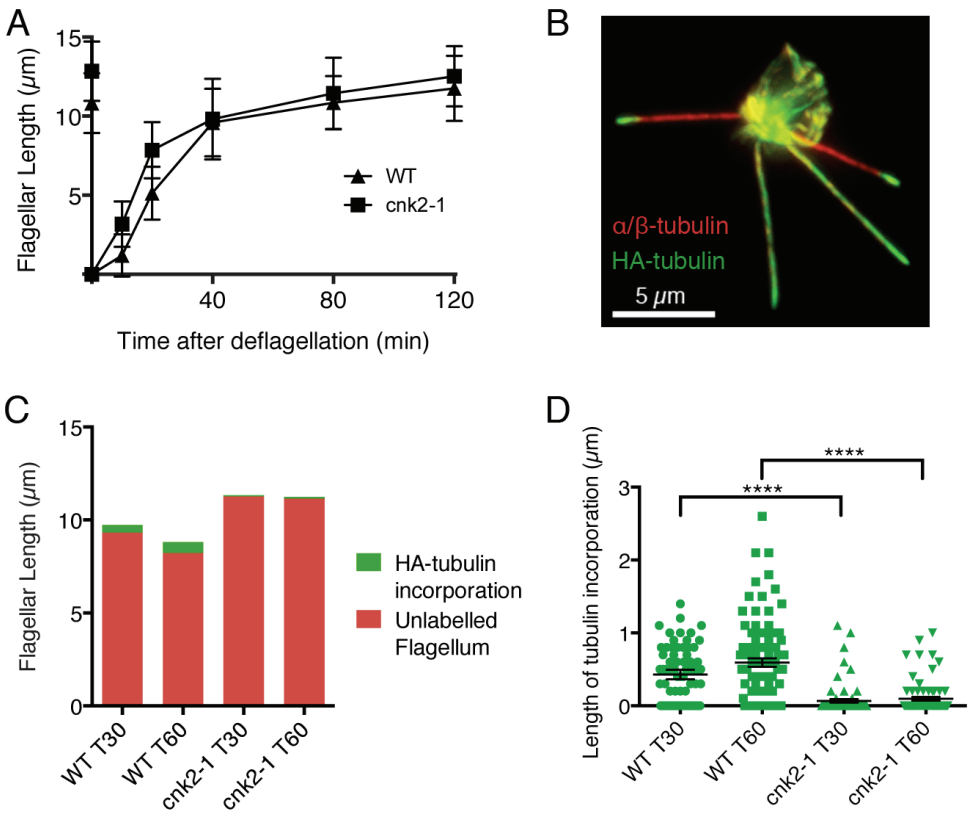

Figure 4.6. Flagellar Assembly is Reduced at Steady-State Length in cnk2-1 Mutant Flagella.

A. Flagellar regeneration kinetics of wild-type and *cnk2-1* mutant flagella were determined by deflagellating cells by pH shock, and measuring flagellar lengths at various time points during regeneration. Flagella from fifty cells were measured at each time point for each strain. Error bars represent 95% confidence interval. **B-D.** Wild-type cells were mated to HA-tubulin cells (WT), or *cnk2-1* cells were mated to *cnk2-1* HA-tubulin cells (*cnk2-1*), and resulting quadriflagellate cells (QFCs) were incubated for 30 or 60 minutes before being fixed and stained with antibodies to α/β-tubulin and HA [8]. **B.** Representative image of a wild-type QFC 60 minutes after mating. **C.** The amount of new tubulin incorporation is measured as the length of the HA-stained section at the distal tip of the flagellum, and flagellar length is measured from the total length of the acetylated tubulin-stained section. **D.** Distributions for the amount of new tubulin incorporation. At least 30 cells from each of two independent experiments were measured at each time point for each strain. Error bars represent 95% confidence interval. Means were compared by Tukey's HSD. **** $p < 0.0001$.

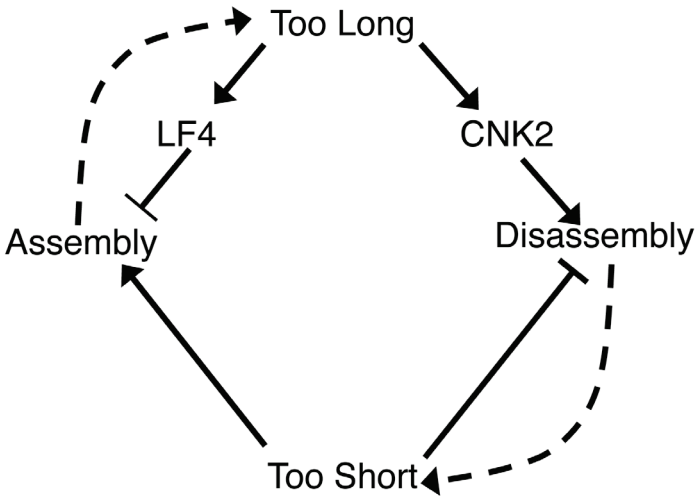

Figure 4.7. A Model for Flagellar Length Control by Feedback Regulation Involving Both Assembly and Disassembly.

Flagella become too long when assembly exceeds disassembly (dashed line, top right). Once they become too long, they can reduce their overall length by activating disassembly via CNK2 and by inhibiting assembly via LF4. Similar regulatory mechanisms could act to inhibit disassembly and activate assembly when flagella become too short.

5. Conclusions and Future Directions

5.1. Nek1, Ciliogenesis, and Nuclear Cycling

In Chapter 2, I reported that Nek1, which normally localizes to centrosomes, is also continually cycling through the nucleus. We know this because blocking nuclear export with the CRM1 inhibitor Leptomycin B causes Nek1 to accumulate in the nucleus. I demonstrated that Nek1 contains at least two functional nuclear localization signals (NLS), one of which was defined by sequence analysis and mutagenesis, the other of which remains cryptic. In Chapter 2, I suggested that the purpose of Nek1 nuclear cycling might be to relay signals between the centrosome/cilium and the nucleus. Here, I will elaborate on the possible nuclear functions of Nek1, the signals that may regulate its nuclear localization, and the relationship to human health and disease.

The *Nek1*$^{kat\text{-}2J}$ mutation in mice is an insertion of a single guanosine at position 996 in the Nek1 cDNA, resulting in a premature stop codon [Upadhya et al., 2000]. Several groups have confirmed that this is a null mutation, and that *Nek1*$^{kat\text{-}2J/kat\text{-}2J}$ homozygotes do not express any detectable Nek1 protein [Polci et al., 2004; Feige et al., 2006]. These mice are characterized by runting, facial dysmorphism, anemia, male sterility, hydrocephalus, and progressive polycystic kidneys [Vogler et al., 1999]. They survive into adulthood and ultimately succumb to renal failure before one year of age, indicating that Nek1 is important for normal development and homeostasis in mice but is not essential for viability [Vogler et al., 1999].

In contrast, null mutations of Nek1 in humans cause short rib-polydactyly syndrome (SRPS) type II or type III, and always result in embryonic lethality [Thiel et al., 2011; Chen et al., 2012a; Chen et al., 2012b; El Hokayem et al., 2012]. Some features of this disorder are similar to the mouse phenotype, including facial dysmorphism and cystic kidneys, but it is distinguished by skeletal abnormalities including short ribs, short limbs, and polydactyly. Cultured fibroblasts from a Nek1 SRPS embryo and from Nek1$^{kat\text{-}2J/kat\text{-}2J}$ mice both produce short, stumpy cilia in a small fraction of cells and no

cilia in the remainder of cells [Shalom et al., 2008; Thiel et al., 2011]. Additionally, they have abnormal acetylated microtubule structures in the cytoplasm [Shalom et al., 2008; Thiel et al., 2011]. Thus, null mutations of Nek1 have similar effects at the cellular level in both humans and mice, but have much more severe effects on development in humans.

SRPS types II and III can also be caused by mutations in *DYNC2H1,* the gene encoding the cytoplasmic dynein retrograde IFT motor; *IFT80*, encoding an IFT complex B protein; and *WDR35*, encoding the IFT121 complex A protein (reviewed by [Huber and Cormier-Daire, 2012]). Mutations in any of these components abolish ciliogenesis, and consequently hedgehog signalling and osteogenesis are severely disrupted. Many of the clinical features of SRPS, such as cystic kidneys and polydactyly, are hallmark features of a variety of ciliopathies (e.g. [Davis and Katsanis, 2012]). These data strongly implicate ciliary defects in the pathology of SRPS, yet Nek1 has been most extensively characterized as a component of the DNA damage response (DDR).

The DNA damage response pathway involves the activation of two kinases, ATM (ataxia telangiectasia mutated) and ATR (ATM- and Rad3-related) in response to DNA double strand breaks (reviewed by [Heijink et al., 2013]). Upon activation, ATM and ATR (in complex with its interacting protein, ATRIP) phosphorylate the checkpoint kinases Chk2 and Chk1, respectively [Heijink et al., 2013]. Chk1 and Chk2 then maintain the Cdc25 phosphatase in its inactive form, which prevents the dephosphorylation and activation of either CyclinE/Cdk2 (causing G1 arrest and S-phase delay) or Cyclin B/Cdk 1 (causing G2 arrest) [Donzelli and Draetta, 2003]. Ultimately, the effect of the activation of these DDR checkpoints is a delay in cell cycle progression until DNA damage can be repaired [Heijink et al., 2013]. ATM and ATR-ATRIP localize to DNA damage foci within the nucleus when this pathway is activated [Heijink et al., 2013].

The role of Nek1 in the DDR may provide the best explanation for the ability of Nek1 to cycle through the nucleus. In cell culture, treatment with ionizing radiation causes Nek1 to accumulate in the nucleus and associate with DNA damage repair proteins at the DNA damage foci [Polci et al., 2004]. Nek1 mutant MEFs are also more susceptible to the deleterious effects of ionizing radiation than wild-type MEFs, and fail to arrest properly at G1/S and G2/M checkpoints in response to DNA damage [Polci et

al., 2004; Chen et al., 2008; Pelegrini et al., 2010]. Recent data indicates that Nek1 functions upstream of ATR-ATRIP, and that its kinase activity is important for phosphorylation and activation of Chk1 [Chen et al., 2011; Liu et al., 2013]. These data suggest that Nek1 cycles through the nucleus and becomes trapped there upon activation of the DDR.

Although the DDR and ciliogenesis are diverse cellular pathways, the dual role of Nek1 in both of these situations may be indicative of a connection. Recent data suggest that the cilium might function as a cell cycle checkpoint, and that a delay in pre-mitotic ciliary resorption causes a delay in cell cycle progression (see Section 1.2, [Pugacheva et al., 2007; Kim et al., 2011; Li et al., 2011; Plotnikova et al., 2012]). However, an exact mechanism for how delayed resorption might lead to cell cycle arrest has not yet been identified. I hypothesize that Nek1 functions at centrosomes to sense the state of the cilium as the cell approaches mitosis. If ciliary resorption is incomplete, Nek1 could relay that signal to the DDR to activate cell cycle arrest. This hypothesis could be tested by inducing delayed pre-mitotic resorption, for example by siRNA of HDAC6, and examining the localization of Nek1 and the activation of DDR components such as Chk1. If my hypothesis is correct, then Chk1 should become phosphorylated and activated in these cells in a Nek1-dependent pathway.

While this hypothesis justifies the role of Nek1, a centrosomal protein, in the DDR, it does not explain its role in ciliogenesis. Recently, it has been proposed that p53, a tumour suppressor that is regulated by both ATM and ATR-ATRIP, promotes quiescence in stem cells (reviewed by [Sperka et al., 2012]). Since ciliation is a hallmark of quiescence, this implicates the DDR in the signals that regulate ciliogenesis. In one study, TEM of fibroblasts from a human Nek1-deficient SRPS patient revealed the absence of ciliary vesicles on the centrioles of serum-depleted quiescent cells [Thiel et al., 2011]. This indicates that Nek1 is involved in the signalling pathways that are involved in the earliest stages of ciliogenesis. Furthermore, CEP164, a component of the centriolar distal appendages that are required for ciliary vesicle formation and basal body docking, also interacts with the DDR pathway, and mutations in the gene encoding CEP164 are associated with a nephronophthisis-type disease [Graser et al., 2007; Chaki et al., 2012]. It would be very informative to examine the effects of p53 on the activity of

Nek1, and to examine the effects of Nek1 on the assembly of centriolar components like CEP164, to determine how Nek1 and the DDR contribute to ciliogenesis.

Lastly, it would be valuable to examine the roles of Nek1 orthologs in other organisms. In *Chlamydomonas*, the Nek1 ortholog is CNK10 [Parker et al., 2007], although they share less than 25% overall sequence identity. Recently, Susan Dutcher's lab identified a *cnk10* mutant in a screen for Taxol-sensitive mutants generated by insertional mutagenesis (H. Lin and S. Dutcher, personal communication). Early characterization has revealed a flagellar regeneration defect, and a mysterious cell survival phenotype that manifests as cell death after two weeks on solid agar media (H. Lin and S. Dutcher, personal communication). It is tantalizing to speculate that this cell survival phenotype is related to a DDR-type pathway in *Chlamydomonas*. This would indicate remarkable functional conservation of the Nek1 clade across billions of years of evolution, despite major sequence divergence.

5.2. Resorption and Deflagellation Converge: Severing at the PSOS

As I described in Section 1.4 (Ciliary Resorption and Deflagellation), evidence from *Chlamydomonas* suggests that flagellar resorption and deflagellation share common mechanisms and/or signalling pathways. In Chapter 3, Jeremy Parker and I described yet another instance of overlap between these two pathways when we demonstrated that pre-mitotic resorption culminates in an axonemal severing event that separates the basal body from the transition zone at the PSOS. We speculated that such a severing event might be essential for cell cycle progression in *Chlamydomonas*, and may be conserved in ciliated eukaryotes.

Further evidence for the essential nature of this severing event comes from Quarmby lab research into the pathways and mechanisms that control deflagellation. In 1998, Finst et al. conducted a genetic screen for *Chlamydomonas* mutants with defects in deflagellation using a combination of insertional and UV mutagenesis (see Section 1.4 for a description of the mutants recovered). This screen produced 4-6 mutant alleles of each of three genes, *adf1, fa1,* and *fa2,* so it appeared to be saturated. However, this

cannot represent a complete parts list for deflagellation, because we know that deflagellation requires a calcium sensor to activate the severing machinery in response to calcium influx and a microtubule severing protein (such as katanin) to directly sever the microtubule axoneme. If pre-mitotic PSOS severing relies on some of the same components as deflagellation severing at the SOFA (Figure 5.1), then these additional components could be missing from the deflagellation screen because they would be essential for cell survival and therefore would not have been uncovered in the screen.

To address this issue, the Quarmby lab is currently conducting a second genetic screen to identify conditional temperature-sensitive (ts) deflagellation mutants, with the hypothesis that some ts deflagellation mutants will be ts-lethal due to defects in cell cycle progression. So far, the screen has produced multiple new alleles of *adf1, fa1,* and *fa2*; one allele of a new gene, *adf2*; a still-unnamed ts mutant with a phenotype ts for fa and non-ts for adf; and 3 ts *fa* mutants that are still in the very early stages of characterization. Whereas *adf* mutants are defective in the calcium influx that activates the severing machinery, *fa* mutants are defective in the severing machinery and its direct regulatory components. This means that PSOS mutants, including the elusive calcium sensor and microtubule severing proteins, should have *fa* phenotypes with respect to deflagellation. Therefore isolating more ts *fa* mutants, and identifying the causative mutations, is the number one priority to assembly the parts list for severing at the PSOS and the SOFA.

It is worth noting that the *Chlamydomonas fa2* mutant also has a delay in cell cycle progression that manifests as large cell size, but that this does not appear to be related to defective PSOS severing. Rasi et al. [2009] observed the presence of flagellar remnants in the mother cell wall of mitotic *fa2-3* mutant cells, indicating that PSOS severing is intact. Live cell imaging of *fa2* mutants during mitosis confirmed that pre-mitotic resorption and PSOS severing proceed normally (my own unpublished observations). However, FA2 may affect cell size and cell cycle progression by coordinating the timing of pre-mitotic resorption with cell cycle. In wild-type cells, after pre-mitotic resorption the cell cortex rotates 90° relative to the cell wall before mitosis proceeds, so the cleavage furrow forms perpendicular to the long axis of the cell. I found that *fa2* mutant cells rarely undergo cortical rotation, so the cleavage furrow forms parallel to the long axis of the cell (data not shown). This may indicate that the cell is

already primed for division before resorption is complete, and that the delay in pre-mitotic resorption leaves the cell without enough time to complete cortical rotation prior to division. That FA2 is also a Nek lends support to the hypothesis that the Neks are coordinators of cilia and the cell cycle.

Phylogenetic analysis of the Neks revealed that FA2, along with CNK2 and its paralog CNK1, belongs to a clade that is only represented in protists [Parker et al., 2007]. Remarkably, when FA2-GFP is expressed in mouse kidney epithelial cells in cell culture, it localizes to the ciliary transition zone and to the proximal end of both mother and daughter centrioles in a pattern that is very similar to what is observed in *Chlamydomonas* cells [Mahjoub et al., 2004]. FA2-GFP also localizes to the cytokinetic midbody that connects the cytoplasm of recently divided daughter cells [Mahjoub et al., 2004]. The presence of FA2-GFP at both of these sites may indicate that a microtubule severing complex, involved in both axonemal severing and midbody abscission, may exist in mammalian cells and may be conserved between mammals and *Chlamydomonas*. Although the phylogenetic analysis of the Neks doesn't indicate a direct mammalian ortholog of FA2, it doesn't rule out the presence of a functional ortholog. One candidate is Nek2, which has a very similar localization pattern in ciliated cells as FA2-GFP [Spalluto et al., 2012]. Furthermore, siRNA of Nek2 in cell culture delays pre-mitotic ciliary resorption until after centrosomes have separated [Spalluto et al., 2012], an effect that bears similarity to the delayed cell cycle progression in *Chlamydomonas fa2* mutants.

In *Chlamydomonas* cells, the transition zone is relatively structurally elaborate, including a large electron-dense "H" structure of unknown function or composition at its core that clearly distinguishes the distal and proximal ends [Ringo, 1967]. Comparatively speaking, the transition zone of primary cilia is simple (reviewed in [Fisch and Dupuis-Williams, 2011]). Whereas the sites of axonemal severing in *Chlamydomonas* cells are positioned at either end of the transition zone, these two sites may be compressed into a single site that executes both stress-related deciliation and pre-mitotic severing in mammalian cilia. If this is the case, then it is likely that FA2-GFP interacts with components of this combined SOFA/PSOS when it is expressed in mammalian cells. Quarmby Lab graduate student Mette Lethan is currently attempting to identify components of the mammalian severing complex by co-immunoprecipitating them with

FA2-GFP. Together with new *Chlamydomonas* mutants identified in the conditional deflagellation mutant screen, these data should provide a thorough list of important components for pre-mitotic severing.

Once the PSOS components have been identified, RNAi experiments could be used to assess the functions of these components in mammalian cells. For example, defects in mitotic entry could indicate that PSOS severing acts as a mitotic checkpoint that prevents cells from going on in mitosis until it is complete. This could be the event that Nek1 communicates to the DDR checkpoint (see section 5.1). Alternatively, in organized tissues where the plane of cell division is important for maintaining tissue architecture, loss of PSOS severing could interfere with spindle orientation and result in disorganization. This type of disorganization is hypothesized to contribute to the formation of kidney cysts [Jonassen et al., 2008], making PSOS components excellent candidates for human ciliopathy genes.

5.3. CNK2 in Ciliary Length Control

In Chapter 4, I demonstrate that a *Chlamydomonas* flagellar Nek, CNK2, regulates both flagellar resorption and length by regulating the rate of axonemal disassembly. I also show that another kinase, LF4, participates in flagellar length control by regulating the rate of assembly. My data provide an important framework for understanding how ciliary length is controlled by demonstrating that rates of assembly and disassembly are both actively regulated when flagella are too long.

The tight control of ciliary length is critical for the function of cilia in many developmental, homeostatic, and sensory processes. In *Chlamydomonas,* flagella that are too long or too short interfere with normal motility. In the wild, this would interfere with a cell's ability to move toward optimal sunlight conditions for photosynthesis. Since mating is also dependent on flagella in *Chlamydomonas*, long or short flagella would severely compromise fitness. Therefore it is likely that wild-type flagellar length has been evolutionarily selected.

In vertebrates, where the primary cilia are the hub of developmental and homeostatic signalling processes, the correct ciliary length is important for their normal

function. When cells are induced to have multiple cilia by inducing supernumerary centrosomes, the same number of signalling molecules (including the Shh effector, Smo) is produced, but they are distributed among a greater number of cilia [Mahjoub and Stearns, 2012]. This dilution dramatically reduces the efficacy of the Shh signalling pathway [Mahjoub and Stearns, 2012]. A similar dilution of the signalling molecules could be created in abnormally long primary cilia, and could be a contributing factor in the etiology of ciliopathies like Meckel Syndrome, which has phenotypes related to defective Shh signalling and has been associated with long primary cilia [Tammachote et al., 2009]. In *Chlamydomonas*, where signals in the flagellum are generated during mating in response to flagellar adhesion, having extra-long flagella could similarly dilute the signals and reduce overall mating efficiency. Since long flagella mutants have reduced mating efficiency compared to wild-type (my own unpublished observations), it could be valuable to determine whether this is due to decreased motility and difficulty in finding mating partners, or due to a dilution of the flagellar agglutinins and the downstream signalling effectors.

In ciliated cells that re-enter the cell cycle, long cilia may interfere with the timing of cell division by delaying the completion of pre-mitotic resorption. Depletion of either Tctex-1 or Nde1 causes long cilia and delays in cell cycle re-entry [Kim et al., 2011; Li et al., 2011; Palmer et al., 2011]. Surprisingly, in *Chlamydomonas*, the presence of very long flagella does not seem to have this effect on the cell cycle. However, to my knowledge, a close-up examination of the growth rates or pre-mitotic resorption has not been conducted yet for any of the five *lf* mutants. My work in Chapter 4 demonstrated that *lf4* mutants have an accelerated rate of disassembly, which cells could take advantage of to complete pre-mitotic resorption rapidly, thereby minimizing the effect on the cell cycle. Alternatively, *lf* mutants could be executing PSOS severing before complete resorption, leaving longer flagellar remnants. Either way, the *Chlamydomonas lf* mutants could be valuable tools for identifying the mechanisms by which cells deal with long cilia during mitosis.

In terminally differentiated cells, such as photoreceptors in the vertebrate eye or sensory neurons in *C. elegans*, long cilia usually degenerate over time probably due to structural instability. The mammalian homolog of *Chlamydomonas* LF4, MAK, also regulates ciliary length. When MAK is mutated in humans or mice, the result is

elongation of the photoreceptor connecting cilium and gradual degeneration of the photoreceptor outer segment [Omori et al., 2010; Ozgül et al., 2011; Tucker et al., 2011]. Mutations in the gene encoding the *C. elegans* homolog of LF4, DYF-5, also cause elongation of the neuronal sensory cilia, accompanied by structural defects [Burghoorn et al., 2007]. The *C. elegans dyf-18* mutant, which disrupts the gene encoding the homolog of the *Chlamydomonas* LF2 CDK-like kinase, has also been characterized, and causes long, curly cilia and mild structural defects similar to those observed in the *dyf-5* mutant [Phirke et al., 2011]. Remarkably, the presence of homologs of both LF4 and LF2 with similar functions in metazoans indicates that the signalling pathways that control ciliary length are highly conserved throughout evolution.

Unlike LF4 or LF2, CNK2 belongs to the same protist-only clade of Neks as FA2 and therefore does not have a direct mammalian ortholog [Parker et al., 2007]. As I have already discussed for FA2 (see Section 5.2), this does not rule out the possibility that mammalian cells have a functional ortholog for CNK2. Brian Bradley demonstrated that CNK2-GFP localizes to the primary cilium in IMCD3 cells (Figure 5.2). These data are especially remarkable because the primary cilium is a much more streamlined structure than the elaborate *Chlamydomonas* motile flagellum, and indicate that core components of the complex with which CNK2 interacts may be conserved.

The ciliary localization of CNK2 in mammalian cells may be a valuable tool for identifying components of this length control complex. This could be done by expressing epitope-tagged CNK2 in IMCD3 cells, performing immunoprecipitation, and identifying interacting proteins by mass spectrometry. I have attempted a similar workflow in *Chlamydomonas*, but was unable to isolate CNK2-HA by immunoprecipitation. In addition to a binding partner approach, the powerful genetics of *Chlamydomonas* could be used to identify new components of the CNK2 resorption/length control pathway. I could enrich for mutants by taking advantage of the fact that *Chlamydomonas* cells are phototactic. Cells that fail to resorb in response to NaPPi or IBMX could be separated from wild-type cells on the basis of their ability to swim towards a light source because they maintain full-length flagella in these treatments. Mutagenesis could also be performed on *cnk2-1* mutant cells to look for second-site mutations that suppress the *cnk2-1* phenotype. Using an insertional mutagenesis approach similar to the one that

generated the *cnk2-1* mutant would allow rapid identification of causative mutations by 3'-RACE [Meslet-Cladière and Vallon, 2012].

This genetic approach may be especially valuable for identifying the elusive length sensor that relays information about incorrect flagellar length to the LF4 and CNK2 signalling pathways. One important system that may contribute to the sensation and regulation of flagellar length is Ca^{2+} [Rosenbaum, 2003]. Importantly, the amount of current generated by Ca^{2+} influx is proportional to the length of the flagella, indicating that number of voltage-gated Ca^{2+} channels in the flagellum also correlates with flagellar length [Beck and Uhl, 1994]. It is reasonable to predict, then, that long flagella would have higher Ca^{2+} current than wild-type length flagella, in which case high levels of Ca^{2+} would cause flagella to shorten. This is consistent with a number of stimuli that cause flagellar resorption. As I mentioned in Section 1.4, when deflagellation-defective *fa* mutants are treated with pH shock, they resorb instead of deflagellating. Since the pH shock induces an influx of Ca^{2+} into the cell, it is possible that this increase in intracellular Ca^{2+} is triggering the resorption response. Moreover, NaPPi and IBMX, the chemicals I used to induce resorption in Chapter 4, may both be influencing intracellular Ca^{2+}. Although it has been hypothesized that NaPPi is acting as a Ca^{2+} chelator, and that low levels of Ca^{2+} are responsible for resorption in NaPPi-treated cells [Lefebvre et al., 1978], preliminary experiments revealed that NaPPi induces a stronger resorption effect in media with high levels of Ca^{2+} (1 mM) than in media with no added Ca^{2+} (Kavisha Gunawardane, unpublished observations). Further experiments are required to determine whether increased Ca^{2+} is, in fact, responsible for the resorption effect of NaPPi. Finally, as IBMX is a cyclic nucleotide phosphodiesterase inhibitor, its effect on *Chlamydomonas* flagella is likely an increase in cAMP and/or cGMP levels. As a second messenger, cAMP is often responsible for inducing Ca^{2+} influx or release from intracellular stores, so IBMX may also be causing an increase in Ca^{2+} within the flagellum. Such a Ca^{2+} signal could be translated into effects on both assembly and disassembly to effect changes in overall flagellar length.

How, then, would changes in Ca^{2+} be translated into changes in the rate of assembly? Since IFT is required to deliver new flagellar subunits to the tip of the flagellum for assembly to occur, it is possible that the regulation of assembly occurs at the level of regulating IFT. From data in *lf4* mutant cells, we know that the rate of

injection of IFT particles is increased in long flagella. If IFT is the key regulatory step in *cnk2-1* mutants, then I would expect to observe a decrease in the overall rate of IFT particle injection into the flagella. If instead I observe no change in the rate of IFT in *cnk2-1* mutants, this would indicate that the rate of assembly is being regulated some other way.

The regulation of assembly rates could alternatively be achieved by regulating the affinity of IFT complexes for their cargos. This is an aspect of IFT that is still largely uncharacterized. Recently, the rate of tubulin transport and incorporation was measured in *C. elegans* cilia [Hao et al., 2011]. However, one cannot observe events related to ciliogenesis, ciliary resorption, or perturbations to ciliary length in *C. elegans*, so this data is only informative for cargo transport for maintenance of steady-state length. In many ways, this makes *Chlamydomonas* the ideal system for studying the relationship between cargo transport and ciliary length. At the 2013 FASEB Biology of Cilia and Flagella meeting, Dr. Karl Lechtreck reported a system for measuring the rate of transport of two *Chlamydomonas* axonemal components that participate in the regulation of motility: DRC4, a component of the dynein regulatory complex, and PF16, a central pair component. This has enabled, for the first time, direct measurement of the correlation between the movement of IFT complex proteins and motors with cargo transport. Although DRC4 and PF16 are important components of the axoneme, they are not required for ciliogenesis and do not directly contribute to axonemal elongation. Once a system for measuring the trafficking of tubulin has been developed, it will be possible to directly measure how the association of IFT particles with tubulin cargo contributes to the regulation of flagellar length. Consistent with my hypothesis that Ca^{2+} may act as the length sensor, intraflagellar Ca^{2+} levels were recently shown to regulate the binding of IFT particles to flagellar membrane glycoproteins to control flagellar surface motility [Shih et al., 2013]. Similar regulation by Ca^{2+} levels could conceivably contribute to regulating the loading of tubulin cargo onto IFT.

It is more difficult to speculate on the ways in which flagellar disassembly is regulated, especially because my data is the first to show that disassembly is regulated at all. However, flagellar microtubules are stable compared to cytoplasmic microtubules, possibly due to the presence of microtubule stabilizing components at the tip of the flagellum. The microtubule +-end tracking protein (+TIP) EB1 localizes to the tips of

Chlamydomonas flagella, and is required for ciliogenesis in mammalian primary cilia [Pedersen et al., 2003; Schroder et al., 2007]. EB1 itself, or other +TIPs, could function to regulate the flagellar microtubule disassembly rate, helping to keep it low during flagellar elongation and increasing it when flagella are too long or need to be resorbed. Microtubule depolymerizing kinesins of the kinesin-13 family, one of which has been identified in *Chlamydomonas*, may also participate in the regulation of disassembly [Piao et al., 2009]. The proteomics and genetics approaches that I have suggested for the flagellar resorption pathway may help identify more components that are involved in regulating both the rates of assembly and disassembly.

Finally, I would like to address the role of CNK2, a Nek, in cell cycle regulation. Previous work in the Quarmby lab demonstrated that overexpression of CNK2 was associated with smaller cell size, while RNAi was associated with larger cell size, and it was concluded that CNK2 regulates the minimum commitment size for division (see section 1.2, [Bradley and Quarmby, 2005]). As part of the characterization of the *cnk2-1* mutant strain, I attempted to examine the commitment size of the mutants but was unable to find a consistent phenotype, nor was I able to identify any genetic interactions between *cnk2-1* and other commitment size mutants. This result is inconclusive and requires further follow-up, but a lack of cell cycle phenotype of the *cnk2-1* mutant would be consistent with the observation that CNK2 is not required for pre-mitotic resorption (Figure 4.2). The cell size phenotype previously reported may have been associated with off-target effects of the RNAi construct used, and possibly to mild cytotoxic effects of overexpressing CNK2 in a wild-type background. This would make CNK2 one of few Neks characterized to-date with no discernible effects on the cell cycle. However, CNK2 and its paralog CNK1 arose from a gene duplication that occurred quite recently in the *Chlamydomonas* lineage [Parker et al., 2007]. Subfunctionalization often occurs as a consequence of gene duplication, where each paralog evolves to perform only a subset of the functions that the single ancestral gene performed. Limited characterization of CNK1 has been performed so far, but I would hypothesize that it has retained the cell cycle functions that have been lost from CNK2. Given the sequence similarity between CNK1 and CNK2, it is also possible that CNK1 was one of the off-target effects of the CNK2 RNAi, and that this was responsible for the observed cell cycle phenotype [Bradley and Quarmby, 2005].

5.4. Perspectives

My work has used *Chlamydomonas* and mouse tissue culture cells to examine the functions of two diverse members of the NIMA-related kinase family, *Chlamydomonas* CNK2 and mouse Nek1. Since I completed my work showing that Nek1 cycles between the nucleus and the centrosomes, a significant amount of data has been produced to show that Nek1 functions in the DNA damage response. This makes Nek1 a dual-role Nek, with functions in both cilia and cell cycle regulation, similar to the original dual-role Nek, *Chlamydomonas* FA2. It will be valuable to tie the ciliary roles of Nek1 to its cell cycle roles to advance our understanding of how cilia and the cell cycle are mutually controlled. Although I did not identify any cell cycle roles for CNK2, I did find that CNK2 participates in an important length control pathway in *Chlamydomonas*. The mechanisms by which length is sensed and assembly and disassembly regulated remain elusive. Nonetheless, ciliary length control may be an excellent target for drug development to treat adult-onset degenerative ciliopathies such as PKD and retinitis pigmentosa. My results with CNK2 provide a framework in which to understand how such treatments could work. Lastly, my work helped to characterize an axonemal severing event that occurs as a (likely) essential last step in pre-mitotic ciliary resorption. The Quarmby lab is already employing multiple strategies to identify components that participate in the execution of this event, and it's reasonable to expect that members of the Nek family will be involved. Altogether, my work significantly advances our understanding of the roles of Neks in regulating cilia and the cell cycle.

5.5. Figures

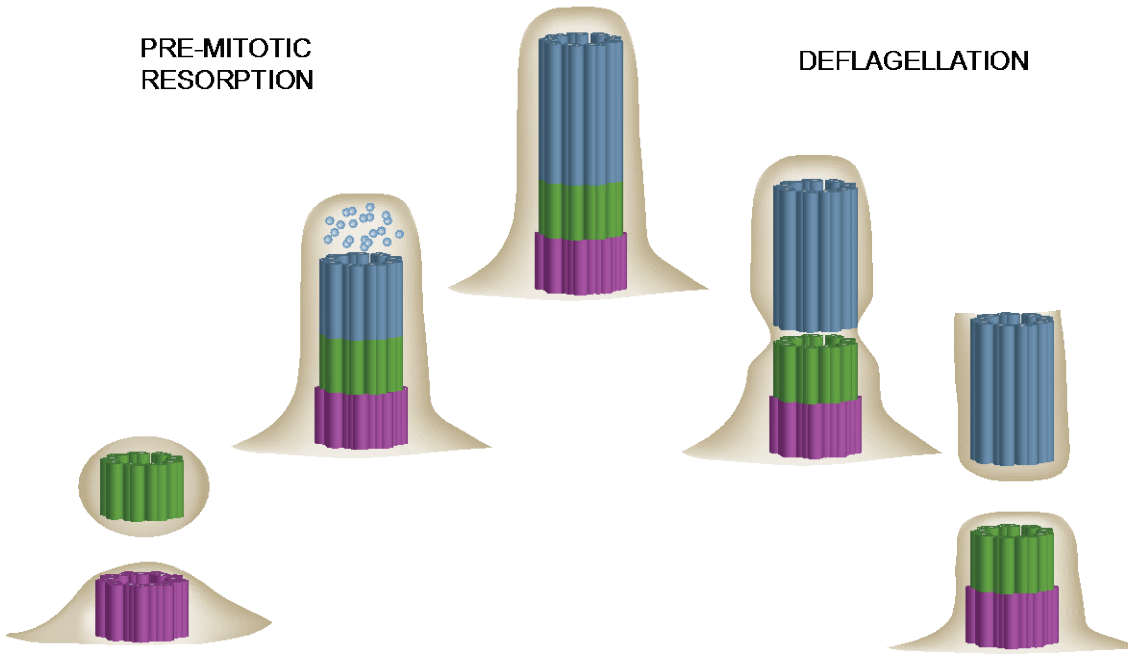

Figure 5.1. Pre-mitotic Resorption vs. Deflagellation.
During pre-mitotic resorption (left side) the cilium is disassembled from the tip-down, and axonemal components are returned to the cell body. Once the axoneme (blue) is disassembled, the remainder of the transition zone (green) is severed from the basal body (pink) at the proximal site of severing (PSOS). The membrane pinches off to seal the cell, leaving the transition zone in a vesicle. During deflagellation (right side) the axoneme is severed at the distal end of the transition zone, at the site of flagellar autotomy (SOFA). As in PSOS severing, the membrane pinches off over the transition zone to seal the cell, and the flagellum is shed.

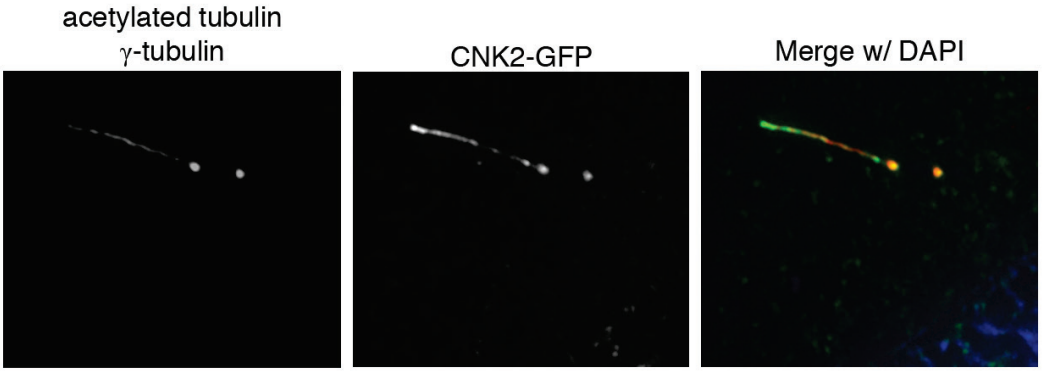

Figure 5.2. Chlamydomonas CNK2-GFP Localizes to Cilia in mouse IMCD3 cells. Mouse inner medullary collecting duct cells were transfected with pEGFP-CNK2 (green), and fixed and stained with antibodies to acetylated tubulin (cilium, red) and γ-tubulin (centrosome, red). Blue: DAPI, nucleus. Image by Brian Bradley.

References

Albee AJ, Kwan AL, Lin H, Granas D, Stormo GD, Dutcher SK. 2013. Identification of Cilia Genes That Affect Cell-Cycle Progression Using Whole-Genome Transcriptome Analysis in Chlamydomonas reinhardtti. *G3 (Bethesda)* 3:979-91.

Allen JJ, Li M, Brinkworth CS, Paulson JL, Wang D, Hubner A, Chou WH, Davis RJ, Burlingame AL, Messing RO, Katayama CD, Hedrick SM, Shokat KM. 2007. A semisynthetic epitope for kinase substrates. *Nat Methods* 4:511-6.

Asleson CM, Lefebvre PA. 1998. Genetic analysis of flagellar length control in Chlamydomonas reinhardtii: a new long-flagella locus and extragenic suppressor mutations. *Genetics* 148:693-702.

Avasthi P, Marley A, Lin H, Gregori-Puigjane E, Shoichet BK, von Zastrow M, Marshall WF. 2012. A chemical screen identifies class a g-protein coupled receptors as regulators of cilia. *ACS Chem Biol* 7:911-9.

Baldari CT, Rosenbaum J. 2010. Intraflagellar transport: it's not just for cilia anymore. *Curr Opin Cell Biol* 22:75-80.

Ballif BA, Villen J, Beausoleil SA, Schwartz D, Gygi SP. 2004. Phosphoproteomic analysis of the developing mouse brain. *Mol Cell Proteomics* 3:1093-1101.

Barr MM, DeModena J, Braun D, Nguyen CQ, Hall DH, Sternberg PW. 2001. The Caenorhabditis elegans autosomal dominant polycystic kidney disease gene homologs lov-1 and pkd-2 act in the same pathway. *Curr Biol* 11:1341-6.

Barr MM, Sternberg PW. 1999. A polycystic kidney-disease gene homologue required for male mating behaviour in C. elegans. *Nature* 401:386-9.

Barsel SE, Wexler DE, Lefebvre PA. 1988. Genetic analysis of long-flagella mutants of Chlamydomonas reinhardtii. *Genetics* 118:637-48.

Beck C, Uhl R. 1994. On the localization of voltage-sensitive calcium channels in the flagella of Chlamydomonas reinhardtii. *J Cell Biol* 125:1119-25.

Belham C, Roig J, Caldwell JA, Aoyama Y, Kemp BE, Comb M, Avruch J. 2003. A mitotic cascade of NIMA family kinases. Nercc1/Nek9 activates the Nek6 and Nek7 kinases. *J Biol Chem* 278:34897-909.

Berbari NF, O'Connor AK, Haycraft CJ, Yoder BK. 2009. The primary cilium as a complex signaling center. *Curr Biol* 19:R526-35.

Berman SA, Wilson NF, Haas NA, Lefebvre PA. 2003. A novel MAP kinase regulates flagellar length in Chlamydomonas. *Curr Biol* 13:1145-9.

Bertuccio CA, Chapin HC, Cai Y, Mistry K, Chauvet V, Somlo S, Caplan MJ. 2009. Polycystin-1 C-terminal cleavage is modulated by polycystin-2 expression. *J Biol Chem* 284:21011-26.

Bisova K, Krylov DM, Umen JG. 2005. Genome-wide annotation and expression profiling of cell cycle regulatory genes in Chlamydomonas reinhardtii. *Plant Physiol* 137:475-91.

Blaineau C, Tessier M, Dubessay P, Tasse L, Crobu L, Pagès M, Bastien P. 2007. A novel microtubule-depolymerizing kinesin involved in length control of a eukaryotic flagellum. *Curr Biol* 17:778-82.

Bradley BA, Quarmby LM. 2005. A NIMA-related kinase, Cnk2p, regulates both flagellar length and cell size in Chlamydomonas. *J Cell Sci* 118:3317-26.

Brazelton WJ, Amundsen CD, Silflow CD, Lefebvre PA. 2001. The bld1 mutation identifies the Chlamydomonas osm-6 homolog as a gene required for flagellar assembly. *Curr Biol* 11:1591-4.

Burghoorn J, Dekkers MP, Rademakers S, de Jong T, Willemsen R, Jansen G. 2007. Mutation of the MAP kinase DYF-5 affects docking and undocking of kinesin-2 motors and reduces their speed in the cilia of Caenorhabditis elegans. *Proc Natl Acad Sci U S A* 104:7157-62.

Cao M, Meng D, Wang L, Bei S, Snell WJ, Pan J. 2013. Activation loop phosphorylation of a protein kinase is a molecular marker of organelle size that dynamically reports flagellar length. *Proc Natl Acad Sci U S A* 110:12337-42.

Caspary T, Larkins CE, Anderson KV. 2007. The graded response to sonic hedgehog depends on cilia architecture. *Dev Cell* 12:767-778.

Cavalier-Smith T. 1974. Basal body and flagellar development during the vegetative cell cycle and the sexual cycle of Chlamydomonas reinhardii. *J Cell Sci* 16:529-56.

Chaki M, Airik R, Ghosh AK, Giles RH, Chen R, Slaats GG, Wang H, Hurd TW, Zhou W, Cluckey A, Gee HY, Ramaswami G, Hong CJ, Hamilton BA, Cervenka I, Ganji RS, Bryja V, Arts HH, van Reeuwijk J, Oud MM, Letteboer SJ, Roepman R, Husson H, Ibraghimov-Beskrovnaya O, Yasunaga T, Walz G, Eley L, Sayer JA, Schermer B, Liebau MC, Benzing T, Le Corre S, Drummond I, Janssen S, Allen SJ, Natarajan S, O'Toole JF, Attanasio M, Saunier S, Antignac C, Koenekoop RK, Ren H, Lopez I, Nayir A, Stoetzel C, Dollfus H, Massoudi R, Gleeson JG, Andreoli SP, Doherty DG, Lindstrad A, Golzio C, Katsanis N, Pape L, Abboud EB, Al-Rajhi AA, Lewis RA, Omran H, Lee EY, Wang S, Sekiguchi JM, Saunders R, Johnson CA, Garner E, Vanselow K, Andersen JS, Shlomai J, Nurnberg G, Nurnberg P, Levy S, Smogorzewska A, Otto EA, Hildebrandt F. 2012. Exome capture reveals ZNF423 and CEP164 mutations, linking renal ciliopathies to DNA damage response signaling. *Cell* 150:533-48.

Chang B, Khanna H, Hawes N, Jimeno D, He S, Lillo C, Parapuram SK, Cheng H, Scott A, Hurd RE, Sayer JA, Otto EA, Attanasio M, O'Toole JF, Jin G, Shou C, Hildebrandt F, Williams DS, Heckenlively JR, Swaroop A. 2006. In-frame deletion in a novel centrosomal/ciliary protein CEP290/NPHP6 perturbs its interaction with RPGR and results in early-onset retinal degeneration in the rd16 mouse. *Hum Mol Genet* 15:1847-57.

Chang J, Baloh RH, Milbrandt J. 2009. The NIMA-family kinase Nek3 regulates microtubule acetylation in neurons. *J Cell Sci* 122:2274-82.

Chauvet V, Tian X, Husson H, Grimm DH, Wang T, Hiesberger T, Igarashi P, Bennett AM, Ibraghimov-Beskrovnaya O, Somlo S, Caplan MJ. 2004. Mechanical stimuli induce cleavage and nuclear translocation of the polycystin-1 C terminus. *J Clin Invest* 114:1433-43.

Chen CP, Chang TY, Chen CY, Wang TY, Tsai FJ, Wu PC, Chern SR, Wang W. 2012a. Short rib-polydactyly syndrome type II (Majewski): prenatal diagnosis, perinatal imaging findings and molecular analysis of the NEK1 gene. *Taiwanese journal of obstetrics & gynecology* 51:100-5.

Chen CP, Chern SR, Chang TY, Su YN, Chen YY, Su JW, Wang W. 2012b. Prenatal diagnosis and molecular genetic analysis of short rib-polydactyly syndrome type III (Verma-Naumoff) in a second-trimester fetus with a homozygous splice site mutation in intron 4 in the NEK1 gene. *Taiwanese journal of obstetrics & gynecology* 51:266-70.

Chen N, Mah A, Blacque OE, Chu J, Phgora K, Bakhoum MW, Newbury CR, Khattra J, Chan S, Go A, Efimenko E, Johnsen R, Phirke P, Swoboda P, Marra M, Moerman DG, Leroux MR, Baillie DL, Stein LD. 2006. Identification of ciliary and ciliopathy genes in Caenorhabditis elegans through comparative genomics. *Genome Biol* 7:R126.

Chen Y, Chen CF, Riley DJ, Chen PL. 2011. Nek1 kinase functions in DNA damage response and checkpoint control through a pathway independent of ATM and ATR. *Cell Cycle* 10:655-63.

Chen Y, Chen PL, Chen CF, Jiang X, Riley DJ. 2008. Never-in-mitosis related kinase 1 functions in DNA damage response and checkpoint control. *Cell Cycle* 7:3194-201.

Chih B, Liu P, Chinn Y, Chalouni C, Komuves LG, Hass PE, Sandoval W, Peterson AS. 2012. A ciliopathy complex at the transition zone protects the cilia as a privileged membrane domain. *Nat Cell Biol* 14:61-72.

Christensen ST, Pedersen LB, Schneider L, Satir P. 2007. Sensory cilia and integration of signal transduction in human health and disease. *Traffic* 8:97-109.

Chu JS, Baillie DL, Chen N. 2010. Convergent evolution of RFX transcription factors and ciliary genes predated the origin of metazoans. *BMC Evol Biol* 10:130.

Clement DL, Mally S, Stock C, Lethan M, Satir P, Schwab A, Pedersen SF, Christensen ST. 2013. PDGFRalpha signaling in the primary cilium regulates NHE1-dependent fibroblast migration via coordinated differential activity of MEK1/2-ERK1/2-p90RSK and AKT signaling pathways. *J Cell Sci* 126:953-65.

Coggins CR, Fouillet XL, Lam R, Morgan KT. 1980. Cigarette smoke induced pathology of the rat respiratory tract: a comparison of the effects of the particulate and vapour phases. *Toxicology* 16:83-101.

Cokol M, Nair R, Rost B. 2000. Finding nuclear localization signals. *EMBO Rep* 1:411-415.

Cole DG. 2009. Intraflagellar Transport. In: Witman GB, editor. *The Chlamydomonas Sourcebook*, Second Edition. Oxford, UK: Academic Press, p. 71-113.

Craige B, Tsao CC, Diener DR, Hou Y, Lechtreck KF, Rosenbaum JL, Witman GB. 2010. CEP290 tethers flagellar transition zone microtubules to the membrane and regulates flagellar protein content. *J Cell Biol* 190:927-40.

Das A, Guo W. 2011. Rabs and the exocyst in ciliogenesis, tubulogenesis and beyond. *Trends Cell Biol* 21:383-6.

Davis EE, Katsanis N. 2012. The ciliopathies: a transitional model into systems biology of human genetic disease. *Current opinion in genetics & development* 22:290-303.

Dentler WL. 1980. Structures linking the tips of ciliary and flagellar microtubules to the membrane. *J Cell Sci* 42:207-20.

Dentler WL, Rosenbaum JL. 1977. Flagellar elongation and shortening in Chlamydomonas. III. structures attached to the tips of flagellar microtubules and their relationship to the directionality of flagellar microtubule assembly. *J Cell Biol* 74:747-59.

Dishinger JF, Kee HL, Jenkins PM, Fan S, Hurd TW, Hammond JW, Truong YN-T, Margolis B, Martens JR, Verhey KJ. 2010. Ciliary entry of the kinesin-2 motor KIF17 is regulated by importin-β2 and RanGTP. *Nat Cell Biol* 12:703-710.

Doles J, Hemann MT. 2010. Nek4 Status Differentially Alters Sensitivity to Distinct Microtubule Poisons. *Cancer Res* 70:1033-1041.

Donzelli M, Draetta GF. 2003. Regulating mammalian checkpoints through Cdc25 inactivation. *EMBO Rep* 4:671-7.

Dunlap K. 1977. Localization of calcium channels in Paramecium caudatum. *J Physiol* 271:119-33.

El Hokayem J, Huber C, Couve A, Aziza J, Baujat G, Bouvier R, Cavalcanti DP, Collins FA, Cordier MP, Delezoide AL, Gonzales M, Johnson D, Le Merrer M, Levy-Mozziconacci A, Loget P, Martin-Coignard D, Martinovic J, Mortier GR, Perez MJ, Roume J, Scarano G, Munnich A, Cormier-Daire V. 2012. NEK1 and DYNC2H1 are both involved in short rib polydactyly Majewski type but not in Beemer Langer cases. *J Med Genet* 49:227-33.

Engel BD, Ishikawa H, Feldman JL, Wilson CW, Chuang P-T, Snedecor J, Williams J, Sun Z, Marshall WF. 2011. A cell-based screen for inhibitors of flagella-driven motility in Chlamydomonas reveals a novel modulator of ciliary length and retrograde actin flow. *Cytoskeleton (Hoboken)* 68:188-203.

Engel BD, Ishikawa H, Wemmer KA, Geimer S, Wakabayashi K-i, Hirono M, Craige B, Pazour GJ, Witman GB, Kamiya R, Marshall WF. 2012. The role of retrograde intraflagellar transport in flagellar assembly, maintenance, and function. *J Cell Biol* 199:151-167.

Engel BD, Ludington WB, Marshall WF. 2009. Intraflagellar transport particle size scales inversely with flagellar length: revisiting the balance-point length control model. *J Cell Biol* 187:81-9.

Evangelista M, Lim TY, Lee J, Parker L, Ashique A, Peterson AS, Ye W, Davis DP, de Sauvage FJ. 2008. Kinome siRNA screen identifies regulators of ciliogenesis and hedgehog signal transduction. *Sci Signal* 1:ra7.

Feige E, Shalom O, Tsuriel S, Yissachar N, Motro B. 2006. Nek1 shares structural and functional similarities with NIMA kinase. *Biochim Biophys Acta* 1763:272-81.

Finst RJ, Kim PJ, Griffis ER, Quarmby LM. 2000. Fa1p is a 171 kDa protein essential for axonemal microtubule severing in Chlamydomonas. *J Cell Sci* 113 (Pt 11):1963-71.

Finst RJ, Kim PJ, Quarmby LM. 1998. Genetics of the deflagellation pathway in Chlamydomonas. *Genetics* 149:927-36.

Fisch C, Dupuis-Williams P. 2011. Ultrastructure of cilia and flagella - back to the future! *Biol Cell* 103:249-70.

Follit JA, Tuft RA, Fogarty KE, Pazour GJ. 2006. The intraflagellar transport protein IFT20 is associated with the Golgi complex and is required for cilia assembly. *Mol Biol Cell* 17:3781-92.

Frank V, den Hollander AI, Bruchle NO, Zonneveld MN, Nurnberg G, Becker C, Du Bois G, Kendziorra H, Roosing S, Senderek J, Nurnberg P, Cremers FP, Zerres K, Bergmann C. 2008. Mutations of the CEP290 gene encoding a centrosomal protein cause Meckel-Gruber syndrome. *Hum Mutat* 29:45-52.

Fry AM, O'Regan L, Sabir SR, Bayliss R. 2012. Cell cycle regulation by the NEK family of protein kinases. *J Cell Sci* 125:4423-4433.

Gaertig J, Wloga D. 2008. Ciliary tubulin and its post-translational modifications. *Curr Top Dev Biol* 85:83-113.

Gaffal KP. 1988. The Basal Body-Root Complex of Chlamydomonas-Reinhardtii during Mitosis. *Protoplasma* 143:118-129.

Garcia-Gonzalo FR, Corbit KC, Sirerol-Piquer MS, Ramaswami G, Otto EA, Noriega TR, Seol AD, Robinson JF, Bennett CL, Josifova DJ, Garcia-Verdugo JM, Katsanis N, Hildebrandt F, Reiter JF. 2011. A transition zone complex regulates mammalian ciliogenesis and ciliary membrane composition. *Nat Genet* 43:776-84.

Gilula NB, Satir P. 1972. The ciliary necklace. A ciliary membrane specialization. *J Cell Biol* 53:494-509.

Goetz SC, Anderson KV. 2010. The primary cilium: a signalling centre during vertebrate development. *Nat Rev Genet* 11:331-44.

Graser S, Stierhof YD, Lavoie SB, Gassner OS, Lamla S, Le Clech M, Nigg EA. 2007. Cep164, a novel centriole appendage protein required for primary cilium formation. *J Cell Biol* 179:321-30.

Habbig S, Bartram MP, Muller RU, Schwarz R, Andriopoulos N, Chen S, Sagmuller JG, Hoehne M, Burst V, Liebau MC, Reinhardt HC, Benzing T, Schermer B. 2011. NPHP4, a cilia-associated protein, negatively regulates the Hippo pathway. *J Cell Biol* 193:633-42.

Hao L, Thein M, Brust-Mascher I, Civelekoglu-Scholey G, Lu Y, Acar S, Prevo B, Shaham S, Scholey JM. 2011. Intraflagellar transport delivers tubulin isotypes to sensory cilium middle and distal segments. *Nat Cell Biol* 13:790-798.

Harris EH. 2009. *The Chlamydomonas Sourcebook* Second Edition. Oxford, U.K.: Academic Press.

Hartzell LB, Hartzell HC, Quarmby LM. 1993. Mechanisms of flagellar excision. I. The role of intracellular acidification. *Exp Cell Res* 208:148-53.

Heijink AM, Krajewska M, MA MvV. 2013. The DNA Damage Response During Mitosis. *Mutation research*.

Heuser T, Raytchev M, Krell J, Porter ME, Nicastro D. 2009. The dynein regulatory complex is the nexin link and a major regulatory node in cilia and flagella. *J Cell Biol* 187:921-33.

Hiesberger T, Gourley E, Erickson A, Koulen P, Ward CJ, Masyuk TV, Larusso NF, Harris PC, Igarashi P. 2006. Proteolytic cleavage and nuclear translocation of fibrocystin is regulated by intracellular Ca2+ and activation of protein kinase C. *J Biol Chem* 281:34357-34364.

Holmes JA, Dutcher SK. 1989. Cellular asymmetry in Chlamydomonas reinhardtii. *J Cell Sci* 94:273-85.

Hoops HJ, Witman GB. 1985. Basal bodies and associated structures are not required for normal flagellar motion or phototaxis in the green alga Chlorogonium elongatum. *J Cell Biol* 100:297-309.

Huber C, Cormier-Daire V. 2012. Ciliary disorder of the skeleton. *American journal of medical genetics Part C, Seminars in medical genetics* 160C:165-74.

Iomini C, Babaev-Khaimov V, Sassaroli M, Piperno G. 2001. Protein particles in Chlamydomonas flagella undergo a transport cycle consisting of four phases. *J Cell Biol* 153:13-24.

Iomini C, Li L, Esparza JM, Dutcher SK. 2009. Retrograde intraflagellar transport mutants identify complex A proteins with multiple genetic interactions in Chlamydomonas reinhardtii. *Genetics* 183:885-96.

Jackson PK. 2011. Do cilia put brakes on the cell cycle? *Nat Cell Biol* 13:340-2.

Janaswami PM, Birkenmeier EH, Cook SA, Rowe LB, Bronson RT, Davisson MT. 1997. Identification and genetic mapping of a new polycystic kidney disease on mouse chromosome 8. *Genomics* 40:101-107.

Jin H, White SR, Shida T, Schulz S, Aguiar M, Gygi SP, Bazan JF, Nachury MV. 2010. The conserved Bardet-Biedl syndrome proteins assemble a coat that traffics membrane proteins to cilia. *Cell* 141:1208-19.

Johnson KA, Rosenbaum JL. 1992. Polarity of flagellar assembly in Chlamydomonas. *J Cell Biol* 119:1605-11.

Johnson UG, Porter KR. 1968. Fine structure of cell division in Chlamydomonas reinhardi. Basal bodies and microtubules. *J Cell Biol* 38:403-25.

Jonassen JA, San Agustin J, Follit JA, Pazour GJ. 2008. Deletion of IFT20 in the mouse kidney causes misorientation of the mitotic spindle and cystic kidney disease. *J Cell Biol* 183:377-84.

Jonassen JA, SanAgustin J, Baker SP, Pazour GJ. 2012. Disruption of IFT complex A causes cystic kidneys without mitotic spindle misorientation. *J Am Soc Nephrol* 23:641-51.

Joo K, Kim CG, Lee M-S, Moon H-Y, Lee S-H, Kim MJ, Kweon H-S, Park W-Y, Kim C-H, Gleeson JG, Kim J. 2013. CCDC41 is required for ciliary vesicle docking to the mother centriole. *Proc Natl Acad Sci U S A*.

Kee HL, Dishinger JF, Blasius TL, Liu CJ, Margolis B, Verhey KJ. 2012. A size-exclusion permeability barrier and nucleoporins characterize a ciliary pore complex that regulates transport into cilia. *Nat Cell Biol* 14:431-7.

Keminer O, Peters R. 1999. Permeability of single nuclear pores. *Biophys J* 77:217-228.

Kim S, Zaghloul NA, Bubenshchikova E, Oh EC, Rankin S, Katsanis N, Obara T, Tsiokas L. 2011. Nde1-mediated inhibition of ciliogenesis affects cell cycle re-entry. *Nat Cell Biol* 13:351-60.

Kindle KL. 1990. High-frequency nuclear transformation of Chlamydomonas reinhardtii. *Proc Natl Acad Sci U S A* 87:1228-32.

King SM, Kamiya R. 2009. Axonemal Dyneins: Assembly, Structure, and Force Generation. In: Witman GB, editor.*The Chlamydomonas Sourcebook*, Second Edition. Oxford, UK: Academic Press, p. 131-208.

Kozminski KG, Beech PL, Rosenbaum JL. 1995. The Chlamydomonas kinesin-like protein FLA10 is involved in motility associated with the flagellar membrane. *J Cell Biol* 131:1517-27.

Kozminski KG, Diener DR, Rosenbaum JL. 1993. High level expression of nonacetylatable alpha-tubulin in Chlamydomonas reinhardtii. *Cell Motil Cytoskeleton* 25:158-70.

Kudo N, Wolff B, Sekimoto T, Schreiner EP, Yoneda Y, Yanagida M, Horinouchi S, Yoshida M. 1998. Leptomycin B inhibition of signal-mediated nuclear export by direct binding to CRM1. *Exp Cell Res* 242:540-547.

la Cour T, Kiemer L, Molgaard A, Gupta R, Skriver K, Brunak S. 2004. Analysis and prediction of leucine-rich nuclear export signals. *Protein Eng Des Sel* 17:527-536.

Lacroix B, van Dijk J, Gold ND, Guizetti J, Aldrian-Herrada G, Rogowski K, Gerlich DW, Janke C. 2010. Tubulin polyglutamylation stimulates spastin-mediated microtubule severing. *J Cell Biol* 189:945-54.

Lai SL, Chien AJ, Moon RT. 2009. Wnt/Fz signaling and the cytoskeleton: potential roles in tumorigenesis. *Cell Res* 19:532-45.

Lechtreck KF, Brown JM, Sampaio JL, Craft JM, Shevchenko A, Evans JE, Witman GB. 2013. Cycling of the signaling protein phospholipase D through cilia requires the BBSome only for the export phase. *J Cell Biol* 201:249-261.

Lechtreck KF, Johnson EC, Sakai T, Cochran D, Ballif BA, Rush J, Pazour GJ, Ikebe M, Witman GB. 2009. The Chlamydomonas reinhardtii BBSome is an IFT cargo required for export of specific signaling proteins from flagella. *J Cell Biol* 187:1117-32.

Lee L. 2011. Mechanisms of mammalian ciliary motility: Insights from primary ciliary dyskinesia genetics. *Gene* 473:57-66.

Lefebvre PA, Nordstrom SA, Moulder JE, Rosenbaum JL. 1978. Flagellar elongation and shortening in Chlamydomonas. IV. Effects of flagellar detachment, regeneration, and resorption on the induction of flagellar protein synthesis. *J Cell Biol* 78:8-27.

Lefebvre PA, Silflow CD, Wieben ED, Rosenbaum JL. 1980. Increased levels of mRNAs for tubulin and other flagellar proteins after amputation or shortening of Chlamydomonas flagella. *Cell* 20:469-77.

Leigh MW, Pittman JE, Carson JL, Ferkol TW, Dell SD, Davis SD, Knowles MR, Zariwala MA. 2009. Clinical and genetic aspects of primary ciliary dyskinesia/Kartagener syndrome. *Genet Med* 11:473-87.

Leitch CC, Zaghloul NA, Davis EE, Stoetzel C, Diaz-Font A, Rix S, Alfadhel M, Lewis RA, Eyaid W, Banin E, Dollfus H, Beales PL, Badano JL, Katsanis N. 2008. Hypomorphic mutations in syndromic encephalocele genes are associated with Bardet-Biedl syndrome. *Nat Genet* 40:443-8.

Letwin K, Mizzen L, Motro B, Ben-David Y, Bernstein A, Pawson T. 1992. A mammalian dual specificity protein kinase, Nek1, is related to the NIMA cell cycle regulator and highly expressed in meiotic germ cells. *EMBO J* 11:3521-31.

Lewin RA, Burrascano C. 1983. Another new kind of Chlamydomonas mutant, with impaired flagellar autotomy. *Experientia* 39:1397-1398.

Lewin RA, Lee KW. 1985. Autotomy of algal flagella: electron microscope studies of Chlamydomonas (Chlorophyceae) and Tetraselmis (Prasinophyceae). *Phycologia* 24:311-316.

Li A, Saito M, Chuang JZ, Tseng YY, Dedesma C, Tomizawa K, Kaitsuka T, Sung CH. 2011. Ciliary transition zone activation of phosphorylated Tctex-1 controls ciliary resorption, S-phase entry and fate of neural progenitors. *Nat Cell Biol* 13:402-11.

Liu S, Ho CK, Ouyang J, Zou L. 2013. Nek1 kinase associates with ATR-ATRIP and primes ATR for efficient DNA damage signaling. *Proc Natl Acad Sci U S A* 110:2175-80.

Liu S, Lu W, Obara T, Kuida S, Lehoczky J, Dewar K, Drummond IA, Beier DR. 2002. A defect in a novel Nek-family kinase causes cystic kidney disease in the mouse and in zebrafish. *Development* 129:5839-46.

Lohret TA, McNally FJ, Quarmby LM. 1998. A role for katanin-mediated axonemal severing during Chlamydomonas deflagellation. *Mol Biol Cell* 9:1195-207.

Lohret TA, Zhao L, Quarmby LM. 1999. Cloning of Chlamydomonas p60 katanin and localization to the site of outer doublet severing during deflagellation. *Cell Motil Cytoskeleton* 43:221-31.

Low SH, Vasanth S, Larson CH, Mukherjee S, Sharma N, Kinter MT, Kane ME, Obara T, Weimbs T. 2006. Polycystin-1, STAT6, and pathway that transduces P100 function in a ciliary mechanosensation and is activated in polycystic kidney disease. *Dev Cell* 10:57-69.

Ludington WB, Shi LZ, Zhu Q, Berns Michael W, Marshall Wallace F. 2012. Organelle Size Equalization by a Constitutive Process. *Curr Biol* 22:2173 - 2179.

Ludington WB, Wemmer KA, Lechtreck KF, Witman GB, Marshall WF. 2013. Avalanche-like behavior in ciliary import. *Proc Natl Acad Sci U S A* 110:3925-3930.

Luo M, Cao M, Kan Y, Li G, Snell W, Pan J. 2011. The Phosphorylation State of an Aurora-Like Kinase Marks the Length of Growing Flagella in Chlamydomonas. *Curr Biol* 21:586 - 591.

Mahjoub MR, Montpetit B, Zhao L, Finst RJ, Goh B, Kim AC, Quarmby LM. 2002. The FA2 gene of Chlamydomonas encodes a NIMA family kinase with roles in cell cycle progression and microtubule severing during deflagellation. *J Cell Sci* 115:1759-68.

Mahjoub MR, Rasi MQ, Quarmby LM. 2004. A NIMA-related kinase, Fa2p, localizes to a novel site in the proximal cilia of Chlamydomonas and mouse kidney cells. *Mol Biol Cell* 15:5172-86.

Mahjoub MR, Stearns T. 2012. Supernumerary centrosomes nucleate extra cilia and compromise primary cilium signaling. *Curr Biol* 22:1628-34.

Mahjoub MR, Trapp ML, Quarmby LM. 2005. NIMA-related kinases defective in murine models of polycystic kidney diseases localize to primary cilia and centrosomes. *J Am Soc Nephrol* 16:3485-9.

Marshall WF. 2008. Basal Bodies: Platforms for building cilia. *Curr Top Dev Biol* 85:1-22.

Marshall WF. 2010. Cilia self-organize in response to planar cell polarity and flow. *Nat Cell Biol* 12:314-5.

Marshall WF, Qin H, Rodrigo Brenni M, Rosenbaum JL. 2005. Flagellar Length Control System: Testing a Simple Model Based on Intraflagellar Transport and Turnover. *Mol Biol Cell* 16:270-278.

Marshall WF, Rosenbaum JL. 2001. Intraflagellar transport balances continuous turnover of outer doublet microtubules: implications for flagellar length control. *J Cell Biol* 155:405-14.

Mazelova J, Astuto-Gribble L, Inoue H, Tam BM, Schonteich E, Prekeris R, Moritz OL, Randazzo PA, Deretic D. 2009. Ciliary targeting motif VxPx directs assembly of a trafficking module through Arf4. *Embo J* 28:183-192.

McVittie A. 1972. Flagellum mutants of Chlamydomonas reinhardii. *J Gen Microbiol* 71:525-40.

Meslet-Cladière L, Vallon O. 2012. A new method to identify flanking sequence tags in chlamydomonas using 3'-RACE. *Plant Methods* 8:21.

Motose H, Hamada T, Yoshimoto K, Murata T, Hasebe M, Watanabe Y, Hashimoto T, Sakai T, Takahashi T. 2011. NIMA-related kinases 6, 4, and 5 interact with each other to regulate microtubule organization during epidermal cell expansion in Arabidopsis thaliana. *Plant J* 67:993-1005.

Motose H, Takatani S, Ikeda T, Takahashi T. 2012. NIMA-related kinases regulate directional cell growth and organ development through microtubule function in Arabidopsis thaliana. *Plant Signal Behav* 7:1552-1555.

Mullins J, McIntosh J. 1982. Isolation and initial characterization of the mammalian midbody. *J Cell Biol* 94:654-661.

Nachury MV, Loktev AV, Zhang Q, Westlake CJ, Peränen J, Merdes A, Slusarski DC, Scheller RH, Bazan JF, Sheffield VC, Jackson PK. 2007. A Core Complex of BBS Proteins Cooperates with the GTPase Rab8 to Promote Ciliary Membrane Biogenesis. *Cell* 129:1201 - 1213.

Nauli SM, Zhou J. 2004. Polycystins and mechanosensation in renal and nodal cilia. *BioEssays : news and reviews in molecular, cellular and developmental biology* 26:844-56.

Nicastro D, Schwartz C, Pierson J, Gaudette R, Porter ME, McIntosh JR. 2006. The molecular architecture of axonemes revealed by cryoelectron tomography. *Science* 313:944-8.

O'Hagan R, Piasecki BP, Silva M, Phirke P, Nguyen KC, Hall DH, Swoboda P, Barr MM. 2011. The Tubulin Deglutamylase CCPP-1 Regulates the Function and Stability of Sensory Cilia in C. elegans. *Curr Biol* 21:1685-94.

O'Regan L, Fry AM. 2009. The Nek6 and Nek7 protein kinases are required for robust mitotic spindle formation and cytokinesis. *Mol Cell Biol* 29:3975-90.

O'Toole ET, Giddings TH, McIntosh JR, Dutcher SK. 2003. Three-dimensional organization of basal bodies from wild-type and delta-tubulin deletion strains of Chlamydomonas reinhardtii. *Mol Biol Cell* 14:2999-3012.

Omori Y, Chaya T, Katoh K, Kajimura N, Sato S, Muraoka K, Ueno S, Koyasu T, Kondo M, Furukawa T. 2010. Negative regulation of ciliary length by ciliary male germ cell-associated kinase (Mak) is required for retinal photoreceptor survival. *Proc Natl Acad Sci U S A* 107:22671-6.

Omoto CK, Gibbons IR, Kamiya R, Shingyoji C, Takahashi K, Witman GB. 1999. Rotation of the central pair microtubules in eukaryotic flagella. *Mol Biol Cell* 10:1-4.

Osmani AH, McGuire SL, O'Donnell KL, Pu RT, Osmani SA. 1991. Role of the cell-cycle-regulated NIMA protein kinase during G2 and mitosis: evidence for two pathways of mitotic regulation. *Cold Spring Harb Symp Quant Biol* 56:549-55.

Otto EA, Schermer B, Obara T, O'Toole JF, Hiller KS, Mueller AM, Ruf RG, Hoefele J, Beekmann F, Landau D, Foreman JW, Goodship JA, Strachan T, Kispert A, Wolf MT, Gagnadoux MF, Nivet H, Antignac C, Walz G, Drummond IA, Benzing T, Hildebrandt F. 2003. Mutations in INVS encoding inversin cause nephronophthisis type 2, linking renal cystic disease to the function of primary cilia and left-right axis determination. *Nat Genet* 34:413-20.

Otto EA, Trapp ML, Schultheiss UT, Helou J, Quarmby LM, Hildebrandt F. 2008. NEK8 mutations affect ciliary and centrosomal localization and may cause nephronophthisis. *J Am Soc Nephrol* 19:587-92.

Ou G, Blacque OE, Snow JJ, Leroux MR, Scholey JM. 2005. Functional coordination of intraflagellar transport motors. *Nature* 436:583-7.

Ozgül RK, Siemiatkowska AM, Yücel D, Myers CA, Collin RWJ, Zonneveld MN, Beryozkin A, Banin E, Hoyng CB, van den Born LI, Bose R, Shen W, Sharon D, Cremers FPM, Klevering BJ, den Hollander AI, Corbo JC. 2011. Exome sequencing and cis-regulatory mapping identify mutations in MAK, a gene encoding a regulator of ciliary length, as a cause of retinitis pigmentosa. *Am J Hum Genet* 89:253-64.

Palmer KJ, MacCarthy-Morrogh L, Smyllie N, Stephens DJ. 2011. A role for Tctex-1 (DYNLT1) in controlling primary cilium length. *Eur J Cell Biol* 90:865-71.

Pan J, Snell WJ. 2005. Chlamydomonas shortens its flagella by activating axonemal disassembly, stimulating IFT particle trafficking, and blocking anterograde cargo loading. *Dev Cell* 9:431-8.

Pan J, Wang Q, Snell WJ. 2004. An aurora kinase is essential for flagellar disassembly in Chlamydomonas. *Dev Cell* 6:445-51.

Pan X, Ou G, Civelekoglu-Scholey G, Blacque OE, Endres NF, Tao L, Mogilner A, Leroux MR, Vale RD, Scholey JM. 2006. Mechanism of transport of IFT particles in C. elegans cilia by the concerted action of kinesin-II and OSM-3 motors. *J Cell Biol* 174:1035-45.

Parker JD, Bradley BA, Mooers AO, Quarmby LM. 2007. Phylogenetic analysis of the Neks reveals early diversification of ciliary-cell cycle kinases. *PLoS One* 2:e1076.

Parker JD, Hilton LK, Diener DR, Rasi MQ, Mahjoub MR, Rosenbaum JL, Quarmby LM. 2010. Centrioles are freed from cilia by severing prior to mitosis. *Cytoskeleton (Hoboken)* 67:425-30.

Parker JDK. 2008. Co-ordinate regulation of cilia and the cell cycle in Chlamydomonas reinhardtii.

Parker JDK, Quarmby LM. 2003. Chlamydomonas fla mutants reveal a link between deflagellation and intraflagellar transport. *BMC Cell Biol* 4:11.

Pazour GJ, Agrin N, Leszyk J, Witman GB. 2005. Proteomic analysis of a eukaryotic cilium. *J Cell Biol* 170:103-13.

Pazour GJ, Bloodgood RA. 2008. Targeting proteins to the ciliary membrane. *Curr Top Dev Biol* 85:115-49.

Pazour GJ, Dickert BL, Vucica Y, Seeley ES, Rosenbaum JL, Witman GB, Cole DG. 2000. Chlamydomonas IFT88 and its mouse homologue, polycystic kidney disease gene tg737, are required for assembly of cilia and flagella. *J Cell Biol* 151:709-18.

Pedersen LB, Geimer S, Sloboda RD, Rosenbaum JL. 2003. The Microtubule plus end-tracking protein EB1 is localized to the flagellar tip and basal bodies in Chlamydomonas reinhardtii. *Curr Biol* 13:1969-74.

Pedersen LB, Rosenbaum JL. 2008. Intraflagellar transport (IFT) role in ciliary assembly, resorption and signalling. *Curr Top Dev Biol* 85:23-61.

Pelegrini AL, Moura DJ, Brenner BL, Ledur PF, Maques GP, Henriques JA, Saffi J, Lenz G. 2010. Nek1 silencing slows down DNA repair and blocks DNA damage-induced cell cycle arrest. *Mutagenesis* 25:447-54.

Phirke P, Efimenko E, Mohan S, Burghoorn J, Crona F, Bakhoum MW, Trieb M, Schuske K, Jorgensen EM, Piasecki BP, Leroux MR, Swoboda P. 2011. Transcriptional profiling of C. elegans DAF-19 uncovers a ciliary base-associated protein and a CDK/CCRK/LF2p-related kinase required for intraflagellar transport. *Dev Biol* 357:235-47.

Piao T, Luo M, Wang L, Guo Y, Li D, Li P, Snell WJ, Pan J. 2009. A microtubule depolymerizing kinesin functions during both flagellar disassembly and flagellar assembly in Chlamydomonas. *Proceedings of the National Academy of Sciences* 106:4713-4718.

Piasecki BP, Burghoorn J, Swoboda P. 2010. Regulatory Factor X (RFX)-mediated transcriptional rewiring of ciliary genes in animals. *Proc Natl Acad Sci U S A* 107:12969-74.

Piasecki BP, Silflow CD. 2009. The UNI1 and UNI2 genes function in the transition of triplet to doublet microtubules between the centriole and cilium in Chlamydomonas. *Mol Biol Cell* 20:368-78.

Pigino G, Geimer S, Lanzavecchia S, Paccagnini E, Cantele F, Diener DR, Rosenbaum JL, Lupetti P. 2009. Electron-tomographic analysis of intraflagellar transport particle trains in situ. *J Cell Biol* 187:135-48.

Piperno G, Siuda E, Henderson S, Segil M, Vaananen H, Sassaroli M. 1998. Distinct mutants of retrograde intraflagellar transport (IFT) share similar morphological and molecular defects. *J Cell Biol* 143:1591-601.

Plotnikova OV, Nikonova AS, Loskutov YV, Kozyulina PY, Pugacheva EN, Golemis EA. 2012. Calmodulin activation of Aurora-A kinase (AURKA) is required during ciliary disassembly and in mitosis. *Mol Biol Cell* 23:2658-70.

Polci R, Peng A, Chen PL, Riley DJ, Chen Y. 2004. NIMA-related protein kinase 1 is involved early in the ionizing radiation-induced DNA damage response. *Cancer Res* 64:8800-3.

Pugacheva EN, Jablonski SA, Hartman TR, Henske EP, Golemis EA. 2007. HEF1-dependent Aurora A activation induces disassembly of the primary cilium. *Cell* 129:1351-63.

Qin H, Diener DR, Geimer S, Cole DG, Rosenbaum JL. 2004. Intraflagellar transport (IFT) cargo. *The Journal of Cell Biology* 164:255-266.

Quarmby LM. 2004. Cellular deflagellation. *Int Rev Cytol* 233:47-91.

Quarmby LM. 2009. Deflagellation. In: Witman GB, editor.*The Chlamydomonas Sourcebook* Second Edition. Oxford, UK: Academic Press, p. 43-69.

Quarmby LM, Hartzell HC. 1994. Two distinct, calcium-mediated, signal transduction pathways can trigger deflagellation in Chlamydomonas reinhardtii. *J Cell Biol* 124:807-15.

Quarmby LM, Leroux MR. 2010. Sensorium: the original raison d'etre of the motile cilium? *J Mol Cell Biol* 2:65-7.

Quarmby LM, Mahjoub MR. 2005. Caught Nek-ing: cilia and centrioles. *J Cell Sci* 118:5161-9.

Quarmby LM, Parker JD. 2005. Cilia and the cell cycle? *J Cell Biol* 169:707-10.

Rasi MQ, Parker JDK, Feldman JL, Marshall WF, Quarmby LM. 2009. Katanin Knockdown Supports a Role for Microtubule Severing in Release of Basal Bodies before Mitosis in Chlamydomonas. *Mol Biol Cell* 20:379-388.

Reiter JF, Blacque OE, Leroux MR. 2012. The base of the cilium: roles for transition fibres and the transition zone in ciliary formation, maintenance and compartmentalization. *EMBO Rep*.

Richards TA, Cavalier-Smith T. 2005. Myosin domain evolution and the primary divergence of eukaryotes. *Nature* 436:1113-8.

Ringo DL. 1967. Flagellar motion and fine structure of the flagellar apparatus in Chlamydomonas. *J Cell Biol* 33:543-571.

Rosenbaum J. 2003. Organelle size regulation: length matters. *Curr Biol* 13:R506-7.

Rosenbaum JL, Child FM. 1967. Flagellar regeneration in protozoan flagellates. *J Cell Biol* 34:345-64.

Rosenbaum JL, Moulder JE, Ringo DL. 1969. Flagellar elongation and shortening in *Chlamydomonas*: The use of cycloheximide and cochicine to study the synthesis and assembly of flagellar proteins. *J Cell Biol* 41:600-619.

Sakato M, King SM. 2004. Design and regulation of the AAA+ microtubule motor dynein. *J Struct Biol* 146:58-71.

Salem H, Rachmin I, Yissachar N, Cohen S, Amiel A, Haffner R, Lavi L, Motro B. 2010. Nek7 kinase targeting leads to early mortality, cytokinesis disturbance and polyploidy. *Oncogene* 29:4046-4057.

Sanders MA, Salisbury JL. 1989. Centrin-mediated microtubule severing during flagellar excision in Chlamydomonas reinhardtii. *J Cell Biol* 108:1751-60.

Sang L, Miller JJ, Corbit KC, Giles RH, Brauer MJ, Otto EA, Baye LM, Wen X, Scales SJ, Kwong M, Huntzicker EG, Sfakianos MK, Sandoval W, Bazan JF, Kulkarni P, Garcia-Gonzalo FR, Seol AD, O'Toole JF, Held S, Reutter HM, Lane WS, Rafiq MA, Noor A, Ansar M, Devi AR, Sheffield VC, Slusarski DC, Vincent JB, Doherty DA, Hildebrandt F, Reiter JF, Jackson PK. 2011. Mapping the NPHP-JBTS-MKS protein network reveals ciliopathy disease genes and pathways. *Cell* 145:513-28.

Satir P, Mitchell DR, Jekely G. 2008. How did the cilium evolve? *Curr Top Dev Biol* 85:63-82.

Sayer JA, Otto EA, O'Toole JF, Nurnberg G, Kennedy MA, Becker C, Hennies HC, Helou J, Attanasio M, Fausett BV, Utsch B, Khanna H, Liu Y, Drummond I, Kawakami I, Kusakabe T, Tsuda M, Ma L, Lee H, Larson RG, Allen SJ, Wilkinson CJ, Nigg EA, Shou C, Lillo C, Williams DS, Hoppe B, Kemper MJ, Neuhaus T, Parisi MA, Glass IA, Petry M, Kispert A, Gloy J, Ganner A, Walz G, Zhu X, Goldman D, Nurnberg P, Swaroop A, Leroux MR, Hildebrandt F. 2006. The centrosomal protein nephrocystin-6 is mutated in Joubert syndrome and activates transcription factor ATF4. *Nat Genet* 38:674-81.

Schneider L, Clement CA, Teilmann SC, Pazour GJ, Hoffmann EK, Satir P, Christensen ST. 2005. PDGFRalphaalpha signaling is regulated through the primary cilium in fibroblasts. *Curr Biol* 15:1861-6.

Schroder JM, Schneider L, Christensen ST, Pedersen LB. 2007. EB1 is required for primary cilia assembly in fibroblasts. *Curr Biol* 17:1134-9.

Shalom O, Shalva N, Altschuler Y, Motro B. 2008. The mammalian Nek1 kinase is involved in primary cilium formation. *FEBS letters* 582:1465-70.

Shida T, Cueva JG, Xu Z, Goodman MB, Nachury MV. 2010. The major alpha-tubulin K40 acetyltransferase alphaTAT1 promotes rapid ciliogenesis and efficient mechanosensation. *Proc Natl Acad Sci U S A* 107:21517-22.

Shih SM, Engel BD, Kocabas F, Bilyard T, Gennerich A, Marshall WF, Yildiz A. 2013. Intraflagellar transport drives flagellar surface motility. *eLife* 2:e00744.

Sillibourne JE, Hurbain I, Grand-Perret T, Goud B, Tran P, Bornens M. 2013. Primary ciliogenesis requires the distal appendage component Cep123. *Biology open* 2:535-45.

Silverman MA, Leroux MR. 2009. Intraflagellar transport and the generation of dynamic, structurally and functionally diverse cilia. *Trends Cell Biol* 19:306-16.

Simons M, Gloy J, Ganner A, Bullerkotte A, Bashkurov M, Kronig C, Schermer B, Benzing T, Cabello OA, Jenny A, Mlodzik M, Polok B, Driever W, Obara T, Walz G. 2005. Inversin, the gene product mutated in nephronophthisis type II, functions as a molecular switch between Wnt signaling pathways. *Nature Genetics* 37:537-543.

Singla V, Romaguera-Ros M, Garcia-Verdugo JM, Reiter JF. 2010. Ofd1, a human disease gene, regulates the length and distal structure of centrioles. *Dev Cell* 18:410-24.

Sizova I, Fuhrmann M, Hegemann P. 2001. A Streptomyces rimosus aphVIII gene coding for a new type phosphotransferase provides stable antibiotic resistance to Chlamydomonas reinhardtii. *Gene* 277:221-9.

Sloboda RD. 2005. Intraflagellar transport and the flagellar tip complex. *J Cell Biochem* 94:266-272.

Song L, Dentler WL. 2001. Flagellar protein dynamics in Chlamydomonas. *J Biol Chem* 276:29754-63.

Spalluto C, Wilson DI, Hearn T. 2012. Nek2 localises to the distal portion of the mother centriole/basal body and is required for timely cilium disassembly at the G2/M transition. *Eur J Cell Biol* 91:675-86.

Sperka T, Wang J, Rudolph KL. 2012. DNA damage checkpoints in stem cells, ageing and cancer. *Nat Rev Mol Cell Biol* 13:579-90.

Sudo H, Baas PW. 2010. Acetylation of microtubules influences their sensitivity to severing by katanin in neurons and fibroblasts. *J Neurosci* 30:7215-26.

Swoboda P, Adler HT, Thomas JH. 2000. The RFX-type transcription factor DAF-19 regulates sensory neuron cilium formation in C. elegans. *Mol Cell* 5:411-21.

Tam L-W, Ranum PT, Lefebvre PA. 2013. CDKL5 regulates flagellar length and localizes to the base of the flagella in Chlamydomonas. *Molecular Biology of the Cell* 24:588-600.

Tammachote R, Hommerding CJ, Sinders RM, Miller CA, Czarnecki PG, Leightner AC, Salisbury JL, Ward CJ, Torres VE, Gattone VH, Harris PC. 2009. Ciliary and centrosomal defects associated with mutation and depletion of the Meckel syndrome genes MKS1 and MKS3. *Human Molecular Genetics* 18:3311-3323.

Tanos BE, Yang HJ, Soni R, Wang WJ, Macaluso FP, Asara JM, Tsou MF. 2013. Centriole distal appendages promote membrane docking, leading to cilia initiation. *Genes Dev* 27:163-8.

Thiel C, Kessler K, Giessl A, Dimmler A, Shalev SA, von der Haar S, Zenker M, Zahnleiter D, Stoss H, Beinder E, Abou Jamra R, Ekici AB, Schroder-Kress N, Aigner T, Kirchner T, Reis A, Brandstatter JH, Rauch A. 2011. NEK1 mutations cause short-rib polydactyly syndrome type majewski. *Am J Hum Genet* 88:106-14.

Tilney LG, Gibbins JR. 1968. Differential effects of antimitotic agents on the stability and behavior of cytoplasmic and ciliary microtubules. *Protoplasma* 65:167-79.

Trapp ML, Galtseva A, Manning DK, Beier DR, Rosenblum ND, Quarmby LM. 2008. Defects in ciliary localization of Nek8 is associated with cystogenesis. *Pediatr Nephrol* 23:377-87.

Tucker BA, Scheetz TE, Mullins RF, DeLuca AP, Hoffmann JM, Johnston RM, Jacobson SG, Sheffield VC, Stone EM. 2011. Exome sequencing and analysis of induced pluripotent stem cells identify the cilia-related gene male germ cell-associated kinase (MAK) as a cause of retinitis pigmentosa. *Proc Natl Acad Sci U S A* 108:E569-76.

Umen JG, Goodenough UW. 2001. Control of cell division by a retinoblastoma protein homolog in Chlamydomonas. *Genes Dev* 15:1652-61.

Upadhya P, Birkenmeier EH, Birkenmeier CS, Barker JE. 2000. Mutations in a NIMA-related kinase gene, Nek1, cause pleiotropic effects including a progressive polycystic kidney disease in mice. *Proc Natl Acad Sci U S A* 97:217-21.

Vogler C, Homan S, Pung A, Thorpe C, Barker J, Birkenmeier EH, Upadhya P. 1999. Clinical and pathologic findings in two new allelic murine models of polycystic kidney disease. *J Am Soc Nephrol* 10:2534-9.

Vorobjev IA, Chentsov YS. 1982. Centrioles in the cell cycle. I. Epithelial cells. *J Cell Biol* 93:938-49.

Walther Z, Vashishtha M, Hall JL. 1994. The Chlamydomonas FLA10 gene encodes a novel kinesin-homologous protein. *J Cell Biol* 126:175-88.

Wargo MJ, Dymek EE, Smith EF. 2005. Calmodulin and PF6 are components of a complex that localizes to the C1 microtubule of the flagellar central apparatus. *J Cell Sci* 118:4655-65.

Waters AM, Beales PL. 2011. Ciliopathies: an expanding disease spectrum. *Pediatr Nephrol* 26:1039-56.

Weiss RL, Goodenough DA, Goodenough UW. 1977. Membrane particle arrays associated with the basal body and with contractile vacuole secretion in Chlamydomonas. *J Cell Biol* 72:133-43.

Wemmer KA, Marshall WF. 2007. Flagellar Length Control in Chlamydomonas—A Paradigm for Organelle Size Regulation.*A Survey of Cell Biology*: Academic Press, p. 175 - 212.

White MC, Quarmby LM. 2008. The NIMA-family kinase, Nek1 affects the stability of centrosomes and ciliogenesis. *BMC Cell Biol* 9:29.

Whitfield JF. 2004. The neuronal primary cilium--an extrasynaptic signaling device. *Cell Signal* 16:763-7.

Williams CL, Li C, Kida K, Inglis PN, Mohan S, Semenec L, Bialas NJ, Stupay RM, Chen N, Blacque OE, Yoder BK, Leroux MR. 2011. MKS and NPHP modules cooperate to establish basal body/transition zone membrane associations and ciliary gate function during ciliogenesis. *J Cell Biol* 192:1023-41.

Wilson GM, Fielding AB, Simon GC, Yu X, Andrews PD, Hames RS, Frey AM, Peden AA, Gould GW, Prekeris R. 2005. The FIP3-Rab11 Protein Complex Regulates Recycling Endosome Targeting to the Cleavage Furrow during Late Cytokinesis. *Mol Biol Cell* 16:849-860.

Wloga D, Camba A, Rogowski K, Manning G, Jerka-Dziadosz M, Gaertig J. 2006. Members of the NIMA-related Kinase Family Promote Disassembly of Cilia by Multiple Mechanisms. *Mol Biol Cell* 17:2799-2810.

Yagi T, Uematsu K, Liu Z, Kamiya R. 2009. Identification of dyneins that localize exclusively to the proximal portion of Chlamydomonas flagella. *J Cell Sci* 122:1306-14.

Yu X, Ng CP, Habacher H, Roy S. 2008. Foxj1 transcription factors are master regulators of the motile ciliogenic program. *Nat Genet* 40:1445-53.

Zaghloul NA, Katsanis N. 2009. Mechanistic insights into Bardet-Biedl syndrome, a model ciliopathy. *J Clin Invest* 119:428-37.

Zanivan S, Gnad F, Wickstrom SA, Geiger T, Macek B, Cox J, Fassler R, Mann M. 2008. Solid Tumor Proteome and Phosphoproteome Analysis by High Resolution Mass Spectrometry. *J Proteome Res* 7:5314-5326.

Zhou J. 2009. Polycystins and primary cilia: primers for cell cycle progression. *Annual review of physiology* 71:83-113.

Appendices

Appendix A.

Regulation of CNK2 by Phosphorylation

Brian Bradley originally observed that expressing full-length kinase-active CNK2-6xHIS in bacteria produces a protein that runs at a substantially higher molecular weight on SDS-PAGE gels (~100 kDa) than either CNK2-6xHIS K40A (presumptive kinase dead) or endogenous CNK2 detected by anti-CNK2 western blot (~72 kDa) (Figure A.1A). I set out to determine whether this apparent increase in molecular weight was due to hyperphosphorylation. I expressed and purified CNK2-6xHIS WT and CNK2-6xHIS K40A from bacteria, and treated the WT sample with protein phosphatase 1 (PP1). Treatment of CNK2-6xHIS WT with PP1 resulted in a decrease in the apparent molecular weight of the protein by SDS-PAGE, although it did not reduce it to the same apparent molecular weight as CNK2-6xHIS K40A (Figure A.1B). To determine conclusively that the size shift was due to hyperphosphorylation, I examined a sample of purified CNK2-6xHIS WT by mass spectrometry. This identified 27 phosphorylated serines and threonines in the purified recombinant protein (Figure A.2).

Given that the K40A recombinant protein does not appear to by hyperphosphorylated, it is likely that the phosphorylation of the WT recombinant protein is due to autophosphorylation. Kinase assays using myelin basic protein as a substrate reveal that WT rCNK2 is kinase active, while K40A rCNK2 is not (Figure A.3). This lends support to the hypothesis that the hyperphosphorylation of WT rCNK2 is due to autophosphorylation.

I next considered whether phosphorylation of CNK2 *in vivo* might be important to regulate its activity. Given that WT rCKN2 is hyperphosphorylated and kinase active, and that CNK2 is required for IBMX-induced flagellar resorption, we reasoned that endogenous CNK2 may become phosphorylated *in vivo* upon IBMX treatment. To test this, I isolated flagella from WT cells after various intervals of IBMX treatment in the presence of phosphatase inhibitors, and detected CNK2 by western blot (Figure A.4). I was unable to detect any size shift in the CNK2 band, indicating at least that CNK2 does not become hyperphosphorylated *in vivo* to the same extent as WT rCNK2.

Although endogenous CNK2 does not appear hyperphosphorylated *in vivo*, I reasoned that phosphorylation of only one or two residues may be required to regulate CNK2 activity. I hypothesized that phosphorylation of threonine in the activation loop may be responsible for activating CNK2, similar to the regulatory mechanism of mouse Nek8 [Zalli et al., 2012]. Alignment of the Nek8 kinase domain with the CNK2 kinase domain, and comparison with the phosphorylated residues identified by mass spectrometry, I determined that CNK2 has four phosphorylated activation loop threonines that may participate in its regulation. My strategy to identify which of these might be key to activating CNK2 was to mutate each residue to an alanine in CNK2-6xHIS and observe whether the protein continued to become hyperphosphorylated. I found that mutating any of the four of these residues abolished the hyperphosphorylation of rCNK2 (Figure A.5). Future experiments should include mutating these threonine residues to glutamate or aspartate to generate “phospho-mimic” rCNK2. If phospho-mimic rCNK2 is hyperphosphorylated *in vitro*, that could indicate that the mutation makes CNK2 constitutively active. This could be followed up by expressing phospho-mimic CNK2 in

Chlamydomonas, where I predict it would cause very short flagella due to constitutive activation of the CNK2-dependent resorption pathways.

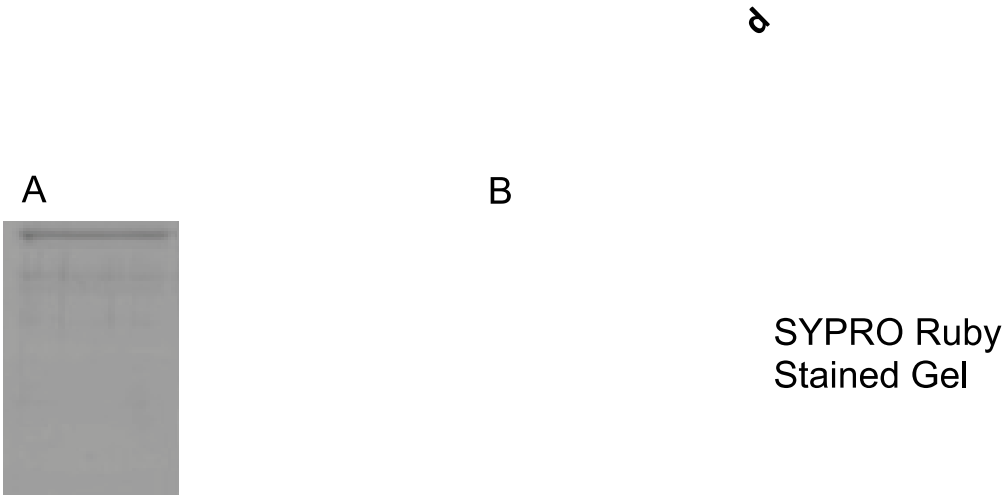

Figure A.1. PP1 treatment indicates that CNK2-6xHIS WT is hyperphosphorylated.

A. CNK2-6xHIS WT (kinase active CNK2) and K40A (kinase dead CNK2) were expressed in bacteria and purified using the HisTrapFF purification system. The purified proteins were run on an 8% SDS-PAGE gel stained with SYPRO Ruby. B. CNK2-6xHIS WT was treated with protein phosphatase 1 (PP1) and run on an SDS-PAGE gel, alongside untreated CNK2-6xHIS WT. The gel was stained with SYPRO Ruby.

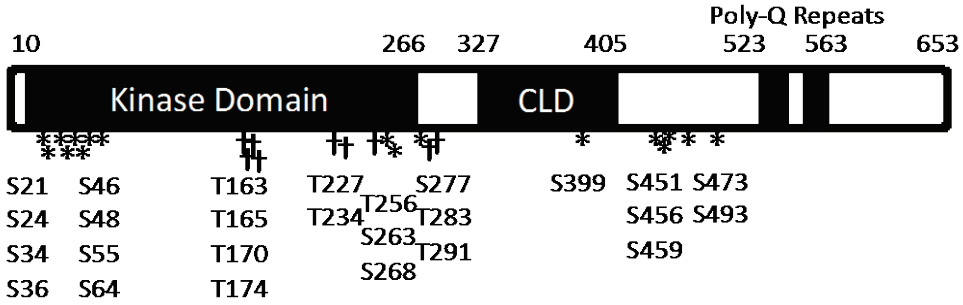

Figure A.2. Mass spectrometry revealed 27 phosphorylated serine and threonine residues in recombinant CNK2-6xHIS.

Purified CNK2-6xHIS was tryptically digested and run on a LTQ-Orbitrap LCMS/MS. Phosphorylation sites are indicated on this schematic of the CNK2 protein.
*Phosphorylated serine residue; †Phosphorylated threonine residue.

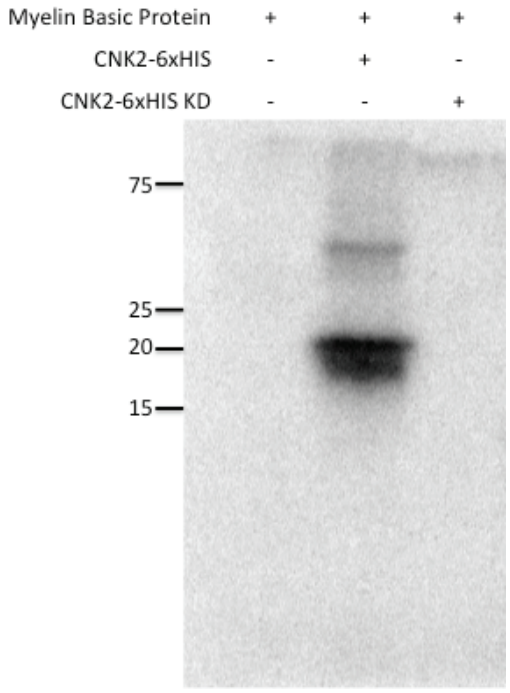

Figure A.3. CNK2-6xHIS WT is kinase active.
Myelin basic protein (MBP) was incubated with either CNK2-6xHIS WT or K40A and γ-^{32}P-ATP, then run on a 12% SDS-PAGE gel and detected by autoradiography. MBP becomes phosphorylated with CNK2-6xHIS WT, but not with K40A.

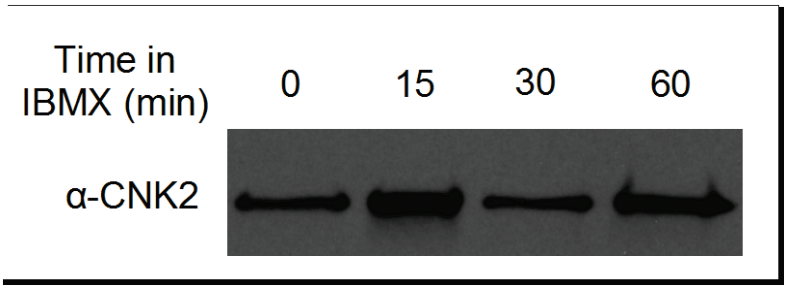

Figure A.4. Endogenous CNK2 does not become hyperphosphorylated in response to IBMX treatment.
Flagella were isolated in the presence of phosphatase inhibitors from WT *Chlamydomonas* cells at various time intervals during treatment with IBMX. Samples were run on an 8% SDS-PAGE gel and detected by anti-CNK2 immunoblotting.

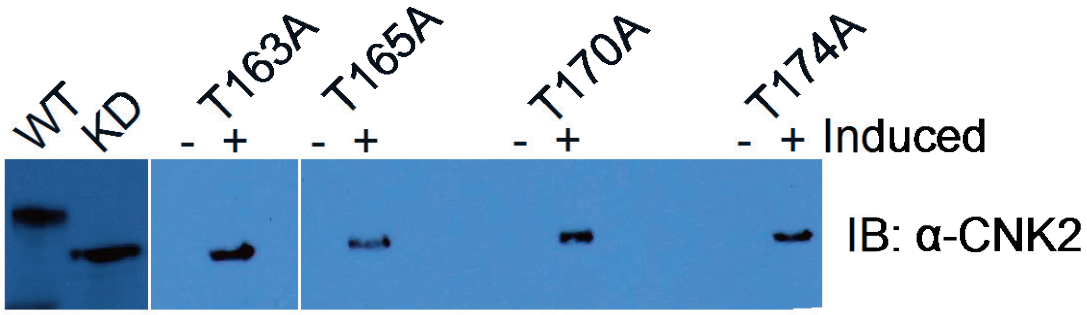

Figure A.5. Mutating putative activation loop threonine residues abolishes hyperphosphorylation of CNK2-6xHIS.

Threonine residues in the putative activation loop of CNK2 were mutated to alanine in CNK2-6xHIS. The constructs were transformed into bacteria and expression was induced with IPTG (+). The samples were run on an 8% SDS-PAGE gel and CNK2-6xHIS was detected by immunoblotting with anti-CNK2.

Appendix B.

Biochemical approaches to identifying CNK2 substrates and binding partners.

Fractionation of wild-type flagella revealed that CNK2 is found associated with the flagellar axoneme in the KCl-extractable fraction (Figure B.1), suggesting that it is associated with an axonemal complex. We reasoned that CNK2 might be associated with a structural component of the flagellum that is lost in motility mutants. Brian Bradley examined the localization of CNK2-HA overexpressed in a wild-type background, and found that it localized normally to the flagella of various structural mutants ([Bradley and Quarmby, 2005] and Table B.1). I followed up on this observation by isolating flagella from a greater number of structural mutants and examining them by anti-CNK2 western blot to confirm that localization of the endogenous CNK2 protein is not affected (Figure B.2 and Table B.1).

To attempt to identify binding partners of CNK2, I performed chemical cross-linking on wild-type axonemes using the zero-length cross-linker EDC (1-Ethyl-3-[3-dimethylaminopropyl] carbodiimide hydrochloride), and examined cross-linked axonemes by anti-CNK2 western blot. The predominant cross-linked product has an apparent molecular weight of approximately 140 kDa, almost exactly twice that of CNK2 (Figure B.3). It is possible that this product is a dimer of CNK2. I planned to repeat this in *cnk2-1* cells expressing CNK2-HA to facilitate immunoprecipitation of CNK2 and its cross-linked binding partners, but was never successful at isolating CNK2-HA by immunoprecipitation.

Lastly, I had planned to use the Shokat method to identify substrates of CNK2. This method involves mutating a “gateway” methionine residue in the kinase domain to a glycine, thereby allowing a bulky ATP analog such as N6-Benzyl-ATP-γ-S to fit into the active site of the modified kinase [Allen et al., 2007]. Upon phosphorylation by the modified kinase, substrates become tagged with the γ-thiophosphate group, which can be immunoprecipitated with a commercial antibody [Allen et al., 2007]. To this end, I generated an M87G mutation in CNK2-6xHIS to first test whether the kinase could utilize the ATP analog. I found that the M87G mutation abolished hyperphosphorylation *in vitro* (Figure B.4A). Furthermore, expressing CNK2-HA M87G in *cnk2-1* mutant cells failed to rescue the NaPPi and IBMX resorption defect (Figure B.4B). I chose to terminate this experiment because it appears that the M87G mutation renders CNK2 kinase dead.

Finally, I examined wild-type and *cnk2-1* mutant flagella, with or without treatment with IBMX or NaPPi, for key phosphorylation events that may be part of the CNK2-dependent resorption pathway. I incubated wild-type and *cnk2-1* cells in phosphate-free media supplemented with $^{32}PO_4$ for 24 hours, then incubated them with either 1 mM IBMX or NaPPi for 10 minutes before isolating flagella in the presence of phosphatase inhibitors. The flagella were then run on SDS-PAGE gels and phosphoproteins were detected by autoradiography. No differences in phosphorylated proteins were detected between treated and untreated samples, or between wild-type and *cnk2-1* (Figure B.5). Thus the experiment was unsuccessful, and could be repeated at some point in the future.

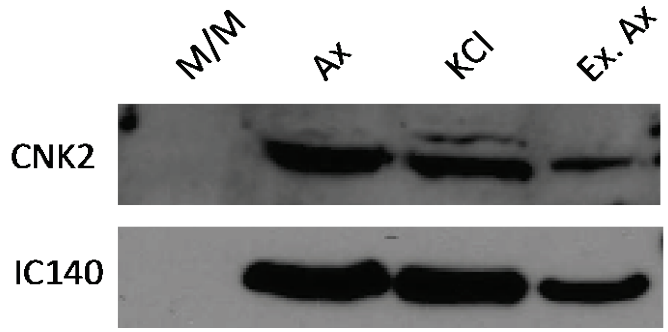

Figure B.1. CNK2 is associated with the flagellar axoneme.
Flagella were isolated from wild-type cells and fractionated into membrane & matrix (M/M), whole axoneme (Ax), KCl extract (KCl), and extracted axoneme (Ex. Ax.) fractions. The fractions were run on an 8% SDS-PAGE gel and examined by western-blotting with anti-CNK2. Anti-IC140 is a positive control for the axoneme and KCl fractions.

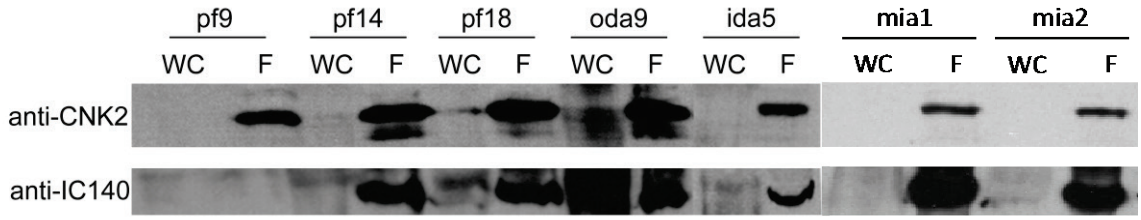

Figure B.2. CNK2 is localized to the flagella of various structural mutants.
Flagella (F) were isolated from various structural motility mutants, run on 8% SDS-PAGE gels, and examined by western-blotting with anti-CNK2. Flagellar fractions were compared to whole cell (WC). Anti-IC140 was used as a loading control, and is missing from *pf9* mutants because it is a component of the inner dynein arms.

Table B.1. The localization of CNK2 in various structural mutants.

Mutant	Structural Defect	CNK2 present in flagella by WB?	CNK2-HA present in flagella by IF? [Bradley and Quarmby, 2005]
pf9	Inner dynein arms	Yes	Yes
pf14	Radial Spokes	Yes	Yes
pf18	Central pair	Yes	Yes
oda9	Outer dynein arms	Yes	Yes
ida5	Inner dynein arms	Yes	Not Done
mia1	MIA complex	Yes	Not Done
mia2	MIA complex	Yes	Not Done
pf3	Nexin-DRC	Not Done	Yes

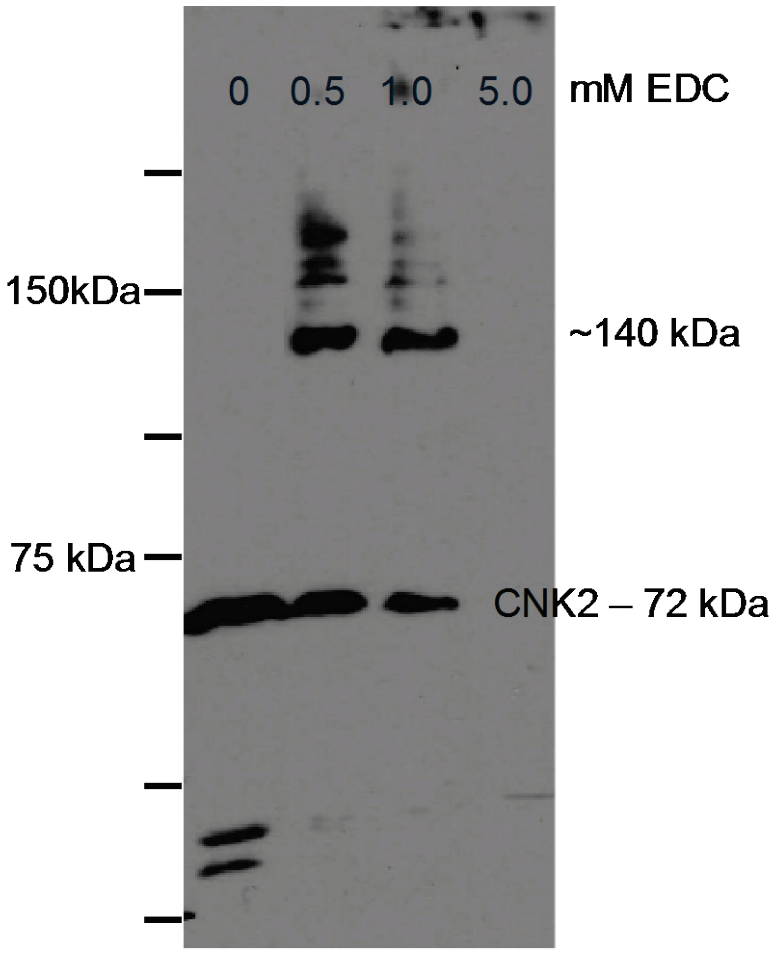

Figure B.3. EDC cross-linking of wild-type axonemes reveals a 140 kDa cross-linked product with CNK2.

Whole flagella were isolated from wild-type *Chlamydomonas* cells and incubated with increasing concentrations of EDC for one hour. The reaction was quenched by adding sample buffer, the samples were run on a 4-20% SDS-PAGE gel, and examined by immunoblotting with anti-CNK2. Endogenous CNK2 is present as a ~72 kDa band, and the primary cross-linked product runs at ~140 kDa.

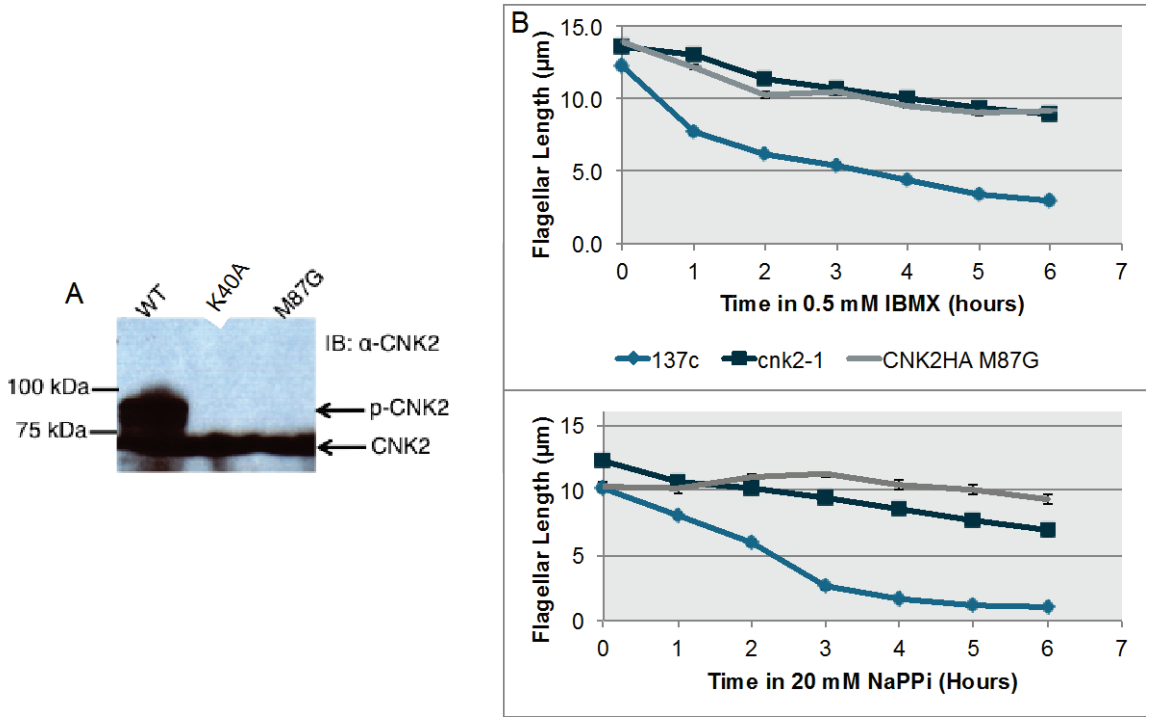

Figure B.4. The gateway M87G mutation renders CNK2 kinase dead.
A. CNK2-6xHIS WT, K40A, and M87G were expressed in bacteria, and CNK2 was detected by anti-CNK2 immunoblotting. Both the K40A and M87G mutations eliminate the hyperphosphorylation of CNK2 (p-CNK2). B. CNK2-HA M87G was expressed in the *cnk2-1* mutant background. These cells were treated with 0.5 mM IBMX or 20 mM NaPPi, and flagellar lengths were measured each hour for six hours, and compared to wild-type (137c) and *cnk2-1* cells. Seventy-five cells were measured at each time point, error bars represent SEM.

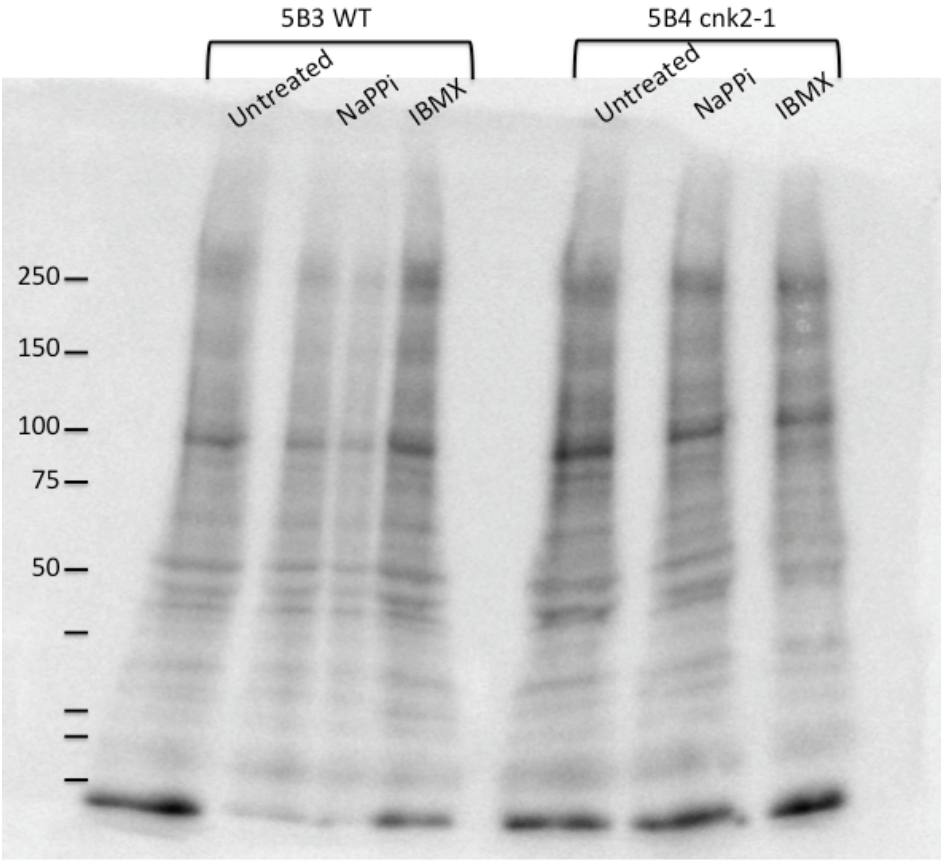

Figure B.5. Identifying flagellar phosphoproteins generated upon treatment with IBMX or NaPPi.

Wild-type or *cnk2-1* cells were incubated in 300 mL tris-acetate media (without phosphate) in the presence of 300 µCi of $^{32}PO_4$ for 24 hours. Each culture was divided equally into three parts and treated with 1 mM IBMX, 20 mM NaPPi, or nothing for 10 minutes. Phosphatase inhibitor cocktail was added and flagella were isolated as usual. Isolated flagella were run on a 4-20% SDS-PAGE gel, and phosphoproteins were detected by autoradiography.